

1978

The Photochemistry Of N-methylphenazonium Methylsulfate In Aqueous Solution

Vivian Seek Chew

Follow this and additional works at: <https://ir.lib.uwo.ca/digitizedtheses>

Recommended Citation

Chew, Vivian Seek, "The Photochemistry Of N-methylphenazonium Methylsulfate In Aqueous Solution" (1978). *Digitized Theses*. 1088.

<https://ir.lib.uwo.ca/digitizedtheses/1088>

This Dissertation is brought to you for free and open access by the Digitized Special Collections at Scholarship@Western. It has been accepted for inclusion in Digitized Theses by an authorized administrator of Scholarship@Western. For more information, please contact tadam@uwo.ca, wlsadmin@uwo.ca.



National Library of Canada

Cataloguing Branch
Canadian Theses Division

Ottawa, Canada
K1A 0N4

Bibliothèque nationale du Canada

Direction du catalogage
Division des thèses canadiennes

NOTICE

The quality of this microfiche is heavily dependent upon the quality of the original thesis submitted for microfilming. Every effort has been made to ensure the highest quality of reproduction possible.

If pages are missing, contact the university which granted the degree.

Some pages may have indistinct print especially if the original pages were typed with a poor typewriter ribbon or if the university sent us a poor photocopy.

Previously copyrighted materials (journal articles, published tests, etc.) are not filmed.

Reproduction in full or in part of this film is governed by the Canadian Copyright Act, R.S.C. 1970, c. C-30. Please read the authorization forms which accompany this thesis.

**THIS DISSERTATION
HAS BEEN MICROFILMED
EXACTLY AS RECEIVED**

AVIS

La qualité de cette microfiche dépend grandement de la qualité de la thèse soumise au microfilmage. Nous avons tout fait pour assurer une qualité supérieure de reproduction.

S'il manque des pages, veuillez communiquer avec l'université qui a conféré le grade.

La qualité d'impression de certaines pages peut laisser à désirer, surtout si les pages originales ont été dactylographiées à l'aide d'un ruban usé ou si l'université nous a fait parvenir une photocopie de mauvaise qualité.

Les documents qui font déjà l'objet d'un droit d'auteur (articles de revue, examens publiés, etc.) ne sont pas microfilmés.

La reproduction, même partielle, de ce microfilm est soumise à la Loi canadienne sur le droit d'auteur, SRC 1970, c. C-30. Veuillez prendre connaissance des formules d'autorisation qui accompagnent cette thèse.

**LA THÈSE A ÉTÉ
MICROFILMÉE TELLE QUE
NOUS L'AVONS REÇUE**

THE PHOTOCHEMISTRY OF N-METHYLPHENAZONIUM
METHYLSULFATE IN AQUEOUS SOLUTION

by

Vivian Seek Fong Chew

Department of Chemistry

Submitted in partial fulfillment
of the requirements for the degree of
Doctor of Philosophy

Faculty of Graduate Studies
The University of Western Ontario
London, Ontario
December, 1977

©

Vivian Seek Fong Chew 1977

ABSTRACT

The photochemistry of NMP^+ (N-methylphenazonium ion) in aqueous solution has been studied using electron spin resonance (ESR) and optical flash photolysis techniques.

When a degassed NMP^+ solution is irradiated with blue light, a stable radical can be detected by ESR immediately after the light is turned on. The radical has been identified from its ESR spectrum and optical absorption spectrum as the semireduced NMP^+ radical cation ($\text{NMPH}^{\dot{+}}$). Pyocyanine is also found as a major product.

A mechanism for the photoreaction is proposed involving the formation of a solvent adduct of the excited singlet state of NMP^+ . This intermediate then donates an $\cdot\text{OH}$ radical to NMP^+ in a concerted reaction to form the semireduced pyocyanine radical cation ($\text{PYH}_2^{\dot{+}}$) and the semireduced NMP^+ neutral radical ($\text{NMP}\cdot$) which is then protonated to form $\text{NMPH}^{\dot{+}}$. $\text{PYH}_2^{\dot{+}}$ then reacts with NMP^+ giving $\text{NMPH}^{\dot{+}}$ and PYH^+ , but $\text{PYH}\cdot$ (the semireduced PYH^+ neutral radical) which can be generated through the ionization of $\text{PYH}_2^{\dot{+}}$, can also react with NMP^+ giving $\text{NMP}\cdot$ and PYH^+ .

The rate constants of the various reactions were determined using an optical flash photolysis technique.

The quantum yield of the formation of $\text{NMPH}^{\dot{+}}$ was determined

using an ESR technique which does not require a knowledge of the absorption coefficient at the wavelength of the incident light. The maximum quantum yield was obtained at pH 3 and drops to 0.29 ± 0.03 at pH 7.

ACKNOWLEDGEMENTS

I would like to thank Prof. James R. Bolton for his help, advice and encouragement during the course of this work.

Acknowledgements are made to the Department of Chemistry and the University of Western Ontario for graduate teaching assistantship, to Drs. Christian Blanchard, C. Anderson Evans, Leonard Fabes, John R. Harbour, Alan R. McIntosh and Prasanna Mohanty for fruitful discussions, and to Mr. Stan Markiewicz for constructing the optical flash photolysis apparatus. Special thanks are due to Prof. Patrick W. M. Jacobs, Prof. John W. Lorimer and Dr. S. King Wong for invaluable discussions and suggestions.

Finally, I would like to thank my husband Calvin for his patience, understanding and encouragement..

TABLE OF CONTENTS

	Page
CERTIFICATE OF EXAMINATION	ii
ABSTRACT	iii
ACKNOWLEDGEMENTS	v
TABLE OF CONTENTS	vi
LIST OF TABLES	x
LIST OF FIGURES	xi
ABBREVIATIONS	xv
CHAPTER 1 INTRODUCTION	1
CHAPTER 2 THE CHEMISTRY AND PHOTOCHEMISTRY OF N-METHYLPHENAZONIUM SALTS AND RELATED COMPOUNDS	7
2.1 HISTORY OF THE USE OF N-METHYLPHENAZONIUM METHYLSULFATE (NMPMS)	7
2.2 NMPMS IN PHOTOPHOSPHORYLATION	15
2.3 CHEMISTRY AND PHOTOCHEMISTRY OF NMP ⁺ SALTS	18
2.3.1 Oxidation States of NMP ⁺	18
2.3.2 Association of NMP ⁺ with Biological Components	19
2.3.3 Photochemical Products from NMP ⁺	21
2.3.4 ESR Studies	25
2.4 PHOTOCHEMISTRY OF RELATED COMPOUNDS	26
2.4.1 Phenazine	26
2.4.2 Pyocyanine	33

CHAPTER 3	EXPERIMENTAL TECHNIQUES AND MATERIALS	34
3.1	BASIC PRINCIPLES OF ELECTRON SPIN RESONANCE (ESR)	34
3.2	FLASH PHOTOLYSIS TECHNIQUES	36
3.2.1	Optical Flash Photolysis	36
3.2.2	Flash Photolysis Electron Spin Resonance (FPESR) Technique	37
3.3	SPIN TRAPPING TECHNIQUE	39
3.4	DETERMINATION OF THE CONCENTRATION AND g FACTOR OF RADICALS	40
3.4.1	Determination of the Absolute Concentration of Radicals	40
3.4.2	Determination of g Factor	41
3.4.3	Determination of Area under Absorption Curves	42
3.4.4	Weighted Least Squares Method	42
3.5	POTENTIOMETRIC TITRATION	44
3.6	DETERMINATION OF FLUORESCENCE QUANTUM YIELD	45
3.7	ESR SPECTROMETER AND ACCESSORIES	46
3.8	OPTICAL FLASH PHOTOLYSIS	52
3.9	LIGHT SOURCES	58
3.10	CHEMICALS AND SAMPLE PREPARATIONS	59
3.11	MISCELLANEOUS INSTRUMENTS	61
CHAPTER 4	RESULTS AND DISCUSSION	62
4.1	THE PROPOSED MECHANISM	62
4.2	PHOTOCHEMICAL GENERATION OF A RADICAL FROM NMPMS	64
4.2.1	Identification of the Radical Formed	64
4.2.2	Analysis of the ESR Spectrum	78

4.2.3	Identification of Other Products	83
4.3	QUANTUM YIELD DETERMINATION	91
4.4	FLUORESCENCE AND REDOX BEHAVIOUR OF NMP^+	107
4.4.1	Fluorescence Behaviour	107
4.4.2	Fluorescence Quantum Yield	107
4.4.3	Reactions Involving the Singlet State	112
4.4.4	Redox Behaviour	117
4.5	OPTICAL FLASH PHOTOLYSIS	126
4.5.1	Rate Constant Determination	126
4.5.2	A Transient Species at 525 nm	140
4.6	pH DEPENDENCE OF THE RATE CONSTANTS AND THE YIELDS	156
4.6.1	Disproportionation of NMPH^+ or NMP^+	165
4.6.2	Competitive Reactions Involving Intermediate X	170
4.6.3	Reactions of PYH_2^+	172
4.7	THE STOICHIOMETRIC RATIO OF NMPH^+ AND PYH^+	176
4.8	EFFECT OF ADDED AGENTS	179
4.8.1	Addition of Spin Traps	179
4.8.2	Effect of Other Solutes	183
4.9	THE NATURE OF THE INTERMEDIATE X	188
4.10	KINETIC SIMULATION	194
4.11	FURTHER WORK AND APPLICATIONS	196
4.11.1	Further Work	196
4.11.2	Possible Applications	197
4.12	SUMMARY	198
	REFERENCES	201

APPENDIX 1	THE COMPUTER PROGRAM FOR THE DOUBLE INTEGRATION	206
APPENDIX 2	THE EXPERIMENTAL SECOND DERIVATIVE OF NMPH ⁺ ESR SPECTRUM AND THE COMPUTER SIMULATED SPECTRUM USING THE HYPERFINE SPLITTING CONSTANTS LISTED IN TABLE 4.1	210
VITA		211

LIST OF TABLES

Table	Description	Page
4.1	The Hyperfine Splitting Constants of the Radical NMPH^+	82
4.2	Summary of the Results in the Quantum Yield Experiments at $\lambda = 476.2 \text{ nm}$	100
4.3	Summary of the Uncertainties in the Quantum Yield Measurements	101
4.4	The Apparent Reduction Potentials of NMP^+ at Various pH's	125
4.5	The Conversion Factor of the Disproportionation Reaction	169
4.6	The Comparison of Hyperfine Splitting Constant of Spin Adducts Formed in NMP^+ to that of $\cdot\text{OH}$ Radical Spin Adducts Using DMPO and PBN as the Spin Traps	182
4.7	Summary of the Rate Constants Obtained in Optical Flash Photolysis Experiments	199

singly protonated form were carried out in ethanol and 6 M hydrochloric acid respectively. $S_0 \rightarrow T$ absorption or phosphorescence of the doubly protonated species was not detected. Fluorescence quantum yields for phenazine were found to be 8.6×10^{-4} in ethanol and 3.0×10^{-5} in hexane solution. Fluorescence emission in ethanol was ascribed to a π, π^* state, and that in hexane was ascribed to a n, π^* state because in hydrocarbon solvents the n, π^* is the lowest excited singlet state.

These investigators also calculated the first and the second pK_a values of phenazine in the lowest π, π^* triplet and π, π^* singlet using Förster's cycle (35). The pK_a 's of the π, π^* triplet and π, π^* singlet of phenazine were reported as 5.7, 4.0 (second pK_a) and 4.1, 6.0 respectively whereas the pK_a values of the ground state of phenazine are -4.30 and 1.21 (36).

The photoreduction of phenazine in strongly acidic methanol (0.1 - 1 M HCl in methanol) and weakly acidic methanol (methanol containing 0.1 M acetic acid and 0.1 M sodium acetate) was investigated by Bailey et al. (37). They indicated that the reactive state under both these conditions is the lowest n, π^* singlet state. They suggested that in weakly acidic methanol the reactive state underwent protonation followed by electron transfer from methanol to produce semiquinone radical. The radical then reacted with the solvent to produce 5,10-dihydrophenazine. In strongly acidic methanol, the authors suggested, monoprotonated phenazine is directly excited and then undergoes a second protonation to give a dication. 5,10-dihydrophenazine is formed after electron transfer to the

4.5	The Optical Absorption Spectrum Obtained (a) after Irradiating NMP^+ in 0.1 M Acetic Acid (b) after Addition of Sodium Borohydride to NMP^+ in 0.1 M Acetic Acid	75
4.6	The First Derivative ESR Spectrum of NMP^+ in 2-propanol	77
4.7	(a) The Expansion of the Low Field End of the Second Derivative ESR Spectrum of NMPH^+ (b) The Computer Simulated Spectrum Using the Four Smallest Hyperfine Splittings Listed in Table 4.1	80
4.8	(a) The Experimental and (b) Computer Simulated First Derivative ESR Spectra of NMPH^+ in Water at pH 3	85
4.9	(a) The Experimental and (b) Computer Simulated First Derivative ESR Spectra of NMPD^+ in D_2O	87
4.10	The Optical Absorption Spectra of Pyocyanine at pH 3 and pH 7	90
4.11	The Relation between the Area under the Absorption Curve and the Peak-to-Peak Amplitude of the ESR Signal	94
4.12	A Typical Trace Obtained in the Quantum Yield Determination Experiment	97
4.13	The pH Dependence of the Quantum Yield of the Formation of NMPH^+	103
4.14	The Relation between the Initial Change in ESR Signal and the Fraction of Light Absorbed by NMP^+ at pH 3	106
4.15	The Fluorescence Spectrum of NMP^+ in Water	109
4.16	The Effect of pH on the Initial Fluorescence Yield of NMP^+ Compared to that in Solution of pH 7	111
4.17	The Relation between the Rate of Formation of NMPH^+ and the Light Intensity	114

4.18	The Relation between the Rate of Formation of NMPH^+ and the Concentration of NMP^+	116
4.19	The Potentiometric Titration of NMP^+ at pH 2	120
4.20	The Potentiometric Titration of NMP^+ at pH 3	122
4.21	The Potentiometric Titration of NMP^+ at pH 7	124
4.22	The Original Traces Obtained in the Optical Flash Photolysis at 443 nm and 525 nm	128
4.23	The First Order Kinetics Plot Measured at 443 nm at pH 3	130
4.24	The First Order Kinetics Plot Measured at 525 nm at pH 3	132
4.25	The Effect of the Concentration of NMP^+ on the Pseudo First Order Rate Constant of Reaction 4.5 Measured at 443 nm and at pH 3	135
4.26	The Effect of the Concentration of NMP^+ on the Pseudo First Order Rate Constant of Reaction 4.8 Measured at 525 nm and at pH 3	137
4.27	The Comparison of Rise Kinetics at 443nm and 525 nm at pH 3	139
4.28	The Comparison of the Rise Kinetics at 525 nm and the Decay Kinetics at 443 nm at pH 3	142
4.29	The Effect of pH on the Maximum Yield of the Fast Decay Transient Detected at 525 nm	144
4.30	The Transient Observed at 525 nm and the Decay Kinetics of the Fast Decay Component.	146
4.31	The Effect of the Concentration of NMP^+ on the Rate Constants of Both Fast and Slow Decay Transients Measured at 525 nm at pH 4.8	149
4.32	The Effect of pH on the Rate Constant of the Fast Decay Transient Detected at 525 nm	151

4.33	The pH Dependence of the Pseudo First Order Rate Constant for the Slow Decay Transient (Reaction 4.7) Observed at 525 nm	154
4.34	The Effect of pH on the Pseudo First Order Rate Constant of Reaction 4.5 Measured at 443 nm	158
4.35	The Effect of pH on the Pseudo First Order Rate Constant for the Formation of Pyocyanine Measured at 525 nm	160
4.36	The Effect of pH on the Ultimate Yield of NMPH^+ Measured at 443 nm	162
4.37	The Effect of pH on the Ultimate Yield of Pyocyanine Measured at 525 nm	164
4.38	The pH Dependence of the Factor $2A/(A_0 - A)$	168
4.39	A Plot of $1/[\text{H}_3\text{O}^+]$ Versus the Ratio of Pseudo First Order Rate Constant Measured at 525 nm to the Concentration of NMP^+	175
4.40	The First Derivative ESR Spectrum Obtained after Irradiation of (a) NMP^+ , (b) 1 % H_2O_2 Solution, Both in the Presence of DMPO	181
4.41	The Effect of the Concentration of Formate Buffer on the Yield of Pyocyanine Compared to that in 10^{-6} M Formate Buffer	185
4.42	Structures of Various Species Involved in the Photohydroxylation of 7,8-Dimethylalloxazine	191



ABBREVIATIONS

a	Hyperfine Splitting Constant
A	Absorbance
ADP	Adenosine Diphosphate
ATP	Adenosine Triphosphate
DMPO	5,5-Dimethyl-1-pyrroline-1-oxide
ϵ	Molar Absorption Coefficient
ESR	Electron Spin Resonance
FPESR	Flash Photolysis Electron Spin Resonance
k_p	Pseudo First Order Rate Constant
NMP^+	N-Methylphenazonium Cation
$NMPH^+$; $NMP\cdot$	Protonated and Unprotonated Semireduced NMP^+
PBN	Phenyl-t-butyl Nitron
PYH^+ ; PY	Protonated and Unprotonated Pyocyanine
PYH_2^+ ; $PYH\cdot$	Protonated and Unprotonated Semireduced Pyocyanine
T	Transmittance
[]	Concentration

The author of this thesis has granted The University of Western Ontario a non-exclusive license to reproduce and distribute copies of this thesis to users of Western Libraries. Copyright remains with the author.

Electronic theses and dissertations available in The University of Western Ontario's institutional repository (Scholarship@Western) are solely for the purpose of private study and research. They may not be copied or reproduced, except as permitted by copyright laws, without written authority of the copyright owner. Any commercial use or publication is strictly prohibited.

The original copyright license attesting to these terms and signed by the author of this thesis may be found in the original print version of the thesis, held by Western Libraries.

The thesis approval page signed by the examining committee may also be found in the original print version of the thesis held in Western Libraries.

Please contact Western Libraries for further information:

E-mail: libadmin@uwo.ca

Telephone: (519) 661-2111 Ext. 84796

Web site: <http://www.lib.uwo.ca/>

CHAPTER 1

INTRODUCTION

In the beginning God created the heaven and the earth. And then He made the light; the sky, dry land and the seas; every sort of grass, seed bearing plants and fruit trees..... On the sixth day God made every kind of animal and then He created man. God gave man the seed bearing plants and fruit trees for food and all the grass and plants to the animals and birds for their food. All life on earth is dependent on a wonderful process - photosynthesis - which converts carbon dioxide and water into carbohydrates and oxygen.

Photosynthesis is only one of the photochemical reactions that are known to us today. Many photochemical systems have been well studied such as the photoreduction of benzophenone in alcohols. Various techniques such as electron spin resonance (ESR), nuclear magnetic resonance (NMR) spectroscopy, mass spectrometry, and flash photolysis have been applied to study the mechanisms of photochemical reactions.

Many photochemical reactions produce radicals and thus the technique of ESR, which is a physical method to detect molecules with one or more unpaired electrons, is of considerable value. For example, the formation of the diphenylhydroxymethyl radical (1), which was detected by ESR, confirmed that hydrogen abstraction by the excited

benzophenone from the solvent ethanol had indeed occurred. At the same time, the intermediates of photochemical reactions are usually very short lived. Thus flash photolysis techniques coupled with rapid detection techniques (such as optical flash photolysis and flash photolysis electron spin resonance (FPESR)) are very useful. In reactions where more than one transient intermediate is created, flash photolysis techniques can also establish the chronological order of the appearance of transients.

During a study of the effect of the dye NMPMS (N-methylphenazonium methylsulfate; this dye is often referred to as PMS) on the kinetics of light - induced free radical production and decay in chromatophores of photosynthetic bacteria, an additional light - induced ESR signal was observed when a red filter was accidentally omitted. The same ESR signal was observed when a control solution containing NMPMS but no chromatophores was illuminated with white light. This stimulated us to investigate the photochemistry of NMP^+ (N-methylphenazonium cation) in aqueous solution with the object of elucidating the mechanism of this reaction.

NMPMS has been shown to catalyze cyclic photophosphorylation, the process where green plants, algae and photosynthetic bacteria use radiant energy to form adenosine triphosphate (ATP) from adenosine diphosphate (ADP) and inorganic phosphate. It was suggested that NMP^+ substantially shortens the chemical pathway for the ATP formation. A knowledge of the mechanism of the NMP^+ photochemical reaction will perhaps help us to understand the role of NMP^+ in cyclic photophosphorylation.

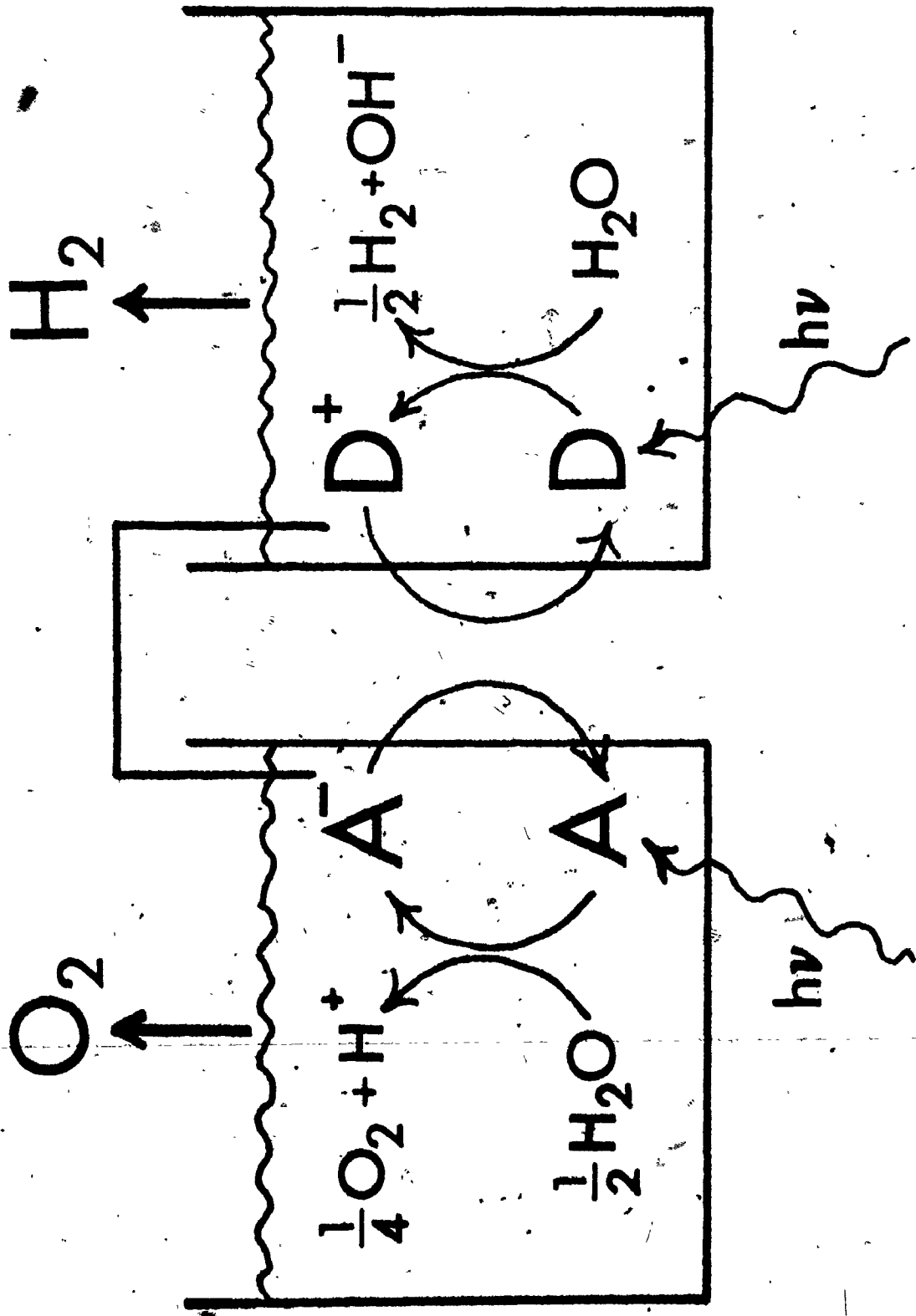
Recently Bolton (2), by drawing analogies with the mechanism of photosynthesis, has proposed a scheme for the sensitized decomposition of water using two coupled photochemical systems. This scheme is shown in Fig. 1.1. D is a strong photochemical reducing agent and A is a strong photochemical oxidizing agent. When the two cells are coupled electrochemically the reverse of the photochemical reactions occur. During the course of this work we have found that NMP^+ can serve as a photochemical oxidizing agent, that is, it can photochemically oxidize itself, formate, acetate and other substrates. Even though the photochemical reaction between NMP^+ and water does not produce oxygen as hoped for in the scheme shown in Fig. 1.1, the understanding of the mechanism of the NMP^+ reaction will provide more information on how a photochemical oxidation reaction occurs.

In the present work it was also found that the semireduced species of NMP^+ is one of the major products of the photochemical reaction of NMP^+ in aqueous solution and is very stable in anaerobic solution. This radical was identified as the semireduced NMP^+ radical cation (NMPH^+) by the hyperfine pattern of the ESR signal and its optical absorption spectrum. Both flash photolysis ESR (FPEER) and optical flash photolysis techniques were used to elucidate the kinetics of formation or removal of various species in the system and the rate constants of the reactions were calculated from these measurements. The quantum yield of the formation of NMPH^+ was determined by an ESR technique which does not require a knowledge of the absorption coefficient of the radical at the wavelength of the incident light. The pH range covered in the present study is from ~ 2 to 7. The reported pK_a values of pyocyanine, NMPH^+ and one of the

Figure 1.1

A Scheme for the Sensitized Decomposition of
Water Using Two Coupled Photochemical Systems (2).

D is a strong photochemical reducing agent and A is
a strong photochemical oxidizing agent.



proposed intermediates, semireduced pyocyanine, are all around 6. Therefore both the protonated and the unprotonated species are involved in the reaction scheme. The severe overlapping in the optical absorption spectra of NMP^+ and the products further complicates the system. The results are discussed in terms of a mechanism involving the addition of water to the excited singlet state and the formation of NMPH^+ and pyocyanine as the final products of the reaction.

CHAPTER 2

THE CHEMISTRY AND PHOTOCHEMISTRY OF N-METHYLPHENAZONIUM SALTS AND RELATED COMPOUNDS

2.1 HISTORY OF THE USE OF N-METHYLPHENAZONIUM METHYLSULFATE (NMPMS)

Kehrmann and Havas (3) were the first to prepare NMPMS in 1913 by treating phenazine with dimethyl sulfate for five minutes at 100 - 110°C. In the same paper, they reported that when an alcoholic solution of NMPMS was treated with a little sodium hydroxide and allowed to stand in the air for a short time a red colour developed. They suggested that the methyl analog of aposafranone (Fig. 2.1a) was formed. If concentrated ammonium hydroxide was used, the product was the 3-aminomethylphenazonium salt (Fig. 2.1b).

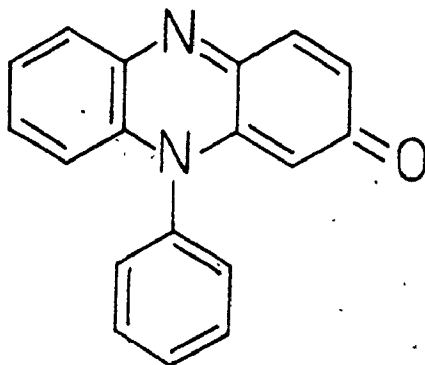
Kehrmann and Havas (3) reported that on adding concentrated potassium iodide to a dilute solution of NMPMS, black - green needles began to separate. They suggested that it was a quinhydrone salt, $C_{13}H_{11}N_2I_3 \cdot 2C_{13}H_{12}N_2$. In the same year, Hantzsch (4) reported that the black - green iodide prepared by Kehrmann and Havas was not a quinhydrone salt but the simple methylphenazonium iodide because, on rubbing with silver nitrate or with silver sulfate in aqueous suspension, the so called quinhydrone salt immediately and smoothly



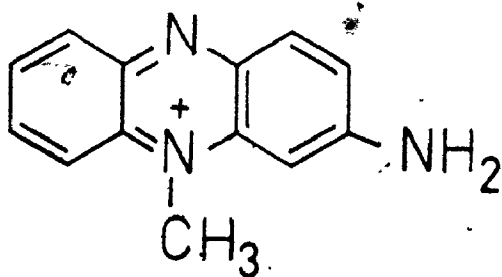
Figure 2.1

Structures of Aposafrazone (a) and
3-Aminomethylphenazonium (b).

a



b



gave the yellow - green nitrate or sulfate and no dihydro salt was formed.

In the next year, Kehrmann and Danecki (5) agreed that the normal red - brown iodide, $C_{13}H_{11}N_2I$, was formed by treating dilute aqueous solution of NMPMS with concentrated aqueous or solid potassium iodide. When the NMPMS solution was first treated with dilute sulfuric or hydrochloric acid and then drop by drop with concentrated potassium iodide, gray - green crystals separated. Black - green crystals were obtained after recrystallization from alcohol. They also suggested that the erroneous analytical results found (3) were probably due to the fact that the preparation consisted of a mixture of the red - brown iodide with a little of the green compound. They reported that the green compound had the formula $C_{13}H_{11}N_2I_3 \cdot C_{13}H_{13}N_2I \cdot 2H_2O$.

Hantzsch (6) reported that when NMPMS was digested with zinc dust and an excess of dilute hydrochloric acid containing a few drops of platinum tetrachloride, the solution first became green, owing to the formation of the meriquinoid salt¹, and then became

¹ The term meriquinoid is applied to compounds which are partially quinoidal such as Würster's salts, while the term holoquinoid is applied to compounds which are completely quinoidal (7). Würster's salts are formed by the one - electron oxidation of aromatic para - diamines, or the one - electron reduction of the corresponding holoquinoids. The redox potential of Würster's salt (a meriquinoid) is half way between that of the diamine and the holoquinoid (8). Although today it is easy to show by

colourless and precipitated as N - methyldihydrophenazine, $\text{NH}(\text{C}_6\text{H}_4)_2\text{NCH}_3$. In the air, especially in aqueous or alcoholic solution, its salts quickly oxidized to green meriquinoid salts.

Michaelis (9) suggested that in acid solution phenazine and related compounds, including N - alkylated derivatives, were oxidized and reduced in distinct one - electron steps, thereby passing through a semireduced intermediate. These semireduced forms are stable in acid and have a characteristic green colour which readily distinguishes them from the fully oxidized or fully reduced compounds. Fig. 2.2 shows the structures of the various oxidation states of NMP^+ and pyocyanine PYH^+ .

Michaelis (9) developed a potentiometric titration method to distinguish a process which involves a meriquinone intermediate from that involving a semiquinone intermediate. R is a compound which can be reversibly oxidized in two successive steps, each involving the loss of one electron. The completely oxidized form of the compound is T. If the intermediate form differs from R and from T only by an electron without change of molecular size, the

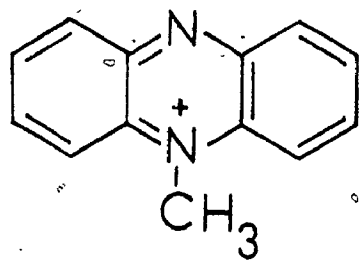
ESR that Würster's salts, or more generally meriquinoids, are paramagnetic salts, early chemists had difficulty in distinguishing between quinhydrones (meriquinones) and semiquinones (meriquinoids).

Figure 2.2

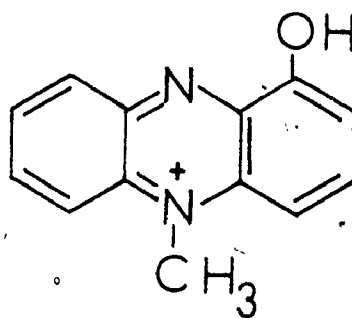
Structures of Various Oxidation States of

NMP^+ and PYH^+

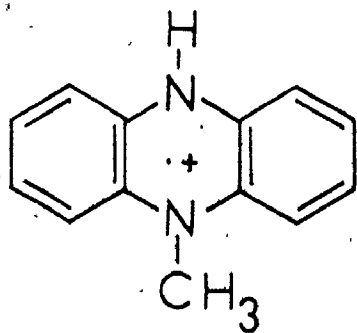
NMPH^+ and PYH_2^+ ; NMPH and PYH_2 are the
protonated semireduced NMP^+ and PYH^+ ;
reduced NMP^+ and PYH^+ respectively.



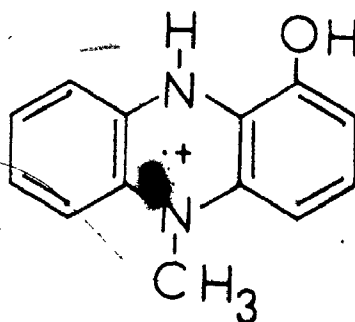
NMP⁺



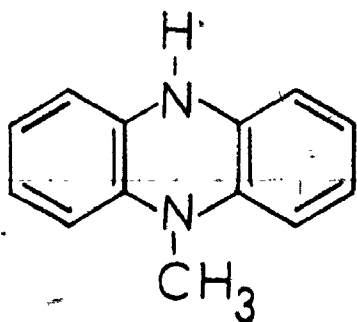
PYH⁺



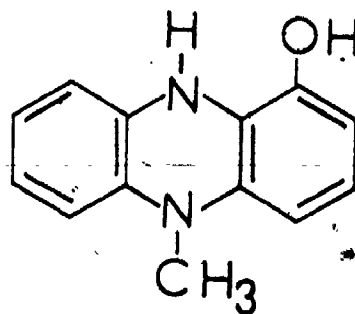
NMPH⁺



PYH₂⁺

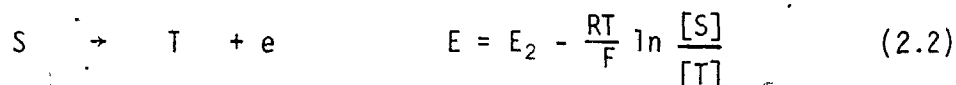
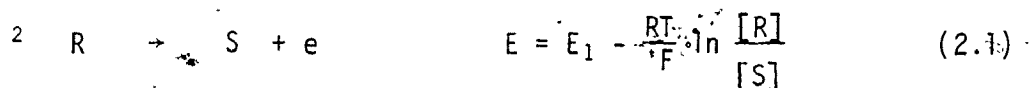


NMPH

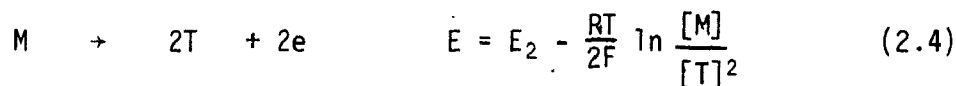
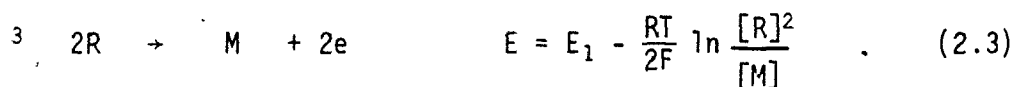


PYH₂

intermediate is called² the semiquinone S. If the intermediate is a compound of one molecule of R and one molecule³ of T, then it is called a meriquinone M. In the case of a meriquinone intermediate reaction, the potential depends on the volume of the solvent in which the initial amount of the substance was dissolved. It is shifted toward the positive side of the reduction potential by 0.03 volt when the volume is varied in the ratio 1 : 10 while for the semiquinone intermediate process the potential is independent of the volume of solvent used.



E is the potential, E_1 and E_2 are the apparent standard potentials of the R - S and S - T systems respectively. E_1 and E_2 are standard potentials only if activities are used in the calculations.



E is the potential, E_1 and E_2 are the apparent standard potentials of the R - M and M - T systems respectively.

2.2 NMPMS IN PHOTOPHOSPHORYLATION

NMPMS has been widely used in photosynthesis studies where it is found to have a stimulating effect on photophosphorylation, the mechanism by which green plants and photosynthetic bacteria use radiant energy to form ATP from ADP and inorganic phosphate.

Newton and Kamen (10) reported that photophosphorylation by Chromatium chromatophore particles is stimulated by catalytic amounts of NMPMS or ascorbate, but that solutions of NMPMS which were exposed to light prior to use as photophosphorylation activators have a decreased activating ability. The activation of the photophosphorylation system of Chromatium by NMPMS required the presence of the dye in the test mixture during assay. They also showed that NMPMS was effective in activating light induced phosphorylation under aerobic and anaerobic conditions; however, in the presence of excess reducing agent, the dye was inactive. The authors also suggested that the most active redox reagents for stimulating photophosphorylation were those which have a standard potential of approximately zero Volts at pH 7.

Hill and Walker (11) studied the effect of 2 - methyl-1,4 naphthoquinone, flavine nucleotide, pyocyanine, NMPMS, anthraquinone-2-sulphonate, etc. on the photophosphorylation reaction in spinach chloroplasts. They found that at low concentration (10^{-5} M) these compounds could increase phosphorylation under aerobic conditions. Of all the substances they tried, NMPMS appeared to be the most active. If the experiment was set up in the dark and oxygen removed as completely as possible, then no increase in

photosynthetic phosphorylation was obtained with NMPMS unless the NMPMS solution had been previously exposed to light in the presence of air. The authors concluded that the activity observed with NMPMS was due to its rapid conversion to pyocyanine in light. However, Geller and Lipmann (12) showed that photophosphorylation in purified cell free preparations of Rhodospirillum rubrum was found to be stimulated strongly by the addition of catalytic amounts of NMPMS, but not by pyocyanine. When the NMPMS - activated system was protected from light absorbed by the dye, a reducing agent such as succinate or lactate was needed. The dye - activated system was relatively unaffected by electron transport inhibitors such as antimycin A. Thus NMPMS seems to bypass the inhibitor - sensitive spots in the system. A maximal rate of photophosphorylation is attained at an intermediate stage of reduction of the components of the electron transport system; completely reduced or oxidized dye inhibits photophosphorylation. Thus it would appear that NMPH^+ is the active agent in stimulating phosphorylation.

Geller (13) studied the effect of reduced NMPMS on photophosphorylation induced in Rhodospirillum rubrum extracts by a .10 μs flash. The author suggested that at least three steps were involved. The first is the light reaction, occurring at the instant of a flash, in which an oxidant and a reductant are formed. This step is unaffected by the presence of the dye. The second step, a slower reaction, is the reduction of the photooxidant at the expense of reduced dye. The third step is the reduction of oxidized dye at the expense of reductant formed in the first step, completing

the cyclic process of electron transport. It was found that addition of reduced NMPMS lowered the yield of ATP formed in a 10 μ s flash. He suggested that, with sufficiently intense illumination for a prolonged period, intermediates accumulated, presumably as a result of the rapidity of photooxidation of the dye compared to the reaction sequence which followed, and thus the yield of ATP obtained with long (2 ms) flashes increased.

2.3 CHEMISTRY AND PHOTOCHEMISTRY OF NMP^+ SALTS

2.3.1. Oxidation States of NMP^+

Using ESR and optical techniques Zaugg (14) studied the spectroscopic and chemical properties of NMP^+ in its three oxidation states at various pH values. The absorption coefficient of recrystallized NMPMS at 387.5 nm in distilled water (pH 5.5) was reported to be $2.63 \times 10^4 \text{ M}^{-1} \text{ cm}^{-1}$.

Fully reduced NMP^+ (NMPH) was prepared (14) by adding dithionite to NMP^+ in 0.2 M hydrochloric acid solution. The colour of the solution first turned to green, then further addition of dithionite caused the disappearance of the green colour and the formation of a white precipitate of NMPH.

The semireduced NMP^+ was prepared (14) by dissolving NMPH in acidic ethanol and allowing air oxidation in the dark at room temperature. During this oxidation, acid is consumed. If the ethanol becomes neutral in pH, red compounds will be formed which probably are the oxidation products containing oxygen at the 2- or 3- position.

Zaugg further reported that the isosbestic points of the oxidation of NMPH to semireduced NMP^+ and semireduced NMP^+ to NMP^+ in aqueous pH ~2 solutions were 355 nm and 409 nm respectively. Also, when excess ascorbic acid was added to an NMP^+ solution at pH 6.9, the NMP^+ was completely reduced to NMPH. NMPH is generated when the solution is made acidic. The semireduced NMP^+ undergoes

disproportionation to regenerate NMP^+ and NMPH when the solution is made basic again. The ESR spectrum of the semireduced species in acidic solution had only nine broad lines; Zaugg did not report any hyperfine splitting constants.

2.3.2 Association of NMP^+ with Biological Components

White and Dearman (15) added NMPMS and a reductant, such as ethanol, to a B. megaterium or E. coli suspension. As a result of metabolic oxidation of the reductant, the contents of the cell became anaerobic quite rapidly, and thereafter NMPMS acted as the principal electron acceptor. An NMPMS free radical was observed by ESR.

Zaugg et al. (16) studied the reactions between fully reduced NMP^+ (NMPH) and chromatophores. They found out that chromatophores of photosynthetic bacteria, R. rubrum, R. spheroides and chromatium vinosum catalyzed a rapid, light - dependent oxidation of NMPH. The photooxidation is coupled to a reduction of ubiquinone (UQ_2 or UQ_6). A back reaction occurs in the dark, allowing for cyclic electron flow. The NMPH-UQ reaction was also catalyzed by extracted bacteriochlorophyll. They suggested that the chromatophores catalyze the photoreduction via bacteriochlorophyll which mediates a direct transfer of electrons from the donor molecule to UQ under the influence of light.

Ishizu et al. (17) investigated the complex of deoxyribonucleic acid (DNA) with NMP^+ and NMPH^+ by ultraviolet - visible and ESR spectrometry. The NMP^+ was less strongly bound than

NMPH⁺ and had fewer binding sites per DNA nucleotide. The binding was reversed by raising the ionic strength. Association of NMPH⁺ with DNA greatly stabilizes it against air oxidation and causes a shift in the Michaelis equilibrium (9) toward the semireduced species.

Nishikimi et al. (18) studied the reduction of nitro blue tetrazolium (NitroBT) by NADH (reduced nicotinamide adenine dinucleotide) under aerobic conditions and found that the rate was negligible. They found that the addition of NMPMS to this system provoked the reaction, and that the rate increased linearly with increasing concentration of NMPMS added. The authors suggested that NMPMS acted as an electron carrier in this system. This reaction was inhibited upon addition of superoxide dismutase. Superoxide dismutase has been shown to catalyze dismutation of the superoxide anion radical (O_2^-) to form molecular oxygen and hydrogen peroxide (19). Nishikimi et al. reported that the amount of inhibition depended on the concentration of superoxide dismutase added. The maximum inhibition obtained was 95 %, indicating that only 5 % of the reduction of NitroBT was due to its direct reaction with reduced NMPMS. They then suggested that the superoxide anion radicals were generated in the reoxidation of reduced NMPMS with oxygen.

When reductants such as NADH or ascorbic acid were added to NMPMS in the presence of hydrogen peroxide, Chayet et al. (20) observed chemiluminescence instrumentally. The emission obeyed consecutive first order kinetics, both reactions being pseudo first order. They suggested that semireduced NMPMS was involved in the light emission reaction.

Cost et al. (21, 22) reported that a reversible light induced electron transfer can be induced between a NMPMS radical and chromatophores from Rhodospirillum rubrum. The NMPMS radical appears to interfere with the transfer of electrons to or from the site normally producing the light induced chromatophore free radical. Using the technique of flash photolysis ESR, Cost and Bolton (23) showed that NMPMS interacts with a reaction centre preparation from the blue - green mutant R26 Rhodospseudomonas spheroides by a specific binding mechanism. A mechanism was proposed involving the interaction of NMPMS radicals on the donor side of P870. It was in this latter study that the direct photochemical production of free radicals from NMPMS was discovered.

2.3.3 Photochemical Products from NMP^+

McIlwain (24) was the first to study the photochemistry of NMPMS. He exposed an aqueous solution of 2 g NMPMS to sunlight in an open flask for one day. The solution was then neutralized and extracted with chloroform. The extract was dried with potassium carbonate and evaporated under reduced pressure. Pyocyanine was collected after petroleum ether was added to the solution.

3-keto-5-methylphenazine and 1-hydroxyphenazine were obtained from the extract with water and dilute aqueous alkali respectively.

Phenazine was collected from the petroleum solution on evaporation.

The yields (in mole percent) of pyocyanine and phenazine were 45 % and 47 % respectively. McIlwain reported that in alkaline solution N-methylphenazonium salts were found to be very unstable even under anaerobic conditions. In aqueous solution, a

precipitate of phenazine and N-methyldihydrophenazine was formed and formaldehyde detected. He suggested that N-methylphenazonium hydroxide is the immediate product of the reaction between N-methylphenazonium salts and alkali.

McIlwain also prepared various highly coloured crystalline compounds such as 5-methylphenazyl-3-sulfonic acid and 5-methylphenazyl-3-cyanide but he was unable to isolate 5-methylphenazyl, that is the unprotonated semireduced NMPMS radical, from solution owing to the ease of its decomposition to phenazine.

Rubaszewska and Grabowski (25) reported that the maxima of the fluorescence spectrum of NMP^+ and NMPH^+ are at 526 nm and 746 nm respectively. The fluorescence of NMPH^+ is on the borderline of the i.r. and can be detected only with an instrument of high sensitivity. They also reported that when NMPMS in aqueous solution was irradiated at 405 nm or 435 nm in the presence of air, it underwent photooxidation to pyocyanine and no free radical formation was observed. They also reported the protolytic pK_a value for the ground state of NMPMS was -3.5. The pK_a value of the first excited singlet state was then determined using the Forster cycle and found to be 3.3.

When NMP^+ was reduced electrolytically in 2-propanol, a solution of semireduced NMP^+ was generated. The product is either NMP^\cdot or NMPH^+ depending on the pH of the solution. NMP^\cdot is the neutral semireduced NMP^+ and NMPH^+ is the protonated semireduced NMP^+ . Dobkowski and Rubaszewska (26) obtained the ESR spectra of both NMP^\cdot and NMPH^+ in 2-propanol. Only the hyperfine splitting constants of

the neutral NMP• radical were reported as they were unable to analyze the ESR spectrum of NMPH⁺. They found that the pK_a values for acridinium and quinolium ions obtained in 2-propanol by means of the glass electrode were 3.2 pK_a units lower than the corresponding pK_a values obtained in aqueous solutions. Thus the equation, $pK_a(\text{water}) = pK_a(2\text{-propanol}) + 3.2$, was used to correlate the aqueous pH scale and the apparent pH values in 2-propanol measured by the glass electrode. They reported that the pK_a values for the ground state and the excited state of NMPH⁺ in water were 5.7 and 10.4 respectively. Recently, Rao and Hayon (27) reported that the pK_a for the ground state of NMPH⁺ in 1 M t-butyl alcohol is 6.8.

NMPH⁺ in 2-propanol (26) was found to be very stable in the dark and under vacuum. There was no change in either ESR or optical absorption spectra after many months of storage. No phenazine was formed during storage of either NMP• or NMPH⁺ in solution. They suggested that dealkylation occurs in the course of, or parallel to, the photochemical (or chemical) reduction of NMP⁺. The authors also observed the quenching of NMP• fluorescence in 2-propanol by water. They suggested it was caused by the formation of the semireduced radical cation NMPH⁺ in the excited state by fast proton transfer. The extremely weak fluorescence of the radical cation was not detected under the conditions of the experiment, so the fluorescence of NMP• is apparently quenched by water. The fluorescence lifetime of NMP• in 2-propanol is 5.1 ns in the absence of oxygen and 4.5 ns in an air saturated solution. The radiative lifetime was calculated to be 340 ns.

When an aqueous NMPMS solution at pH 7.4 was exposed to UV light by Marzotko et al. (28), paper chromatographic separation yielded five different fractions, one of which was usually unchanged NMP⁺. Optical absorption maxima of various species in methanol were given, but the products were not identified.

Kehrmann and Danecki (5) reported that when a dilute aqueous NMPMS solution was treated drop by drop with tin (II) chloride in hydrochloric acid a small permanent precipitate of the meriquinoid SnCl₂ compound was formed which was then redissolved by slow addition of the holoquinoid salt and shaking, and then salted out with solid sodium chloride. A green meriquinoid iodide was obtained with a structure C₁₃H₁₁N₂I · C₁₃H₁₃N₂I · H₂O. Kehrmann (29) then showed in 1915 that when meriquinoid iodide and iodine were added to just enough boiling alcohol and cooled, fine, dark needles of the compound C₂₆H₂₄N₄I₄ · EtOH quickly separated according to the following equation

$$C_{13}H_{11}N_2I \cdot C_{13}H_{13}N_2I + I_2 \rightarrow C_{26}H_{24}N_4I_4$$

The periodide was in all aspects identical to a compound previously described by Kehrmann and Danecki (5). This is perhaps the first published report of the preparation of a free radical salt even though the authors did not recognize that the meriquinoid iodide is actually a radical (a semiquinone).

In 1972, Takagi et al. (30) reported the preparation of a methylphenazonium radical cation salt. The method is based on the photoreduction of NMPMS in acid solution containing oxalate or tartrate. The radical salts are stable for several months even if kept in air at room temperature. The structure was checked by

elemental analysis. The presence of the ring NH in the perchlorate salt was verified by an absorption at $\sim 2600 \text{ cm}^{-1}$ in the i.r. spectrum which had been absent in the starting material NMPMS. The ESR spectrum of the perchlorate salt is the same as that of the chemically semireduced NMP^+ in absolute alcohol. Furthermore, the ESR spectra of the solid salts show a strongly narrowed singlet. These observations all indicate that it is indeed a radical salt.

2.3.4 ESR Studies

The ESR spectrum of the semireduced NMP^+ species was first reported by Zaugg (14) in aqueous solution. The spectrum at pH 3 consists of nine broad lines.

Dobkowski and Rubaszewska (26) recently reported the hyperfine splitting constants of N-methylphenazyl radical ($\text{NMP}\cdot$) (5-methylphenazyl) generated by cathodic reduction on a platinum cathode in 0.1 M LiCl isopropanol. Oxygen was removed from the solution by bubbling argon through it. $a^{\text{N}} = 6.47 \text{ G}$, $a_{\text{N-Me}}^{\text{N}} = 4.52 \text{ G}$, $a_{\text{N-Me}}^{\text{H}} = 3.91 \text{ G}$, $a_{1,9}^{\text{H}} = 3.2 \text{ G}$, $a_{4,6}^{\text{H}} = 2.48 \text{ G}$ and $a_{2,3,7,8}^{\text{H}} = 0.75 \text{ G}$. They could not resolve the hyperfine splitting constants of the semireduced NMP^+ radical cation (NMPH^+) and only reported estimated values.

2.4 PHOTOCHEMISTRY OF RELATED COMPOUNDS

2.4.1 Phenazine

The photoreduction and photoaddition reactions of acridine and phenazine are among the most studied of such reactions of heterocyclic compounds. Probably this is so because the primary non-radical products can be isolated from both compounds and the high efficiency of these reactions make these compounds attractive for detailed kinetic investigation.

The first reports of the photoreduction of phenazine were by Dufraisse et al. (31) who investigated photoreactions of phenazine in various alcohols. Toromanoff (32) showed that the products in methanol were molecular complexes of 5,10 dihydrophenazine and phenazine.

Phenazine had been thought to be a non - fluorescent molecule (33). However, fluorescence, phosphorescence and corresponding absorption spectra of phenazine and both its protonated forms were measured by Grabowski and Pakula (34) in 1969. The 0 - 0 energies of phenazine, the singly protonated species and the doubly protonated species in the lowest π, π^* triplet are 15475 cm^{-1} , 14175 cm^{-1} and about 9300 cm^{-1} respectively. Corresponding energies of the lowest singlet state are 23500 cm^{-1} , 21250 cm^{-1} and 17300 cm^{-1} . The absorption and fluorescence spectra of phenazine, singly protonated phenazine and doubly protonated phenazine were measured in ethanol, 6M sulfuric acid and concentrated sulfuric acid respectively. The phosphorescence measurements of phenazine and its

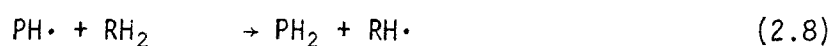
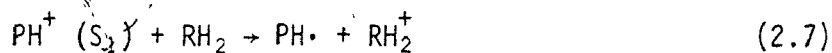
singly protonated form were carried out in ethanol and 6 M hydrochloric acid respectively. $S_0 \rightarrow T$ absorption or phosphorescence of the doubly protonated species was not detected. Fluorescence quantum yields for phenazine were found to be 8.6×10^{-4} in ethanol and 3.0×10^{-5} in hexane solution. Fluorescence emission in ethanol was ascribed to a π, π^* state, and that in hexane was ascribed to a n, π^* state because in hydrocarbon solvents the n, π^* is the lowest excited singlet state.

These investigators also calculated the first and the second pK_a values of phenazine in the lowest π, π^* triplet and π, π^* singlet using Förster's cycle (35). The pK_a 's of the π, π^* triplet and π, π^* singlet of phenazine were reported as 5.7, 4.0 (second pK_a) and 4.1, 6.0 respectively whereas the pK_a values of the ground state of phenazine are -4.30 and 1.21 (36).

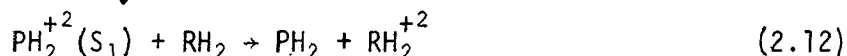
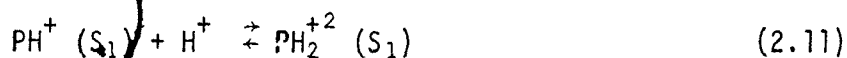
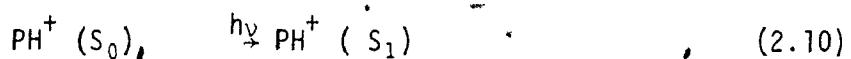
The photoreduction of phenazine in strongly acidic methanol (0.1 - 1 M HCl in methanol) and weakly acidic methanol (methanol containing 0.1 M acetic acid and 0.1 M sodium acetate) was investigated by Bailey et al. (37). They indicated that the reactive state under both these conditions is the lowest n, π^* singlet state. They suggested that in weakly acidic methanol the reactive state underwent protonation followed by electron transfer from methanol to produce semiquinone radical. The radical then reacted with the solvent to produce 5,10-dihydrophenazine. In strongly acidic methanol, the authors suggested, monoprotonated phenazine is directly excited and then undergoes a second protonation to give a dication. 5,10-dihydrophenazine is formed after electron transfer to the

dication. The protonated excited phenazine triplet was found not to be reactive in that study. The proposed mechanisms may be summarized as follows.

In weakly acidic methanol:



In strongly acidic methanol:



where P is the ground state phenazine

PH^+ is the monoprotonated phenazine cation

$PH\cdot$ is the phenazine semireduced radical

PH_2 is 5,10-dihydrophenazine

PH_2^{+2} is the doubly protonated phenazine

RH_2 is methanol

Using kinetic and flash photolysis methods, Davis *et al.* (38) showed that the lowest π, π^* triplet of phenazine is unreactive in the photoreduction of phenazine by isopropanol, triethylamine and tri-n-butylstannane. They also ruled out the π, π^* singlet as the reactive species on the basis of lifetime considerations. They interpreted their data in terms of an n, π^* singlet with a lifetime of about 1 ns as the reactant. The rate constants for the reduction

with triethylamine and the stannane were determined from Stern-Volmer plots and found to be close to that expected for a diffusion controlled rate. In isopropanol, the reaction is about 10^3 times slower.

Japar and Abrahamson (39) then gave additional evidence using the flash photolysis technique that the low - lying n, π^* singlet is the reactive species in the photoreduction of phenazine in strong hydrogen - bonding solvents. They suggested that the radiative lifetime of the lowest n, π^* singlet state should be on the order of 0.1 μ s (if not complicated by radiationless decay). As the formation of dihydrophenazine cation radical was observed during the first 150 μ s immediately after the photolytic flash, it is not the primary product of the photoreduction. They then proposed that monoprotonated semireduced phenazine radical ($PH\cdot$) is the primary product. Due to a strong overlapping of the optical spectra of the triplet, dihydrophenazine cation radical and $PH\cdot$ in trifluoroethanol, no direct evidence for the presence of $PH\cdot$ was observed. These authors further suggested $PH\cdot$ can form the cation radical by either disproportionation or abstraction of acidic hydrogen. The quantum yield of formation of the dihydrophenazine cation radical in trifluoroethanol was found to be 0.08 ± 0.015 .

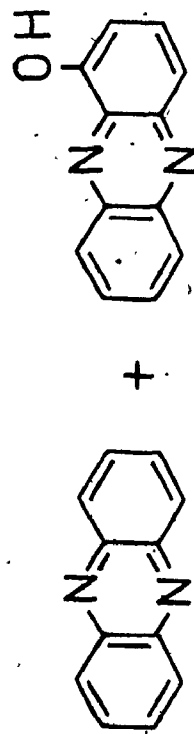
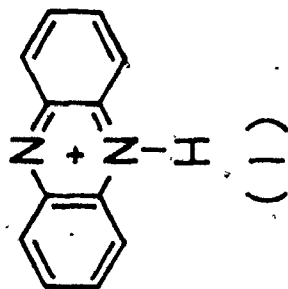
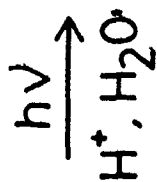
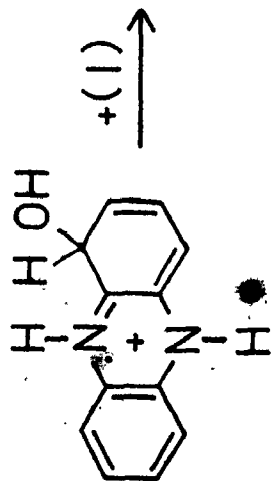
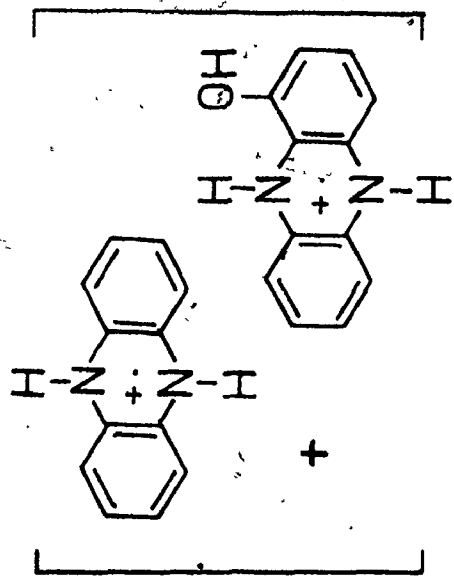
When a solution of phenazine in 2M aqueous phosphoric acid solution was irradiated under nitrogen atmosphere, Wake et al. (40) obtained a green solution containing a green precipitate. The solution was oxidized by air, neutralized with sodium carbonate and then extracted with ether. The products were solvent addition

products. They proposed a mechanism, which is shown in Fig. 2.3, involving a 1 : 1 mixture of phenazonium and 1-hydroxyphenazonium cation radicals. The structure of the solvent addition product was identified either by comparison with an authentic sample or by its physical properties and an elemental analysis.

Kawata et al. (41) investigated the photoreduction of phenazine in aqueous sulfuric acid solution. The pH dependence of the quantum yield in acidic solution for disappearance of phenazine was examined in aerated and deaerated aqueous sulfuric acid solutions. The maximum quantum yield was observed at pH 0.5 in both cases. They suggested that the increase in the quantum yield at pH between 2.5 and 0.5 with decreasing pH is due to the protolytic equilibrium in the ground state. At pH less than 0.5 and H_0 (Hammett acidity function) between 0 and -0.5, the yield decreases and falls to nil as pH or H_0 decreases. The authors indicated that the decrease in quantum yield is caused by the decrease in the amount of water in the medium or by the suppression of the photoreaction process by the doubly protonated phenazine in the excited singlet state. They identified the dihydrophenazine cation radical as the main product. The formation of hydrogen peroxide was confirmed by the colour change of the potassium hexacyanoferrate (III) - iron (III) ammonium sulfate solution from red to dark green. They did not report the relative yield of the radical cation and hydrogen peroxide. The dihydrophenazine cation radical is easily oxidized by air to give 1-hydroxyphenazine in the dark.

Figure 2.3

The Proposed Mechanism of Wake et al. (40) for
the Photoreduction of Phenazine in Acidic Solution.



i) oxidation
ii) OH⁻

2.4.2 Pyocyanine

Pyocyanine is a compound which is stable enough for potentiometric titration and hence was the first compound studied by Friedheim and Michaelis (42), even though the potentiometric method was first applied to the study of the benzidine compounds by Clark et al. (43). In the latter case the potential obtained during the titration showed rapid drifts, so that no real insight into the mechanism of the process could be obtained.

Pyocyanine can be reversibly oxidized and reduced (42). For pH values greater than 6, the slope of the potentiometric titration curves indicates there is only one two - electron transfer step, while for pH values less than 6, there are two one - electron transfer steps. The apparent standard potentials of pyocyanine at various pH values were also given (42). The pK_a values of pyocyanine, semireduced pyocyanine and fully reduced pyocyanine were determined by Voriskova (44) and found to be 4.88, 5.63 and 9.36 respectively.

CHAPTER 3

EXPERIMENTAL TECHNIQUES AND MATERIALS

3.1 BASIC PRINCIPLES OF ELECTRON SPIN RESONANCE (ESR)

Electron spin resonance spectroscopy is a technique designed to detect molecules with one or more unpaired electrons, such as free radicals, triplet states of molecules, most transition metal ions etc., without altering or destroying the molecules.

In the presence of an external magnetic field, the energy levels of various spin states of unpaired electrons are no longer degenerate. For a molecule with one unpaired electron, the energy gap between two states is

$$\Delta E = g\beta H \quad (3.1a)$$

where g is called the g factor and is a dimensionless number whose value for a free electron is 2.0023, β is the Bohr magneton, and H is the intensity of the applied field.

A transition from one state to the other occurs when the system is exposed to an electromagnetic radiation with a frequency ν , where

$$h\nu = g\beta H \quad (3.1b)$$

This is the basic resonance condition of ESR.

Because of the high frequency (100 kHz) modulation detection system used in most ESR spectrometers, typical ESR signals appear as the first derivative of the absorption lines. However, with the use of an additional modulation frequency (1 kHz was used in this work) and a second phase sensitive detector the second derivative of the absorption line may be obtained. The second derivative presentation is very sensitive to small changes in slope of the absorption lines, hence the resolution is improved. For further information beyond this brief outline, please refer to Ref. (45 - 47).

3.2 FLASH PHOTOLYSIS TECHNIQUES

Flash photolysis is a method whereby a nonequilibrium state can be created in a reaction system in a short interval of time. It is applicable to gases, liquids and solids, and to the whole available temperature range. The concentration of intermediates can be measured directly as a function of time and their physical and chemical properties can be determined. In the flash photolysis technique, the reactants are irradiated with an intense flash of visible or ultraviolet light. The intensity of the flash must be sufficient to produce a measurable change in chemical composition, but the duration of the flash must be short compared with that of ensuing reactions to be studied.

3.2.1 Optical Flash Photolysis

Flash photolysis coupled with optical detection of intermediates has proven to be a useful device in the study of transient intermediates in photochemical reactions (48). There are two main techniques for detection and estimation of intermediates.

- a. Flash spectroscopy: A second spectroflash, of short duration, is fired at any chosen time after the photolysis flash. A spectrograph is used to record the absorption spectra of reaction intermediates photographically.
- b. Kinetic spectrophotometry: The light from a continuous light source is passed through the reaction cell. A photodetector (usually photomultiplier and oscilloscope) is used to record the change in light intensity at a specified wavelength which in turn is set by a monochromator. By

changing the wavelength of monochromator, the kinetic behaviour of various intermediates, reactants or products can be determined.

The high sensitivity of the photomultiplier and in some cases high absorption coefficients of the intermediates make the detection of small concentrations of some intermediates possible. The investigation of some primary processes (49) is made possible using newly developed picosecond laser pulses. However, overlapping of absorption bands from several species, the small absorption coefficients of some of the species concerned, and the lack of detail in optical absorption bands are some limitations of the optical detection technique which make it difficult to identify or even detect some intermediates.

3.2.2 Flash Photolysis Electron Spin Resonance (FPESR) Technique

The flash photolysis technique was first coupled with ESR by Bennett et al. in 1967 (50). Since then FPESR has become popular in the study of photochemical and photobiological processes (23,51-53). Usually, a computer of average transients (CAT) is needed to improve the signal - to - noise ratio. The improvement in the signal - to - noise ratio of the data increases as the square root of the number of measurements. A delay unit is used to trigger the CAT at a set amount of time prior to the triggering of each flash. In this way a base line can be recorded to be used later in the determination of signal amplitude. FPESR is used to monitor the kinetics of growth or decay of paramagnetic intermediate species in the system. The ESR spectra of the intermediates can be obtained when

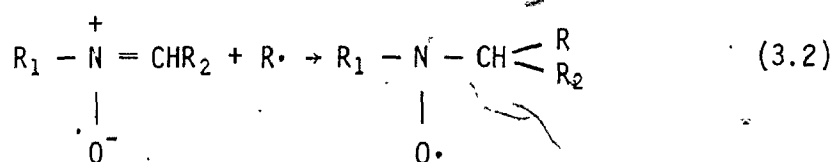
the system is coupled with a rapid scan generator or the profile of the signal can be constructed using the signal amplitude of the kinetic scan at various magnetic fields. From the g factor and hyperfine pattern of the spectrum one can, in favourable cases, identify the paramagnetic species.

ESR is a sensitive technique: radical concentrations as low as 10^{-9} M have been detected, but transient radicals with ESR spectra having broad lines may be difficult to observe, even with extensive signal averaging. This is because the signal amplitude is approximately proportional to the inverse square of the peak - to - peak linewidth. If the ESR spectra of two or more free radicals do overlap, the resulting spectra can often be resolved by varying instrumental conditions such as modulation amplitude and the incident microwave power. FPESR allows detection of transients with lifetimes as short as a few microseconds. Unfortunately, the uncertainty principle prevents ESR detection of transients with lifetimes less than ~ 1 μ s.

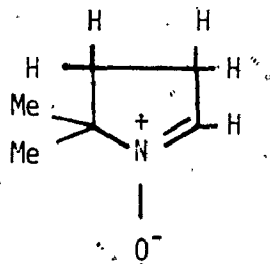
For a detailed comparison of optical flash photolysis and flash photolysis ESR, please refer to Ref. 54.

3.3 SPIN TRAPPING TECHNIQUE

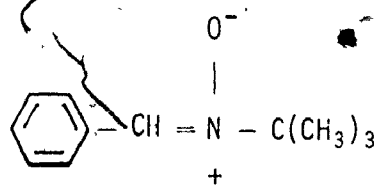
An indirect technique called spin trapping for the detection and identification of low concentrations of free radicals in reacting systems has been reviewed by Janzen (55). It involves trapping of a reactive free radical by an addition reaction to an unsaturated function to produce a more stable radical called a spin adduct, detectable by ESR, whose hyperfine coupling parameters may permit identification of the initial radical trapped. The basic reaction can be described as



The two nitron spin traps which have found wide use are 5,5 dimethyl-1-pyrroline-1-oxide (DMPO) and phenyl-t-butyl nitron (PBN)



DMPO



PBN

DMPO has the advantage that the β hydrogen hyperfine splitting of the spin adduct is quite sensitive to the nature of $R \cdot$ (56) whereas PBN has the advantage of forming very stable spin adducts.

3.4 DETERMINATION OF THE CONCENTRATION AND g FACTOR OF RADICALS

3.4.1 Determination of the Absolute Concentration of Radicals

The absolute concentration of an unknown radical can be obtained by comparing the area enclosed by an ESR absorption curve to a concentration standard under the following conditions (57):

- the same incident microwave power;
- no microwave power saturation of either standard or unknown radicals;
- use of the same solvent and sample tube at the same temperature.

The concentration of the paramagnetic species [X] is given by (57)

$$[X] = \frac{[\text{Std}] \text{Area}_x R_x (\text{Scan}_x)^2 G_{\text{std}} M_{\text{std}} (g_{\text{std}})^2 (S(S+1))_{\text{std}}}{\text{Area}_{\text{std}} R_{\text{std}} (\text{Scan}_{\text{std}})^2 G_x M_x (g_x)^2 (S(S+1))_x} \quad (3.3)$$

The subscripts x and std refer to the unknown and the standard respectively. Area is the measured area under the absorption curve (arbitrary units as long as they are the same for the unknown and standard). Scan is the horizontal scale (in gauss per unit length) on the chart paper. G is the relative gain of the signal amplifier. M is the modulation amplitude. $R = \sum D_j / D_k$ where D_k is the degeneracy of the line for which the area is being determined and $\sum D_j$ is the sum of the degeneracies of all the lines in the spectrum; R is only required when hyperfine splitting is present. g is the g factor of the paramagnetic species. S is the spin quantum number.

We can rewrite the resonance condition (Eq. 3.1b) as

$$g = h\nu / \beta H \quad (3.4)$$

The absolute measurement of a g factor can be obtained if the microwave frequency and the resonant magnetic field are known.

The frequency of the microwaves can be measured by a frequency meter and absolute magnetic field measurements can be made using a gauss meter (by measuring the frequency at which a water sample exhibits proton magnetic resonance). Due to a number of systematic errors (58) absolute measurements are rarely attempted.

3.4.2 Determination of g Factors

The g factor of an unknown radical can be found using a standard with a well - known g factor and the following equation

$$g_{\text{std}} H_{\text{std}} = g_x H_x \quad (3.5)$$

where g_{std} , g_x are the g factors of the standard and the unknown respectively and H_{std} , H_x are the resonant magnetic fields for the standard and unknown respectively. The microwave frequency must be kept constant during the measurement. The above equation can be rewritten as (59)

$$g_x = g_{\text{std}} H_{\text{std}} / H_x \quad (3.6)$$

$$= g_{\text{std}} (1 + \Delta H / (H_{\text{std}} - \Delta H)) \quad (3.7)$$

$$\Delta H = H_{\text{std}} - H_x \quad (3.8)$$

If the g_{std} and g_x are very close, then ΔH will be small compared with H_{std} , and

$$g_x \approx g_{\text{std}} (1 + \Delta H / H_{\text{std}}) \quad (3.9)$$

and accurate results will depend only on an accurate measurement of ΔH . The above equation should not be used when the g factor of the unknown is greatly different from the standard. Then either a

standard with a g factor close to that of the unknown should be used or the exact formula, Eq. 3.7, should be used.

3.4.3 Determination of Area under the Absorption Curves

Because of the high frequency (100 kHz) modulation detection system used in most ESR spectrometers, typical ESR signals appear as the first derivative of the absorption curve. To obtain the area under the absorption curve a double integration of the ESR spectrum is required. The method of Loveland et al. (60) was employed in this work because the base line drift is automatically corrected for and the calculation is suited to both symmetric and asymmetric curves.

The equation used was

$$\text{Area} = \frac{h^2}{3} \sum_{i=1}^n (2n - 3i + 1) Y_i \quad (3.10)$$

where Y_i is the value of the derivative in the i -th interval, h is the interval width, n is the total number of intervals and Area is the area under the ESR absorption curve. The print-out of the computer program used is shown in Appendix 1.

3.4.4 Weighted Linear Least Squares Method

The weighted linear least squares method (61) was used in this work to obtain rate constants. This method was used to account properly for the instrumental uncertainties.

For a function $x = f(u)$, the square of the standard deviation σ_x , is $\sigma_u^2(dx/du)^2$. The weighting factor is equal to $1/(dx/du)^2$ and σ_u^2 is usually assumed to be constant.

For the function $x = \log c$ where c is a concentration, as in the case of determining the first order rate constant by optical flash photolysis,

$$\left(\frac{dx}{dc}\right)^2 = \left(\frac{d(\log c)}{dc}\right)^2 = 1/c^2 \quad (3.11)$$

the weighting factor is c^2 . Similarly, for a second order reaction with function $x = 1/c$,

$$\left(\frac{d(1/c)}{dc}\right)^2 = 1/c^4 \quad (3.12)$$

and c^4 is the weighting factor.

3.5 POTENTIOMETRIC TITRATION.

In potentiometric titrations of NMP^+ , a saturated calomel electrode was used as a reference electrode and a platinum electrode as measuring electrode. A model 8691-2 millivolt potentiometer from Leeds and Northrup was employed.

The following equation was used to determine the apparent standard potential E° of a system,

$$E = E^\circ - \frac{0.059}{n} \log \frac{x}{u - x} \quad (3.13)$$

where u is the amount of reductant used up at the end point of titration, x is the amount of reductant used at a given time during the titration and n is the number of electrons involved in the reduction. The slope of the linear plot of potential E versus $\log (x/(u - x))$ is equal to $-0.059/n$ (that is, -0.059 for $n = 1$, -0.030 for $n = 2$). From the intercept, the apparent standard potential E° can then be calculated. Also from the magnitude of the slope one can determine whether the reduction is a one - electron reduction step ($n = 1$) or a two - electron step ($n = 2$).

3.6 DETERMINATION OF FLUORESCENCE QUANTUM YIELD

A Perkin - Elmer fluorescence spectrophotometer model MDF - 4 was used to record the fluorescence spectra and to determine the fluorescence quantum yield.

The fluorescence quantum yield of NMP⁺ was determined by comparing fluorescence data of NMP⁺ with data obtained for a standard. Quinine sulfate in 0.5 M sulfuric acid was used as the standard. Quinine sulfate was obtained from the Matheson Company and recrystallized three times from hot water. The fluorescence yield of quinine sulfate in 0.5 M sulfuric acid is 0.55 ± 0.03 (62) at 457 nm.

The fluorescence quantum yield of an unknown can be found using the following equation (63)

$$\phi_x = \frac{\phi_{std} \text{Area}_x A_{std} I_{std} n_x^2}{\text{Area}_{std} A_x I_x n_{std}^2} \quad (3.14)$$

the subscripts x and std refer to the unknown and the standard respectively. ϕ is the quantum yield, A and I is the calculated absorbance and relative intensity of the exciting light at the excitation wavelength λ , Area is the area under the emission curve and n is the index of refraction of the solvent. The above equation is only good for dilute solutions (with absorbance less than 0.05). Use of dilute solutions minimizes reabsorption, re-emission and use of the same instrument and cuvette minimizes error from instrumental geometries.

3.7 ESR SPECTROMETER AND ACCESSORIES

A Varian E 12 spectrometer equipped with V3900 12 inch magnet and Hall probe field control system was used in conjunction with a Fabritek 1072 computer of average transients (Nicolet Corp.). The resulting data were read onto an X - Y recorder (Model 7035 B Hewlett - Packard Company) or to a Tally Tape perforator (Tally Corp.) for storage on paper tape which could be used for computer analysis. With the Varian E 12 instrument, it is possible to remove the sample tube containing the standard solution, replace it, retune the spectrometer and obtain the same recorder trace to within 1 per cent of the signal amplitude on the chart paper.

Normally a model E231 TE₁₀₂ multi - purpose cavity with slotted walls allowing about 50 % irradiation to be transmitted was used. For quantum yield measurements, a model E234 TE₁₀₃ optical transmission cavity which permits full irradiation of the active portion of the sample was employed. It contains two optical windows facing each other so that the light intensity after passing through the sample cell can be measured.

Light intensities were determined with a radiometer (Model 65 A radiometer and 6551 probe, Yellow Springs Instrument Company) which in turn had been calibrated against an Eppley 12 - junction bismuth - silver thermopile by the manufacturer. The laser (for details please refer to Section 3.9) was positioned so that the laser beam passed through the centre of the windows of the TE₁₀₃ cavity. The location of the sensor was adjusted so that maximum

light intensity reading was obtained. The radiometer was coupled to a Varian G2000 strip chart recorder to record the light intensity on paper for later calculation. The conversion factor of the reading from the chart paper to the reading of the radiometer was determined before the experiments. Fig. 3.1 shows a block diagram for the quantum yield measurement. A Uniblitz (Model 300 - SD Vincent Associates) shutter was also used to cut off the laser beam to avoid heating up the sensor of the radiometer. It usually takes about half an hour to warm up the laser. The laser was left on all the time during the experiment and 'light' mode was used so that the light intensity would remain constant throughout the experiment. The light intensity was measured both before and after the experiment to ensure its constancy. Usually an average value was used in the calculation.

For some experiments, a flash photolysis apparatus manufactured by Photochemical Research Associates (Model 610 A) was used in conjunction with the ESR. The flash lamp used was a Novatron 185 (Xenon Corp.). A trigger unit, the pulser, was used to start the CAT scan before the lamp discharge pulse was applied to provide an initial base line for kinetic studies. The flash photolysis ESR (FPESR) technique has been described elsewhere (54). Fig. 3.2 shows a block diagram of the apparatus.

Figure 3.1

The Block Diagram for the Quantum Yield Measurement.

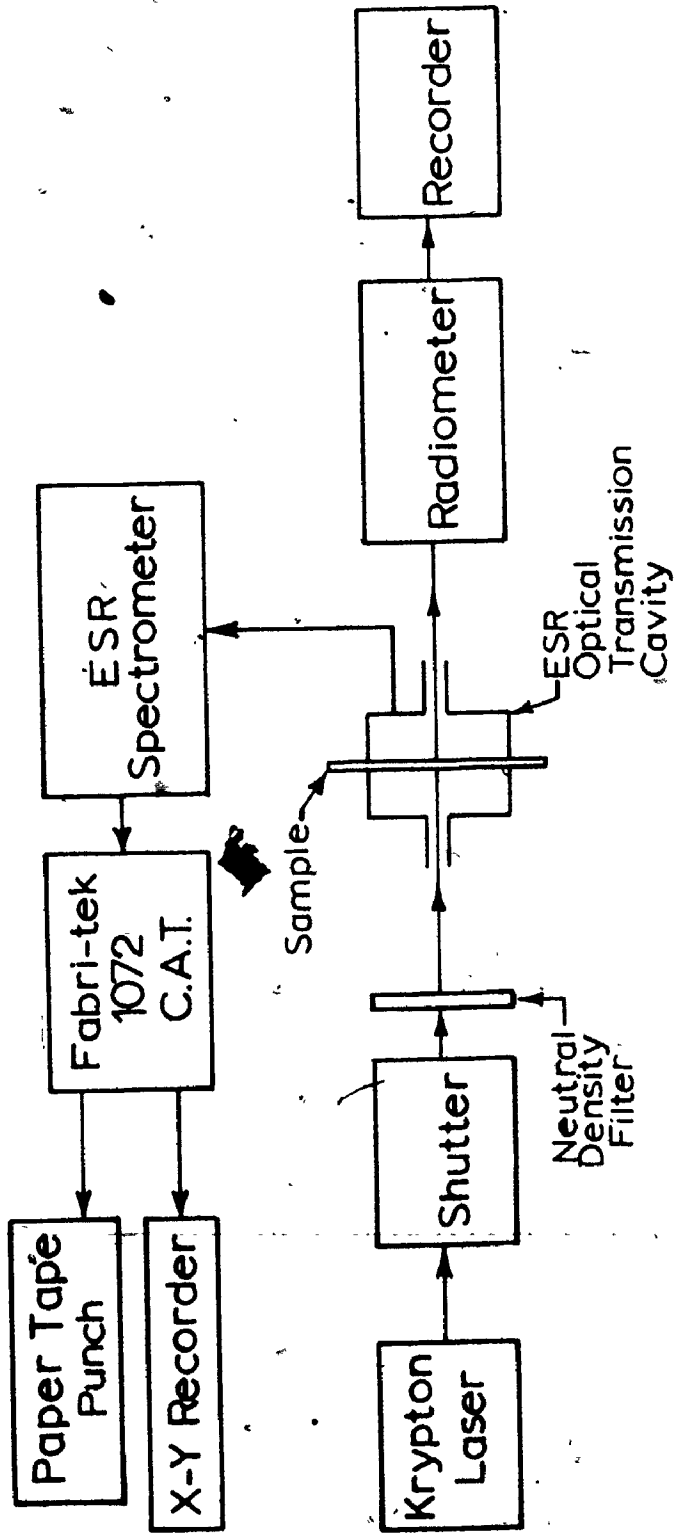
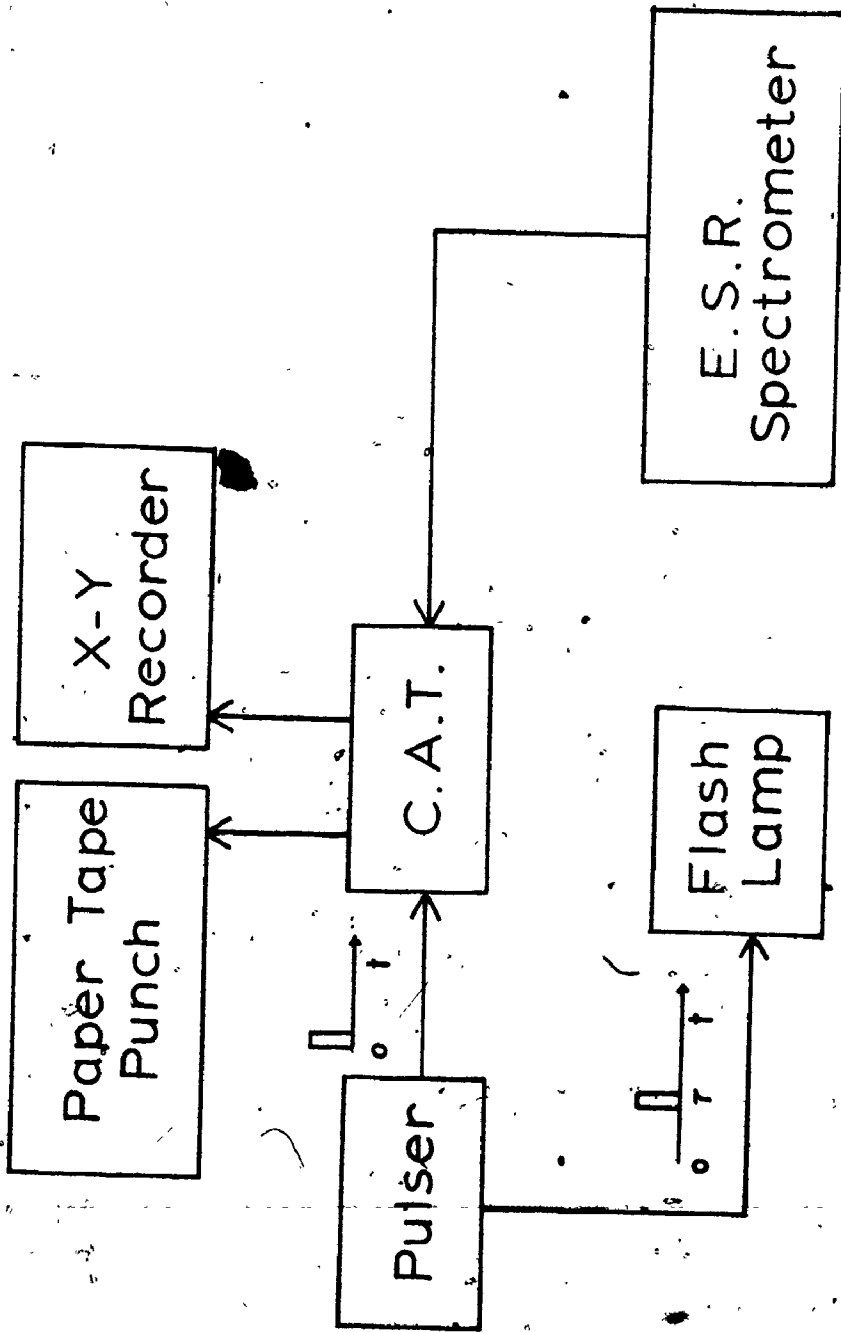


Figure 3.2

The Block Diagram for the Flash Photolysis Electron
Spin Resonance (FPESR) Experiment.



3.8 OPTICAL FLASH PHOTOLYSIS

A block diagram of the set-up is shown in Fig. 3.3. A FX-1C-6 flash lamp from Electro-optics division E, G&G Inc. was used. The photolysis flash lamp and the reaction cell were housed in an aluminium box. A 100 W quartz-halogen projector lamp was used as the continuous light source. A Bausch and Lomb high intensity grating monochromator 33-87-07, an IP-28 photomultiplier and a Tektronix 7613 storage oscilloscope were employed to detect and record the change of the intensity of the continuous light source at the wavelength set by the monochromator. The apparatus was placed on an I beam to minimize vibration. An oscilloscope camera from Tektronix Inc. (Model C 12) was fitted to the screen of the oscilloscope to record the results photographically. A trigger generator in the form of a spark gap was used to trigger the firing of the photolysis flash lamp and the start of recording of the oscilloscope. In most of the experiments, a Corning CS 0-52 filter was placed between the continuous light source and the reaction cell to cut off any light with wavelengths shorter than 340 nm.

For each measurement (Fig. 3.4), the oscilloscope was first triggered with the shutter closed T_0 , then with the shutter open T_{100} and finally 9 kV was applied to the photolysis flash lamp. The shutter was reopened and then the photolysis lamp fired. The oscilloscope was triggered simultaneously to record the change in the transmittance of the solution T_t . About two seconds after the firing of the photolysis lamp the oscilloscope was triggered again

Figure 3.3

The Apparatus for the Optical Flash Photolysis.

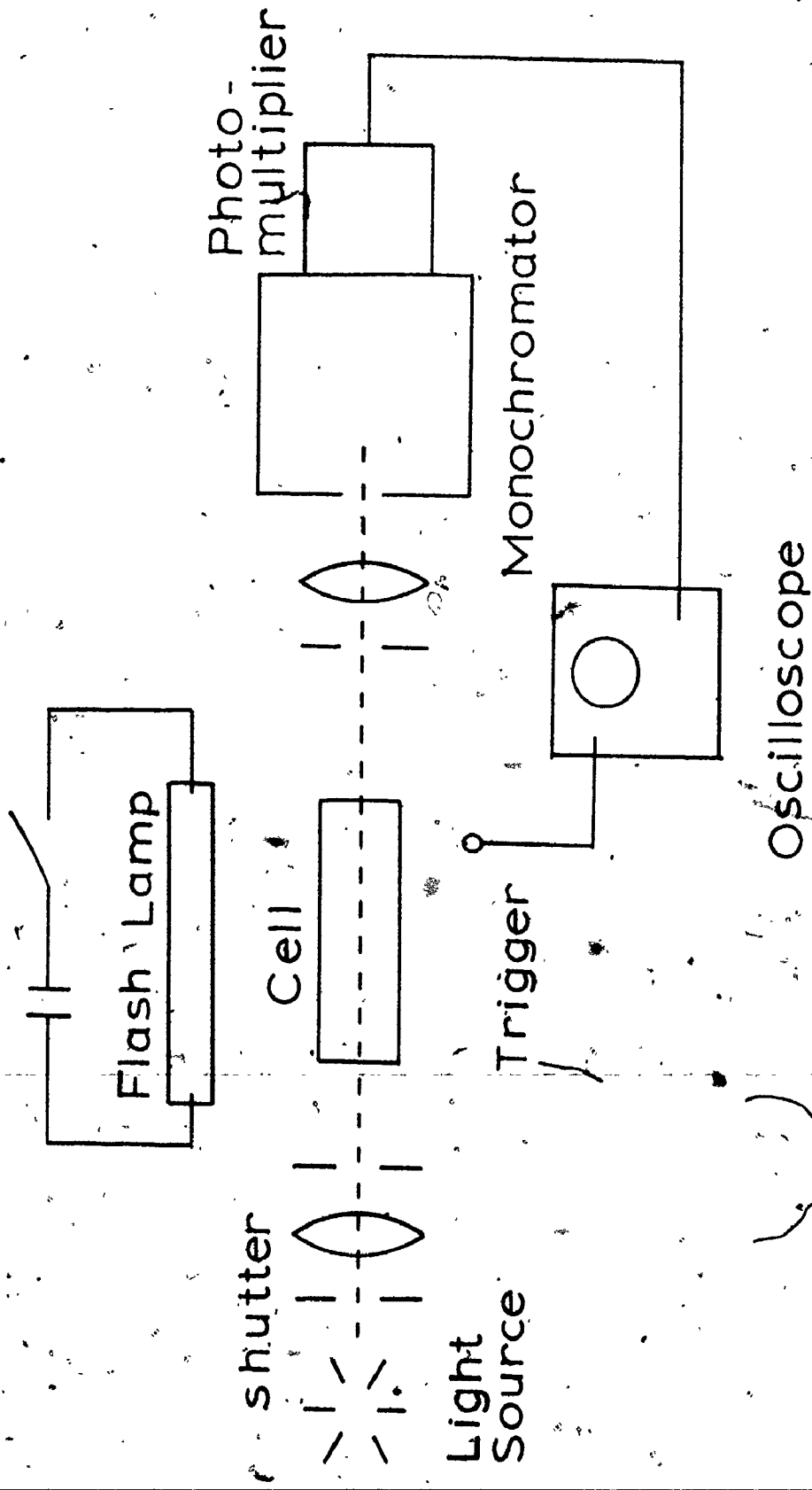
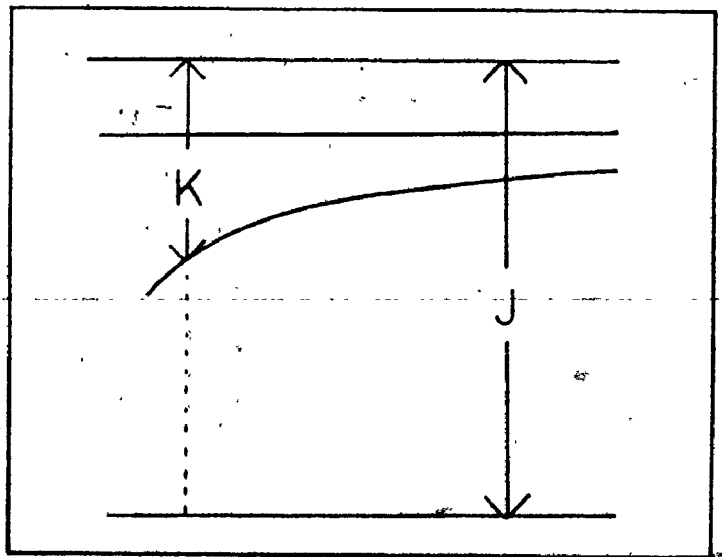
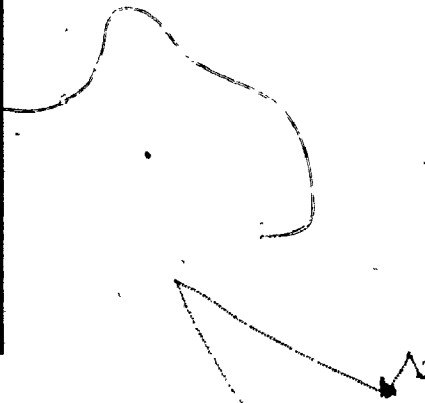
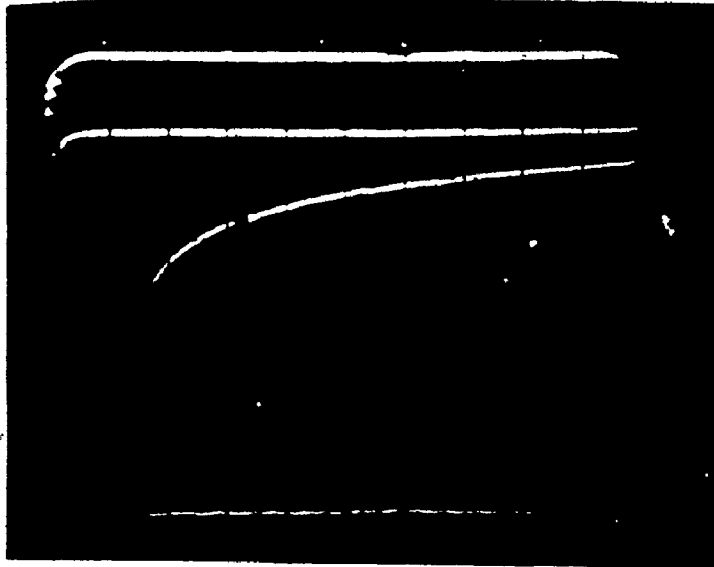


Figure 3.4

A Typical Trace Obtained in the Optical Flash
Photolysis Experiment.



T_0
 T_∞
 T_t

T_{100}

t_1

to record T_{∞} which can be used to calculate the concentration of the transient at infinite time. If the transient absorbs only a small fraction of the light, the signal on the oscilloscope must be amplified for greater accuracy; the light - off trace T_0 will not appear on the screen. In this case, the (light on - light off) amplitude must be determined by reducing the oscilloscope amplification because this factor is needed in the calculation.

Since the oscilloscope only records the change in light intensity detected by the photomultiplier, the difference between the light on and light off traces J corresponds to the light intensity at 100 % transmission (Fig. 3.4). Similarly the difference between the light off and the transient trace T_t at any point K corresponds to the light transmitted at that time. The time scale was set by the horizontal scale on the oscilloscope. Transmittance T at time t_1 is equal to the ratio between K and J . Using the following relation, $A = \log (1/T) = \log (J/K)$, the absorbance at time t_1 can then be calculated.

3.9 LIGHT SOURCES.

Steady state illumination was supplied by a custom - designed light source housing a 600 W General Electric FFJ lamp. Light was collected by an ellipsoidal reflector and then passed through a water filter and a Corning CS 3- 75 yellow green filter having 80 % transmission at 460 nm and none below 370 nm. The 476.2 nm line of a krypton CW laser (Spectra - Physics Model 164 - 01) was also used especially in the quantum yield measurements. The CW laser was shuttered with a Vincent Associates Model 300 - B "Uniblitiz" electronic programmable shutter drive and controlled with a 6 mm Model 26 shutter. The 472.7 nm line of an Argon CW laser (Spectra - Physics Model 164 - 03) was also used. A Koehler Illuminator Model LKR was used for steady state illumination in experiments not involving ESR measurements and a water filter was placed between the lamp and the sample cell. The UV irradiation source was a Hanovia Model 977B 1 kW Hg - Xe lamp in a Schoeffel Model LH 151N lamp housing.

3.10 CHEMICALS AND SAMPLE PREPARATIONS

NMPMS was obtained from Sigma Chemical Company and used without further purification. (During the study of the interaction of NMPMS with reaction centre preparations, Cost and Bolton (23) found that recrystallization of NMPMS was not necessary). PBN (Phenyl-t-butyl nitron) was a gift from Dr. E. G. Janzen and DMP₀ (5,5-dimethyl-1-pyrroline-1-oxide) was a gift from Dr. K. S. Chen.

Chemically semireduced NMPMS was prepared by adding 1 mg of sodium borohydride to 0.75 mg NMPMS in 10 ml 0.1 M acetic acid solution (pH ~3).

In the quantum yield experiment, the concentrations of NMPMS solutions were kept below 3.6×10^{-3} M, so that the absorbance at 476.2 nm was below 0.1 within the flat cell (thickness 0.0332 cm); that is the light intensity gradient across the cell is kept small. The solvent was 5×10^{-4} M phosphate pH 7 buffer solution unless otherwise stated. The samples were thoroughly degassed on a vacuum line using 5 - 7 freeze - pump - thaw cycles until the vacuum gauge measured no pressure change above 10^{-4} torr during the pumping portion of the degassing cycle. For the rest of the experiments NMPMS solutions were purged with nitrogen gas for at least ten minutes before irradiation.

For the optical flash photolysis experiment, 1×10^{-5} M NMPMS was used so that about half of the photolysis light was absorbed ($A \sim 0.3$). Concentrated sodium hydroxide or hydrochloric

acid was added to 5×10^{-3} M potassium phthalate solution to buffer the solution to various pH values. There was no significant change in the rate constant measured at 443 nm when the buffer concentration was changed from 5×10^{-3} M to 5×10^{-5} M. 5×10^{-3} M buffer was used in this work. NMPMS solution was purged with nitrogen for fifteen minutes at the side arm of the apparatus and at the same time nitrogen gas was passed through the 19.5 cm long quartz reaction cell. NMPMS solution was then poured into the reaction vessel just before irradiation. A fresh sample was used for each measurement.

Pyocyanine was prepared as reported (24), but a 5×10^{-2} M phosphate pH 7 buffer was used as the solvent instead of pure water. NMPMS solution was exposed to light for about 20 hours. The solution had then become dark blue. It was filtered through glass wool. First chloroform was used to extract mainly pyocyanine from the neutral aqueous layer. Then 1% sulfuric acid was added to the chloroform extracted layer to extract pyocyanine (64). All other chloroform soluble substances remained in the chloroform layer. The red aqueous layer was then neutralized by sodium carbonate and the colour of the solution changed from red to blue. Pyocyanine was then again extracted by chloroform which was evaporated under reduced pressure. Hot hexane was added to the concentrated solution. Deep blue crystals were then collected. Semireduced pyocyanine can be prepared by adding ascorbic acid to a nitrogen purged pyocyanine solution.

3.11 MISCELLANEOUS INSTRUMENTS

All optical absorption measurements were carried out on a Cary 118 spectrometer.

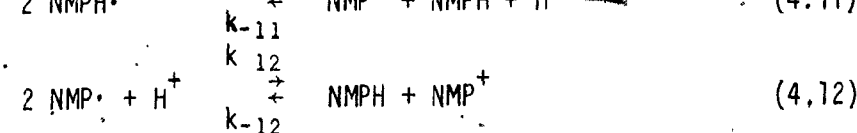
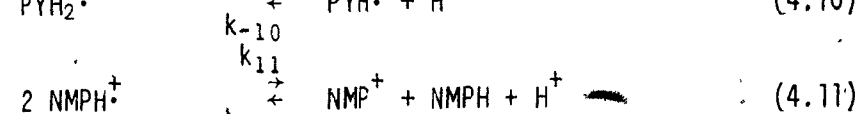
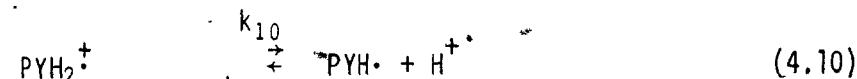
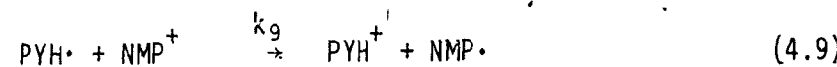
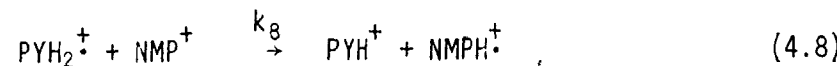
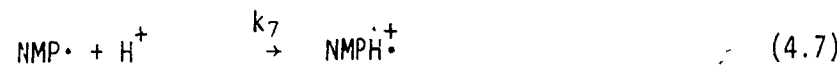
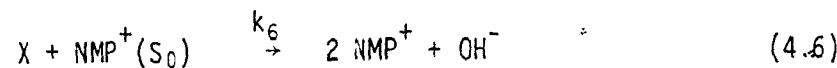
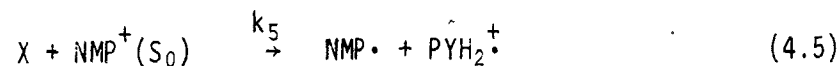
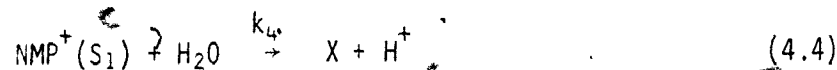
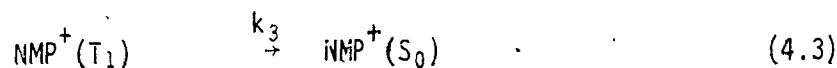
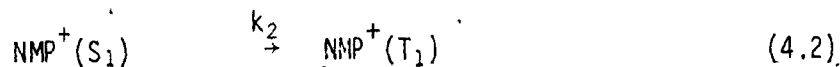
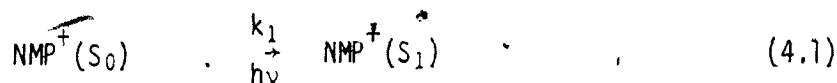
pH values of the solutions were measured using a Corning Model 7 pH meter.

CHAPTER 4

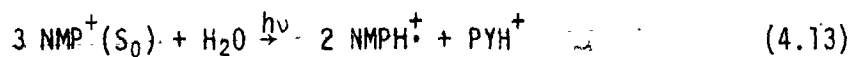
RESULTS AND DISCUSSION

4.1 THE PROPOSED MECHANISM

This work involves the investigation of the mechanism of the photochemistry of NMP^+ in aqueous solution. We propose the following mechanism for this reaction. The results which will be presented in this chapter are discussed in the context of the proposed mechanism as support for the individual steps in the proposed mechanism. In the discussion that follows, the reactions below will be referred to often. Thus the reader will find it convenient to open out the following page for easy reference.



Overall reaction



X is an intermediate of unknown structure. It will be shown that the reactive state is singlet, disproportionation is not important and Reaction 4.6 is a possible side reaction. So Reactions 4.2, 4.3, 4.6, 4.11 and 4.12 are omitted in the overall reaction.

4.2 - PHOTOCHEMICAL GENERATION OF A RADICAL FROM NMPMS

When a degassed yellow solution of NMPMS is irradiated with blue light, the solution turns green and a paramagnetic species is formed, as detected by ESR, immediately after the light is turned on. There is no significant change in the ESR signal ten minutes after the light is turned off. However, in a system in which not all the oxygen has been removed, the ESR signal completely decays away in ten minutes.

4.2.1 Identification of the Radical Formed

Fig. 4.1 shows the ESR spectra of the light - induced species in water and in D_2O . The total magnetic field span of the spectrum is shorter in D_2O . In water, the spectrum consists of nine groups, which can be separated into more than 120 hyperfine components under low modulation amplitude (0.1 G). When the spectrum is moderately overmodulated (4 G), the spectrum shows nine broad lines which is similar to the spectrum reported by Zaugg (14). There is a marked change in the hyperfine splitting pattern when the solvent is changed from water to D_2O . A single deuterium ($I = 1$) gives a triplet instead of a doublet hyperfine pattern for a hydrogen ($I = 1/2$). If all other factors are the same, the deuterium hyperfine splitting is only about one - seventh that of the hydrogen. The reduction in hyperfine splitting constant of the light - induced species in D_2O can readily be interpreted as due to one (or more) exchangeable proton(s) being replaced by a deuteron(s).

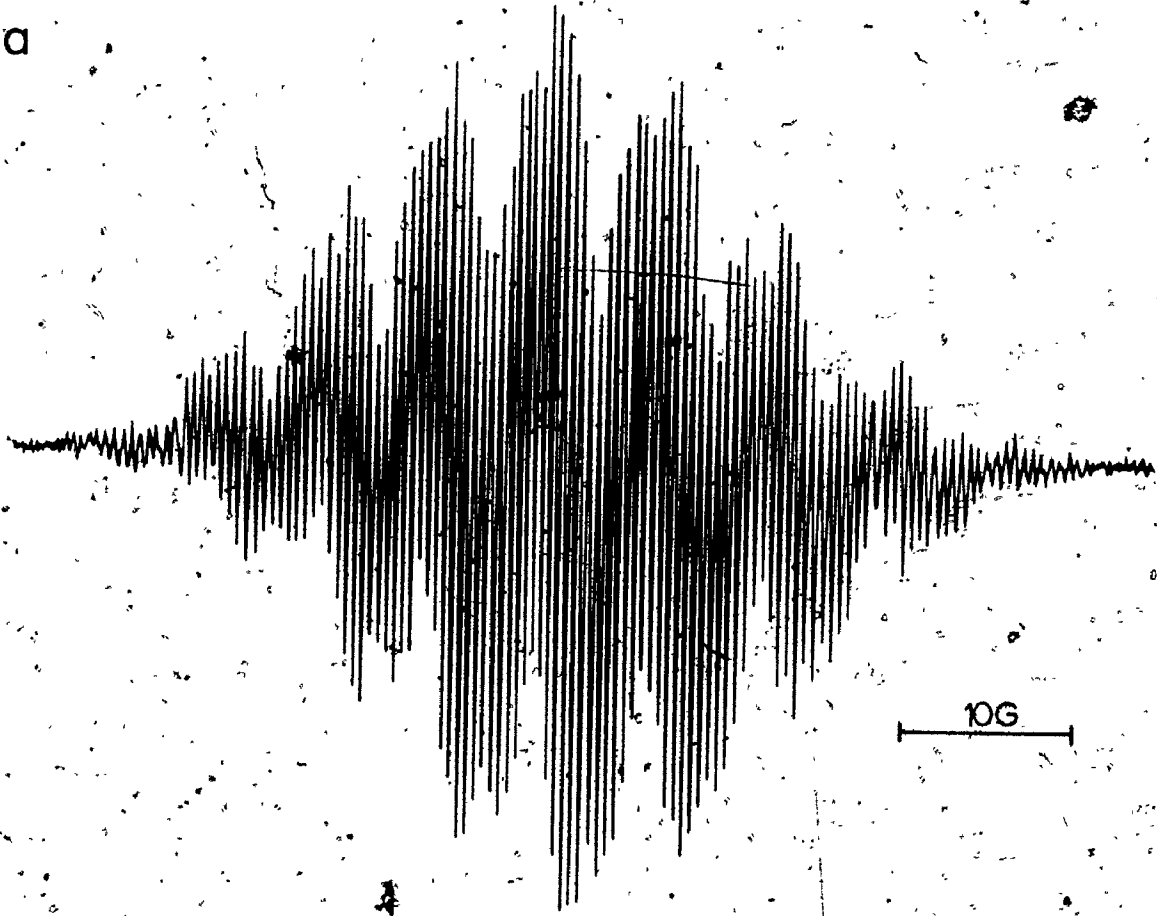
The addition of sodium borohydride to a solution of NMPMS

Figure 4.1

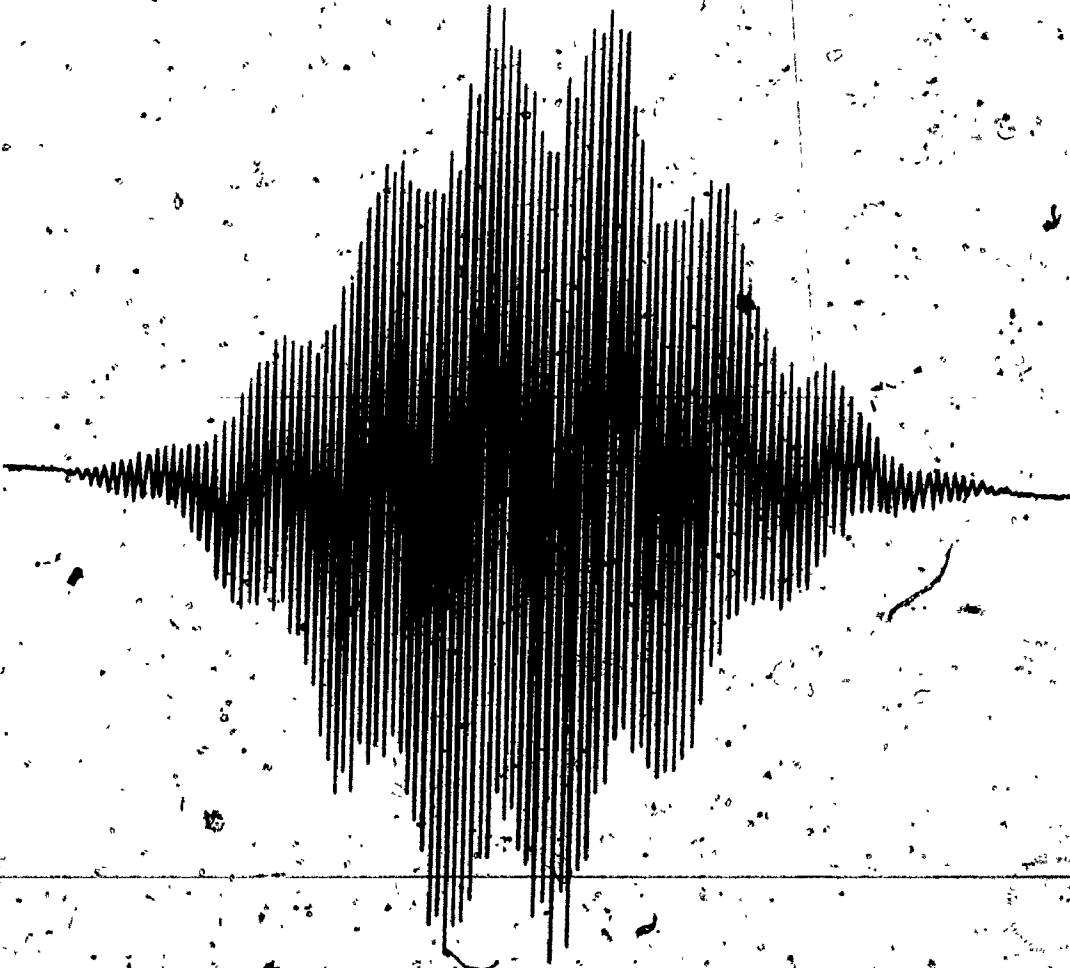
The First Derivative ESR Spectrum of the Light Induced Radical Formed from NMP^+ (a) in H_2O ; (b) in D_2O at pH 3.

Modulation amplitude 0.08 G, time constant 0.3 s, scan time 16 min., microwave power 10 mW.

a



b



leads to the establishment of a Michaelis equilibrium involving the fully oxidized, fully reduced and semireduced NMPMS (see the scheme proposed by King (65) shown in Fig. 4.2). Fig. 4.3 and 4.4 show the absorption spectra of NMP^+ and NMPH^+ perchlorate at pH 3. Fig. 4.5 curve (a) shows the optical spectrum obtained after irradiating NMP^+ in 0.1 M acetic acid solution. Curve (b) in Fig. 4.5 shows the optical spectrum of chemically semireduced NMP^+ in 0.1 M acetic acid solution. The strong absorbance below 400 nm is due to the NMP^+ remaining in the solution. Both curves are very similar, showing a peak at 443 nm which is not present in the optical absorption spectrum of NMP^+ (Fig. 4.3); however, the optical spectrum of NMPH^+ perchlorate does show a peak at 443 nm (Fig. 4.4). Both chemically semireduced NMP^+ and the photoinduced species in 0.1 M acetic acid give virtually identical ESR spectra. This means that the light-induced species is either the neutral radical $\text{NMP}\cdot$ or the radical cation NMPH^+ . NMPH^+ is the protonated form of the neutral radical $\text{NMP}\cdot$. The N_{10} position is the only position for which proton exchange is expected. Since $\text{NMP}\cdot$ does not have any exchangeable protons, its ESR spectrum should not be altered by changing the solvent from water to D_2O . Besides, Dobkowski and Rubaszewska (26) have reported the ESR spectrum of $\text{NMP}\cdot$ in isopropanol and its hyperfine splitting constants. The ESR spectrum of $\text{NMP}\cdot$ in isopropanol (Fig. 4.6) is totally different from the ESR spectrum of the light-induced species in aqueous solution. Hence, we can conclude that the light-induced species is a semireduced NMP^+ , probably the NMPH^+ radical cation.

Figure 4.2

King's Scheme (65) for the Reduction of NMP^+

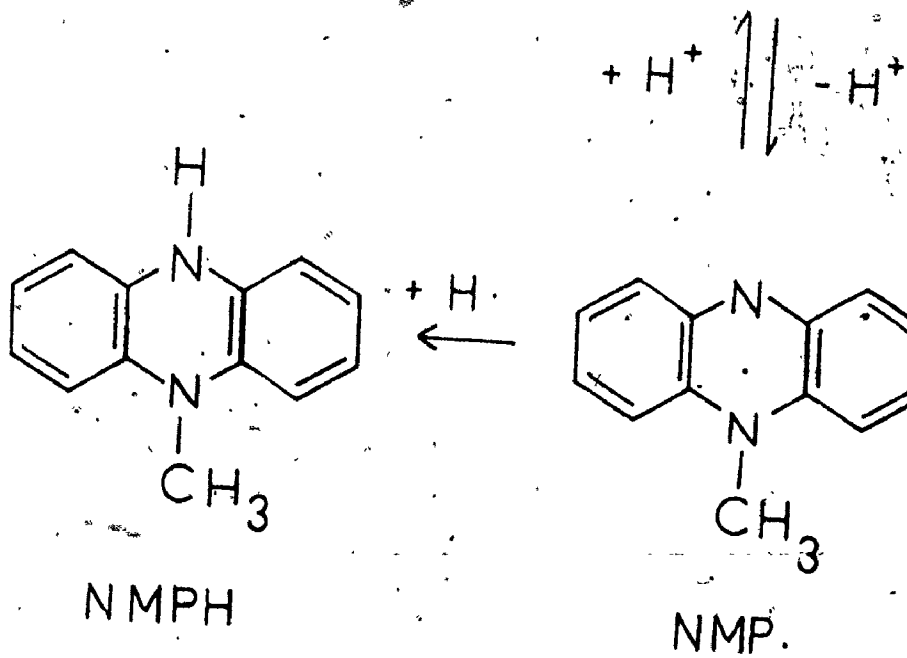
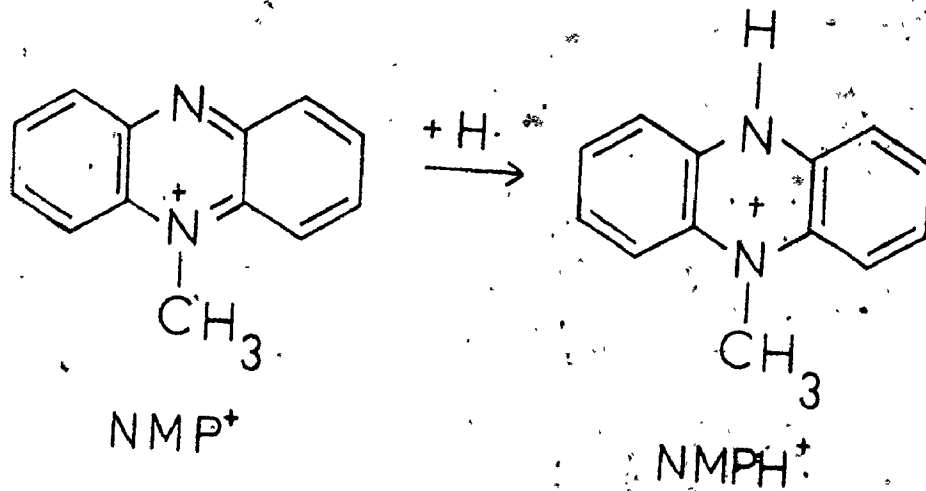


Figure 4.3

The Optical Absorption Spectrum of NMP^+ at pH 3.

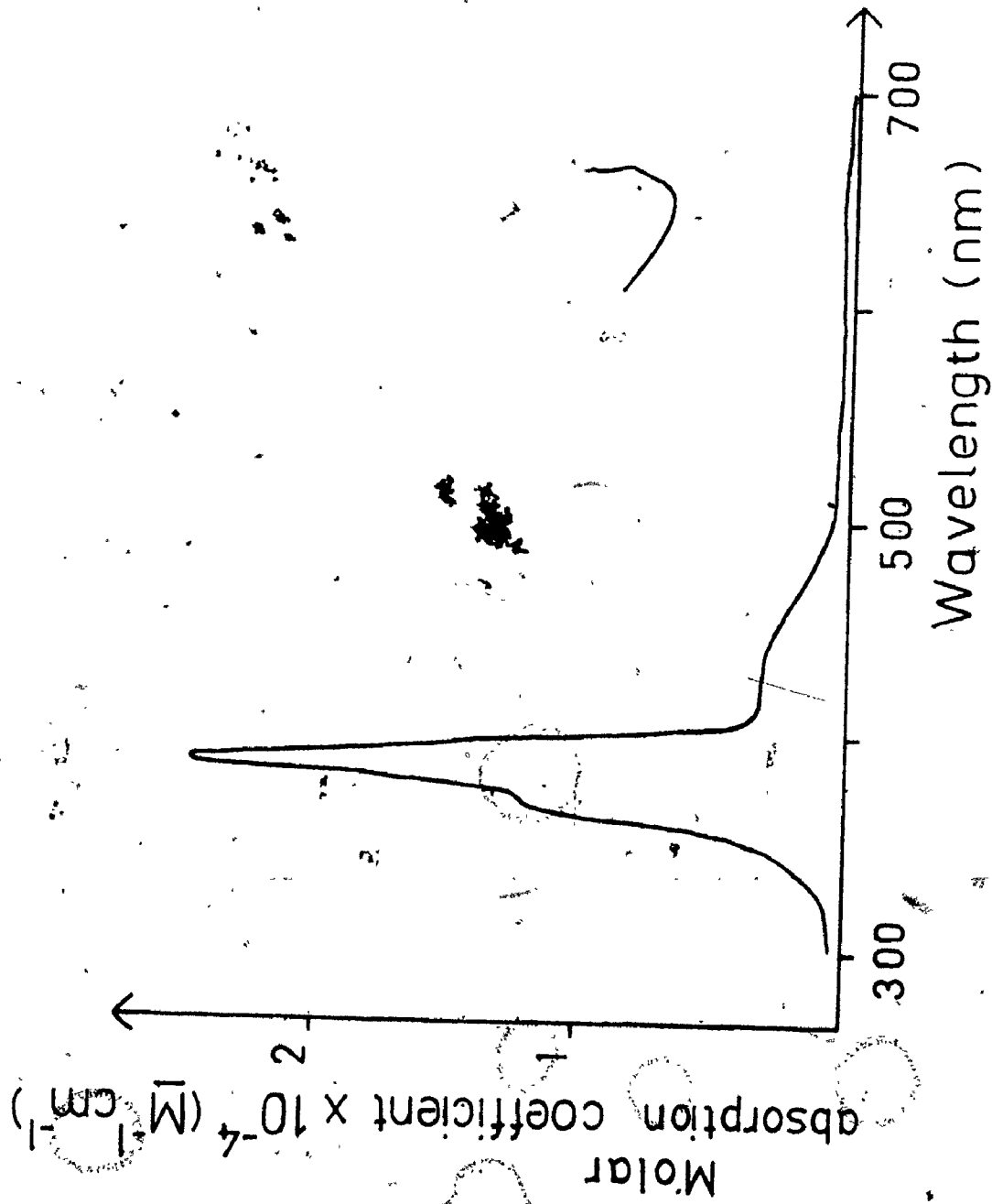


Figure 4.4

The Optical Absorption Spectrum of NMPH^+

Perchlorate at pH 3.

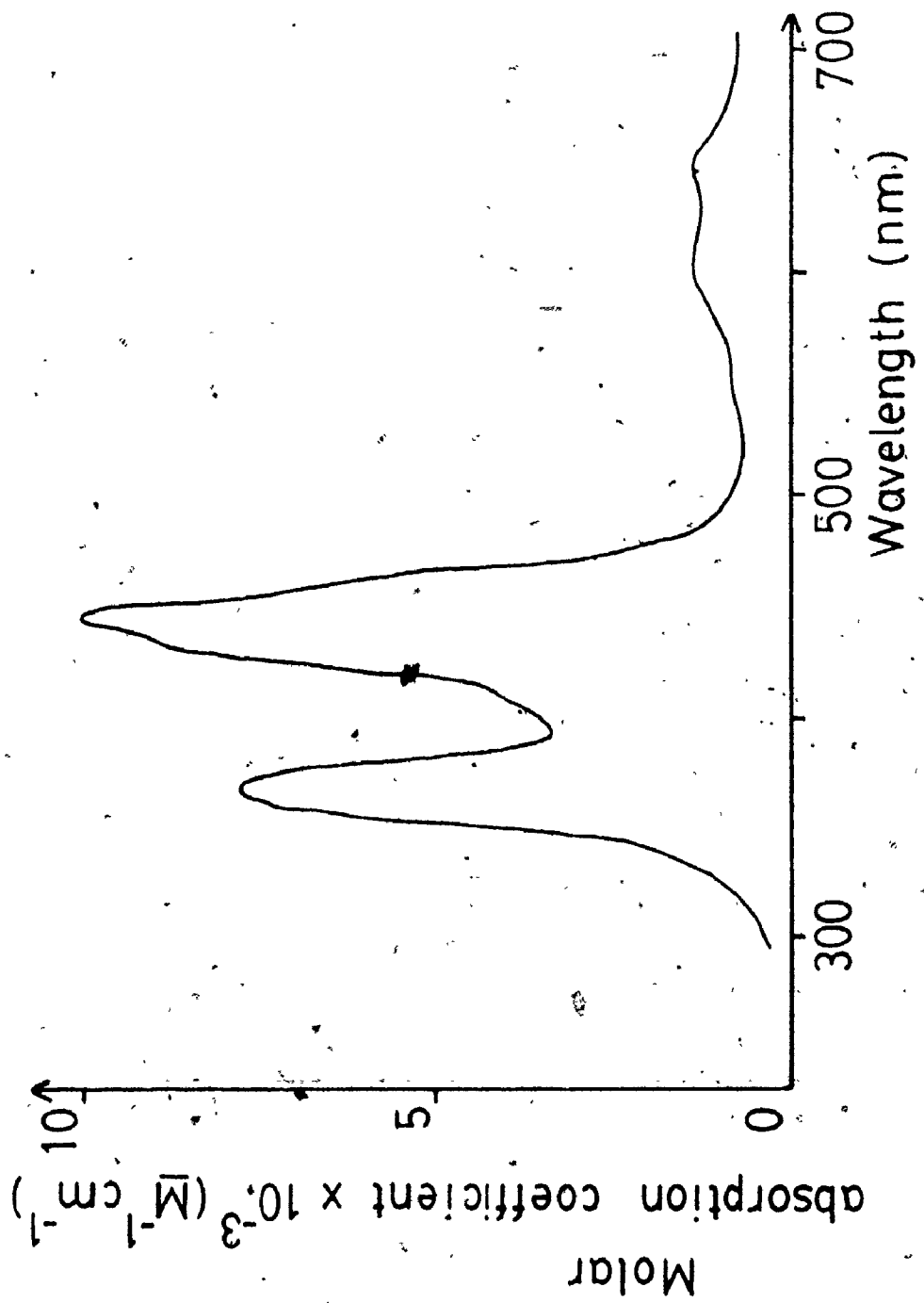


Figure 4.5

The Optical Absorption Spectrum Obtained (a) after Irradiating NMP^+ in 0.1 M Acetic Acid, (b) after Addition of Sodium Borohydride to NMP^+ in 0.1 M Acetic Acid.

The dotted line is the optical absorption spectrum of the starting material NMP^+ .

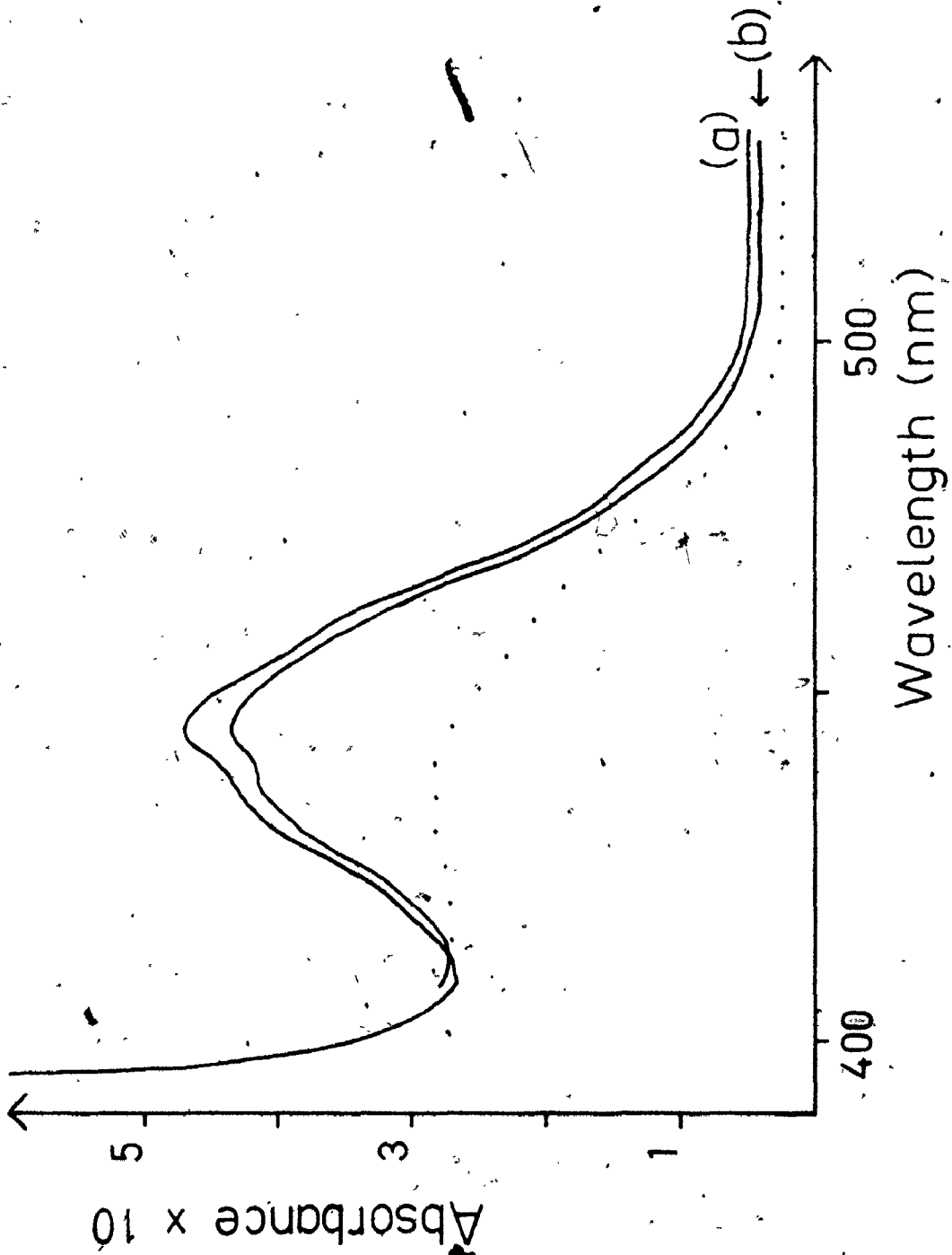
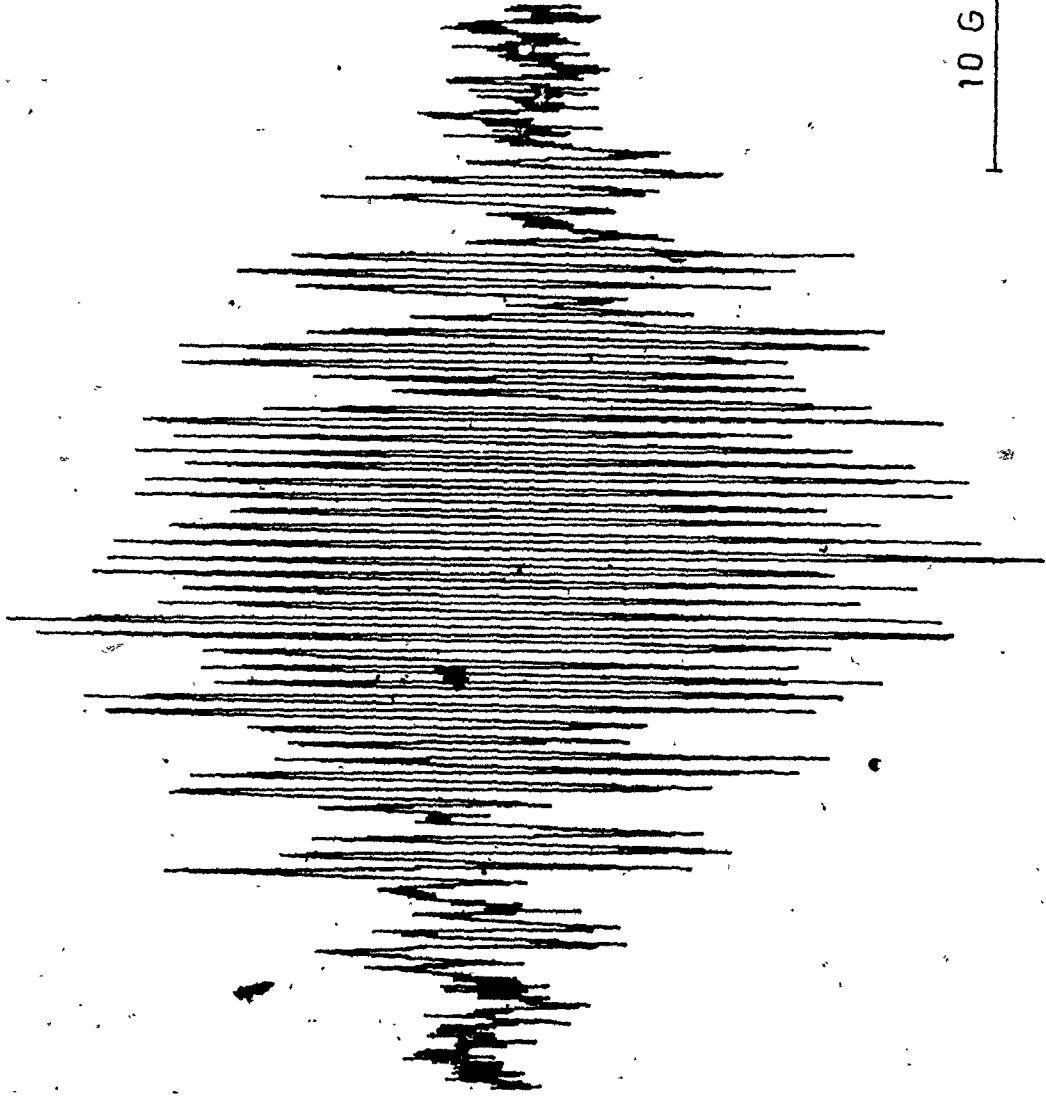


Figure 4.6

The First Derivative ESR Spectrum of NMP.

in 2-propanol

Modulation amplitude 0.32 G, time constant 0.3 s,
scan time 16 min., microwave power 10 mW.



10 G

4.2.2 Analysis of the ESR Spectrum

The $\text{NMPH}^{\cdot+}$ radical cation has eight distinct sets of magnetic nuclei and thus the ESR spectrum of $\text{NMPH}^{\cdot+}$ should consist of 5832 lines; nevertheless, only about 120 lines are observed in the first derivative spectrum shown in Fig. 4.1a. In order to obtain improved resolution, the second derivative of the light-induced ESR absorption spectrum at pH 3 was recorded. An attempt was made to analyse the hyperfine structure of the light-induced species using this second derivative spectrum.

From the expansion of the tail part of the spectrum (Fig. 4.7a), it was found that the ratio of the three small hyperfine splitting constants is coincidentally about 1:2:3. Each group consists of two equivalent protons. The intensity profile of the combination of these three groups should be about 1 : 2 : 3 : 6 : 7 : 8 : 10 : 8 : 7 : 6 : 3 : 1. The smallest hyperfine splitting is equal to the separation of the two outermost lines and found to be 0.45 G. A fourth proton hyperfine splitting (namely 2.03 G) is discernible. Fig. 4.7b shows the simulated spectrum using only these four small hyperfine splitting constants.

The splitting of the N-H proton was estimated from the difference in the total span from outside line to outside line of the ESR spectra obtained in water and in D_2O . If $\Delta H(\text{H}_2\text{O})$ is the total extent for the spectrum in H_2O and $\Delta H(\text{D}_2\text{O})$ is the extent of the spectrum in D_2O , then

$$\Delta H(\text{H}_2\text{O}) - \Delta H(\text{D}_2\text{O}) = a_{\text{NH}}^{\text{H}} - 2 a_{\text{ND}}^{\text{D}} \quad (4.14)$$

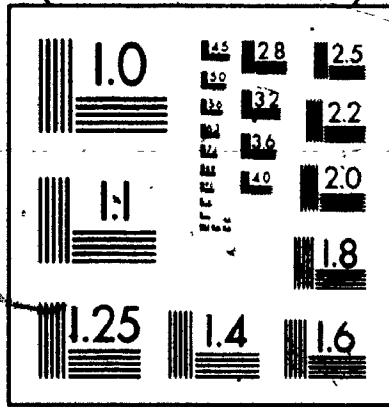
Figure 4.7

(a) The Expansion of the Low Field End of the Second Derivative ESR Spectrum of NMPH^+ and (b) The Computer Stimulated Spectrum Using the Four Smallest Hyperfine Splittings Listed in Table 4.1.

Modulation amplitude 0.1 G, time constant 10⁻⁵ s, scan time 1 hr., microwave power 1 mW, modulation frequencies 100 kHz and 1 kHz, linewidth used in the simulation 0.15 G.

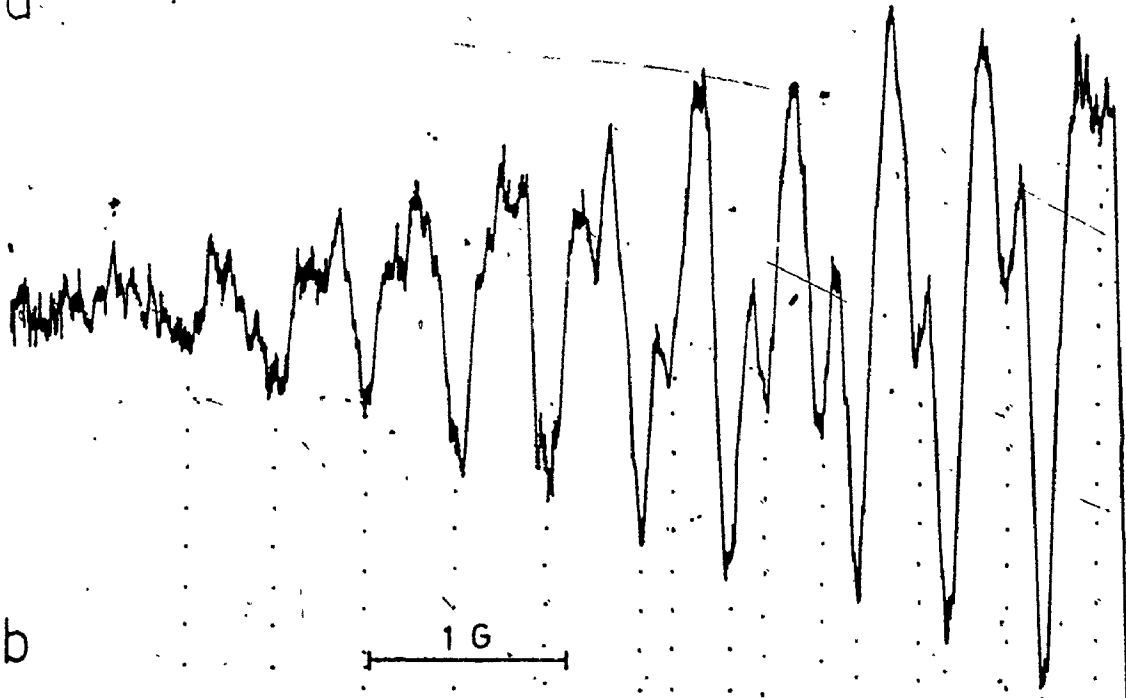
Note that the peak of the second derivative line is towards the bottom of the page.

2

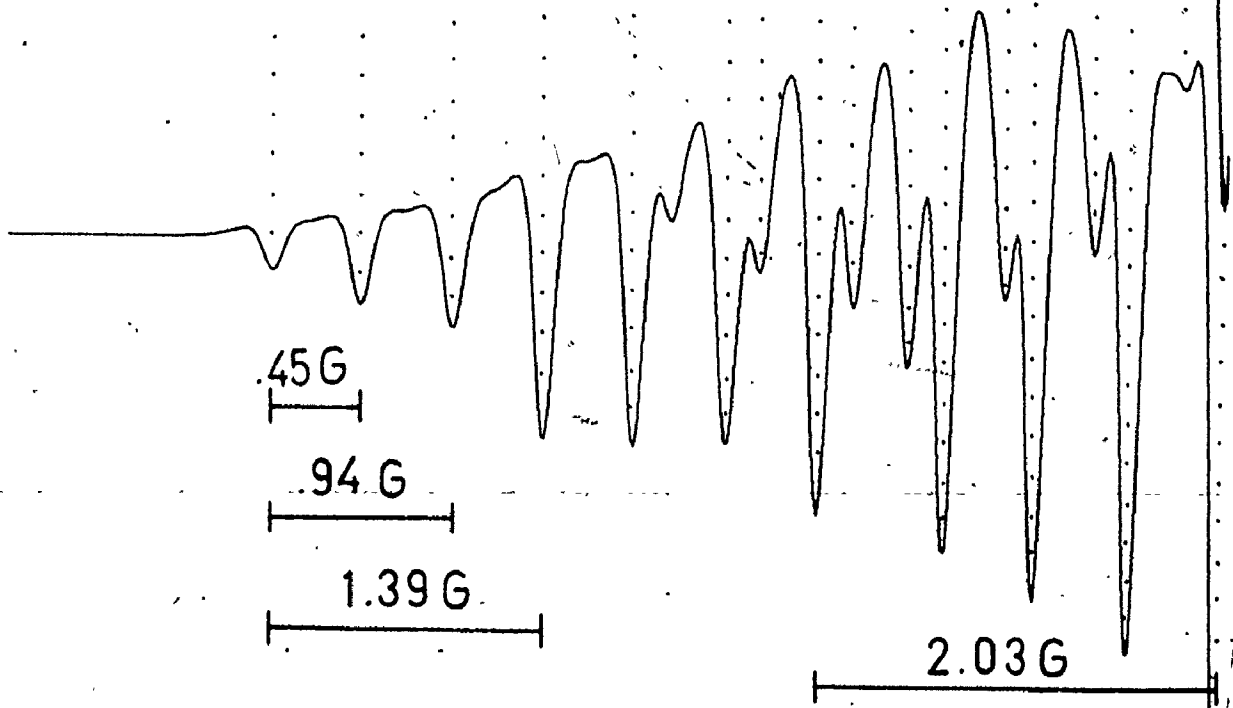


Metre A4441 Or 80 G024 B41P C/100 24/01 8/94

a



b



From the ratio of magnetogyric ratio of H to D, $a_{ND}^D = 0.1535 a_{NH}^H$, then

$$a_{NH}^H = 1.443 (H(H_2O) - \Delta H(D_2O)) \quad (4.15)$$

It has been shown that a_{NH}^H is about 5 - 10 % greater than the a_{NH}^N for radical cations containing nitrogen heteroatoms (66), and a_{Me}^H is about 5 % less than a_{NMe}^N . Using these two guidelines and the relation that the total span of the ESR spectrum must be equal to $\sum n_i I_i a_i$ (where n_i is the number of equivalent nuclei of type i , I_i is the nuclear spin quantum number of the i -th set and a_i is the hyperfine splitting for a nucleus in the i -th set) the best fit to the ESR spectrum of the light - induced species was obtained after a number of false attempts with the hyperfine splitting constants shown in Table 4.1. Most of the hyperfine splitting constants are within the estimated ranges suggested by Dobkowski and Rubaszewska (26).

The second derivative ESR spectrum and the computer simulated spectrum are shown in Appendix 2. The line positions and fine structure of the second derivative spectrum constructed from the above information agrees very well with the experimental spectrum, but the relative intensity of the outer to centre lines is not exactly as predicted. There are two possible reasons for this discrepancy. First, because there is severe overlap in the centre of the spectrum, a small change in hyperfine splitting constants may affect the relative intensity of the observed lines. The second and more likely reason is that the $NMPH^+$ radical cation is a moderately large molecule which will have a slower tumbling rate than a small radical. The slower tumbling rate will result in a greater broadening of the outer lines of the ESR spectrum relative to the inner lines (45).

Table 4.1

The Hyperfine Splitting Constants of the
Radical NMPH⁺

$$a_{\text{NMe}}^{\text{N}} = 6.93 \text{ G}$$

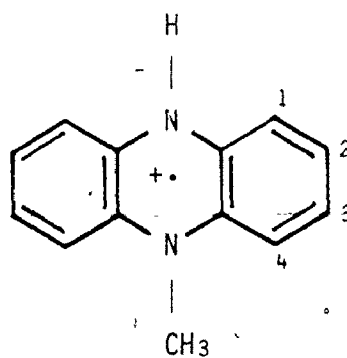
$$a_{\text{NMe}}^{\text{H}} = 6.35 \text{ G (3 protons)}$$

$$a_{\text{NH}}^{\text{N}} = 6.00 \text{ G}$$

$$a_{\text{NH}}^{\text{H}} = 6.45 \text{ G (1 proton)}$$

$$(a_2^{\text{H}}, a_3^{\text{H}}) = \{ \begin{array}{l} 2.03 \text{ G (2 protons)} \\ 1.39 \text{ G (2 protons)} \end{array} \}^*$$

$$(a_1^{\text{H}}, a_4^{\text{H}}) = \{ \begin{array}{l} 0.94 \text{ G (2 protons)} \\ 0.45 \text{ G (2 protons)} \end{array} \}^*$$



* Assignment of the four small ring proton hyperfine splittings is not certain - see page 83.

The exact hyperfine splitting constants of the ring protons should not be more than 0.03 G away from the values listed in Table 4.1. The error in the four major splittings could be as high as 0.05 G. This analysis indicates without doubt that there is indeed a proton attached to the nitrogen.

Fig. 4.8 shows the experimental spectrum (a) and the simulated spectrum (b) of $\text{NMPH}^{\cdot+}$ in water. When a_{NH}^{H} was substituted by a_{ND}^{D} ($=0.99$ G, $I = 1$) in the simulation, the resulting $\text{NMPD}^{\cdot+}$ spectrum is shown in Fig. 4.9b which is also very similar to the actual spectrum (Fig. 4.9a).

The average of the two larger ring proton splittings of $\text{NMPH}^{\cdot+}$ is 1.7 G and the two smaller splittings is 0.69 G. These average values are very close to the hyperfine splittings of the ring protons of phenazine cation radical where $a_1^{\text{H}} = 0.66$ G and $a_2^{\text{H}} = 1.71$ G (66). Probably the two large proton splittings correspond to the hydrogen at 2 and 3 positions while the two small splittings correspond to the hydrogen at 1 and 4 positions. A molecular orbital calculation would perhaps give a better indication of the exact assignment but such a calculation was not attempted.

In summary, the stable radical formed in the present system is a semireduced $\text{NMP}^{\cdot+}$ and has one exchangeable proton. Hence, the light - induced radical species is without doubt $\text{NMPH}^{\cdot+}$.

4.2.3 Identification of Other Products

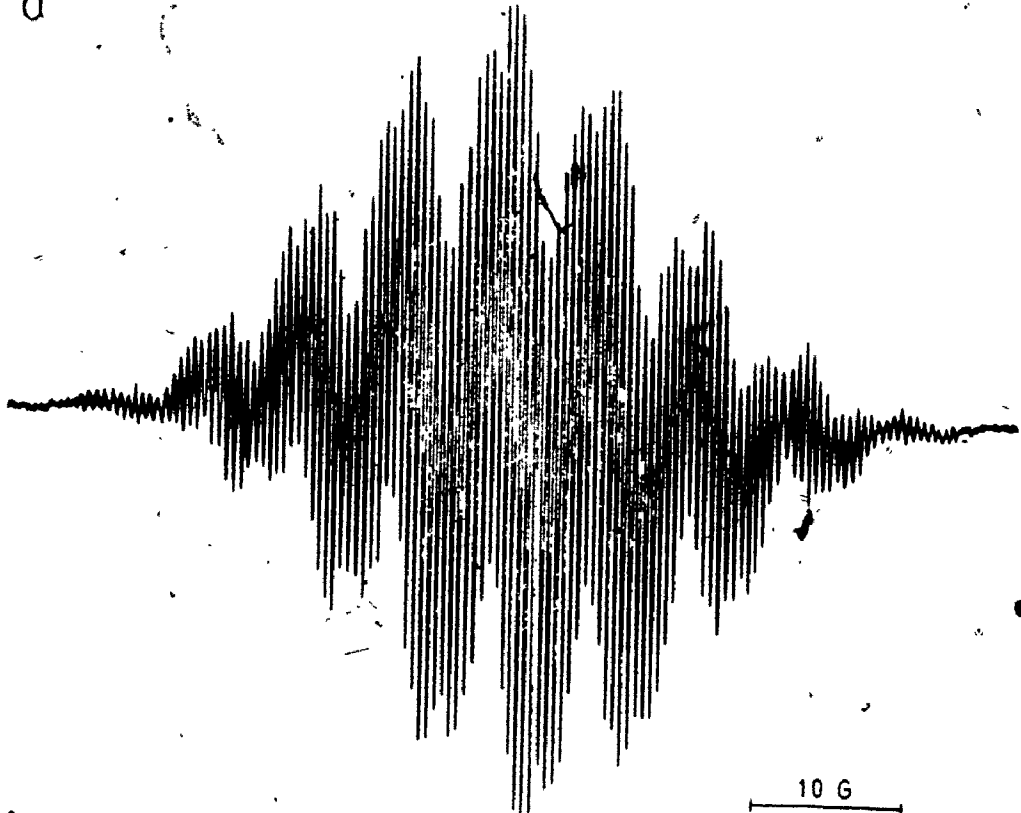
When a vacuum degassed $\text{NMP}^{\cdot+}$ ($\sim 10^{-5}$ M) solution at pH 7 was irradiated with a krypton laser, the colour of the solution changed

Figure 4.8

(a) The Experimental and (b) Computer Simulated (Using
Hyperfine Splittings Given in Table 4.1) First Derivative
ESR Spectra of NMPH^+ in Water at pH 3

Modulation amplitude 0.08 G, time constant 0.1 s,
scan time 16 min., microwave power 10 mW, linewidth
used in simulation 0.15 G.

a



10 G

b

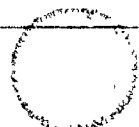
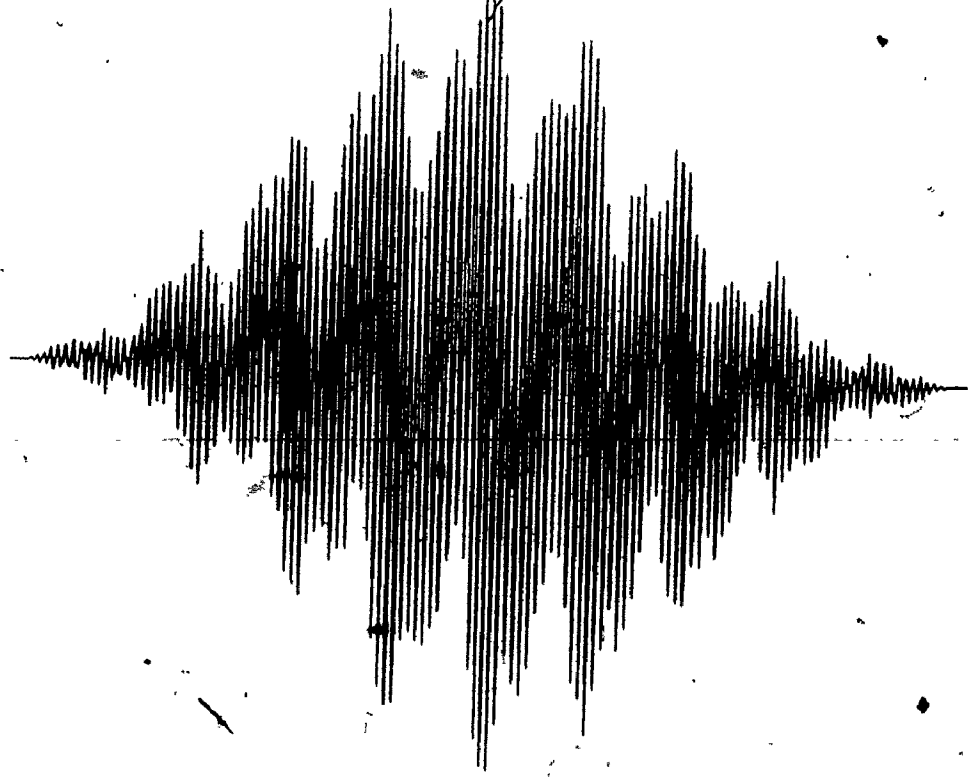


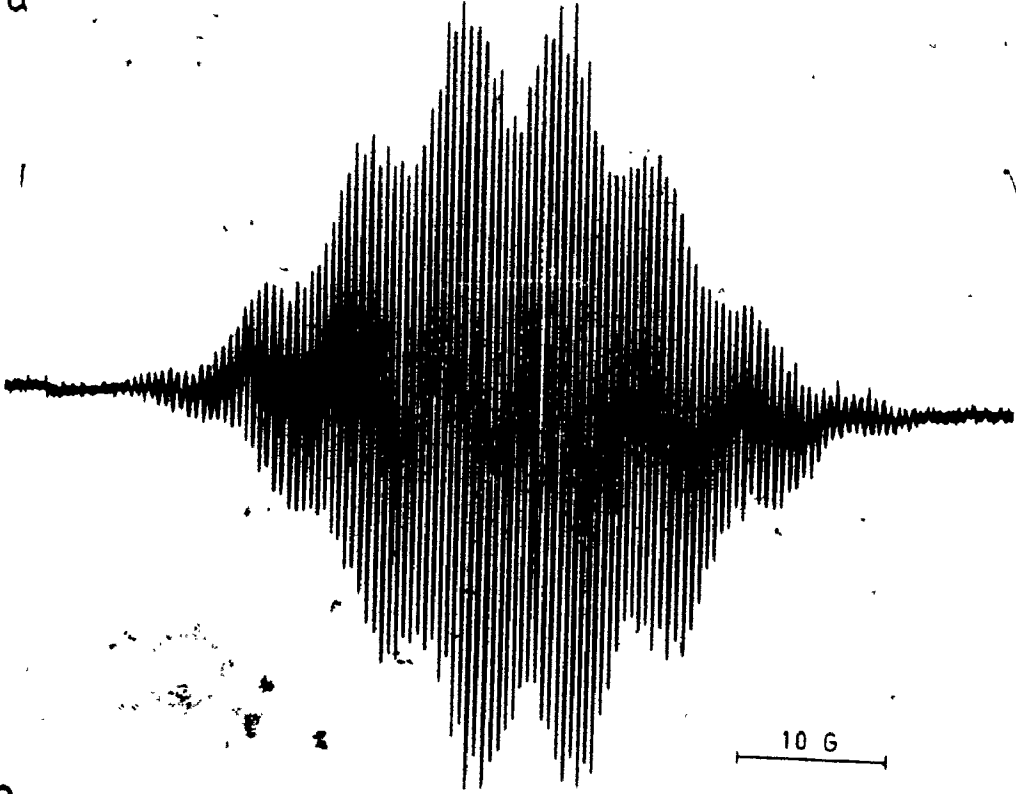
Figure 4.9

(a) The Experimental and (b) Computer Simulated First Derivative ESR Spectra of NMPD[•] in D₂O.

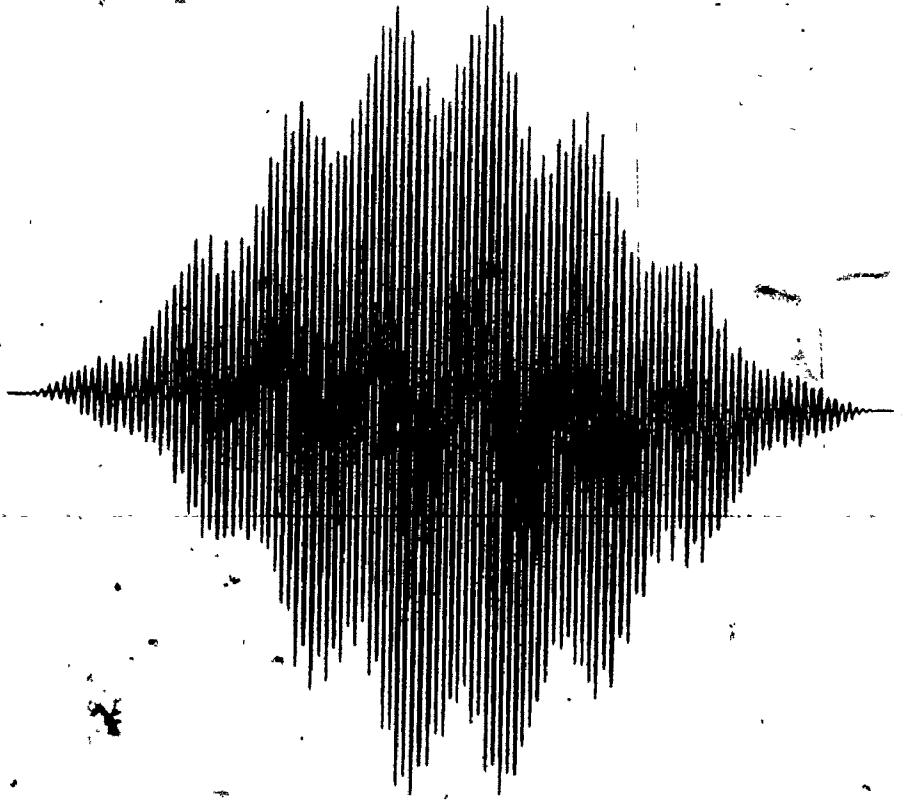
Hyperfine splittings given in Table 4.1 with $a_{ND}^D = 0.99$ G were used.

Modulation amplitude 0.08 G, time constant 0.1 s, scan time 16 min., microwave power 10 mW, linewidth used in the simulation 0.15 G.

a



b



gradually from yellow to blue. A large absorption peak was observed at 310 nm which is fairly weak in the chemically reduced solution. After the system was opened to the air, the absorbance at 310 nm remained unchanged. Hence, this peak does not originate from NMPH^+ which is not stable at pH 7 in the presence of oxygen.

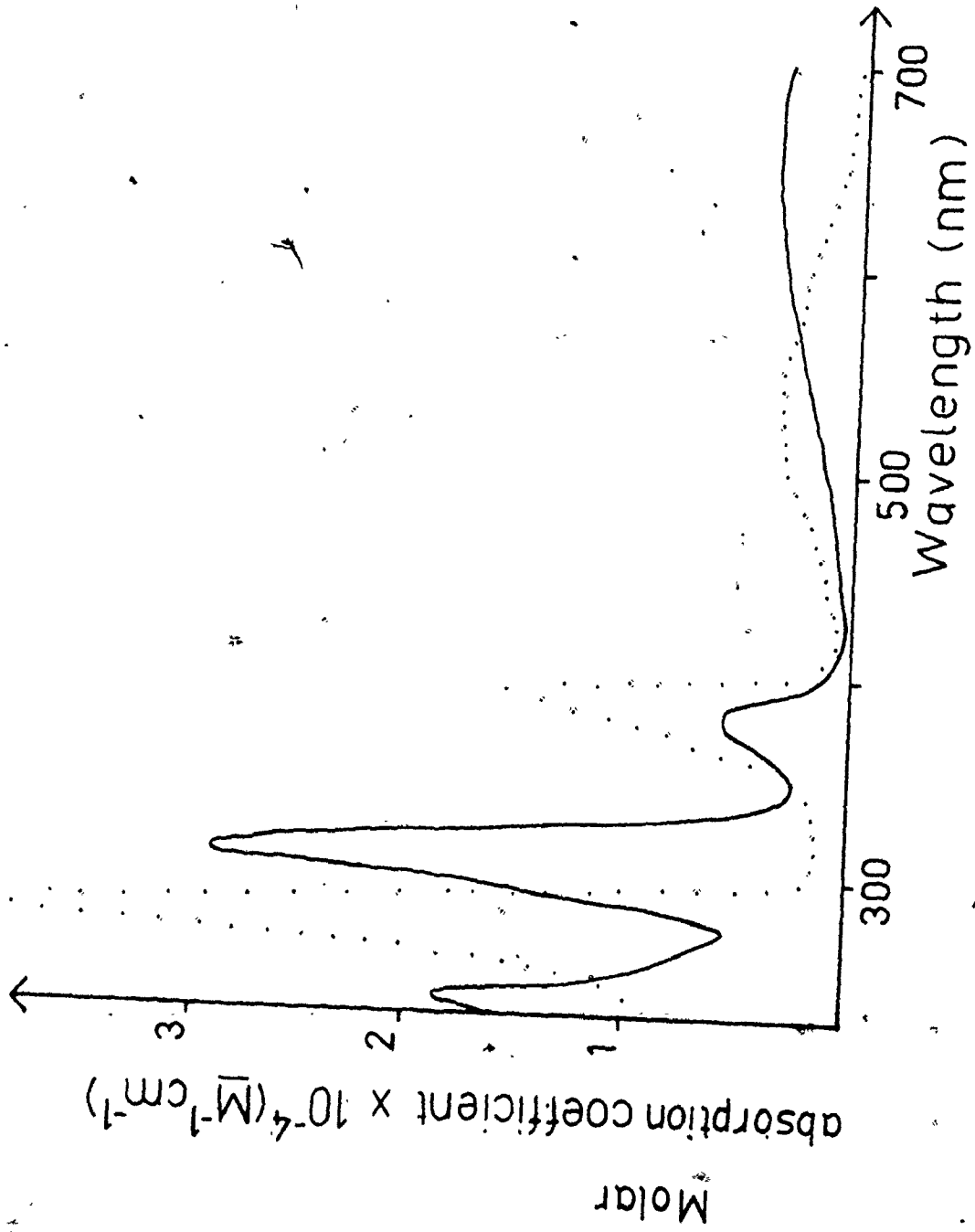
) McIlwain (24) reported that, under the influence of visible light, oxidation of NMP^+ salts in the presence of air produced mainly pyocyanine, together with phenazine and small amounts of 4-hydroxyphenazine and 3-keto-N-methylphenazine.

When a drop of concentrated acetic acid was added to the blue solution (the final pH of the solution was ~ 4), the colour of the solution turned to red. The 310 nm absorption peak disappeared as a 278 nm peak appeared. This pH dependence is similar to that of pyocyanine. The optical absorption spectra of pyocyanine at pH 3 and 7 (Fig. 4.10) are different because the pK_a value of pyocyanine is 4.9 (44). That is, at a pH lower than 4.9, the protonated form PYH^+ (which is red) dominates, while at a pH higher than 4.9, the unprotonated form PY (which is blue) predominates. The concentration of pyocyanine was calculated from the absorbance at 310 nm. It was found that the amount of pyocyanine formed was comparable to the amount of NMP^+ used up in the reaction. As a result of these observations we conclude that pyocyanine is a major product in the present system.

At no time was any evidence obtained for demethylation of NMP^+ to form phenazine at pH < 7 .

Figure 4.10

The Optical Absorption Spectra of Pyocyanine
at pH 3 (dotted lined) and 7.



4.3 QUANTUM YIELD DETERMINATION :

In photochemistry, the quantum yield ϕ_z of product Z resulting from the photodecomposition of X, $X + h\nu \rightarrow Z$, is defined as

$$\phi_z = \frac{\text{Molecules of Z formed}}{\text{Quanta of light absorbed by X}} \quad (4.16)$$

The value of the denominator can be calculated from a measurement of the absorbed light energy and the excitation wavelength. The value of the numerator is usually found by chemical analysis. When Z is paramagnetic and detectable by ESR, the concentration of Z in a sample can be determined by comparing the sample under study with a standard (for details see Section 3.4.1).

Loach and Walsh (67) reported that there is a 1 : 1 correspondence between the concentrations of photoreduced spins in chromatophores of R. rubrum as measured by the ESR technique and by an absorbance change at 865 nm. The quantum yields for the photoreduced species in chromatophores determined by ESR agree very well with the previous reported values (68, 57) which were determined optically. In their experiments, they used an equation to relate number of spins to peak - to - peak amplitude of ESR signal. The line shapes of the signals, that is Gaussian or Lorentzian, are required in the calculation. In order to relate the concentration to the total number of spins, the effective volume of the cell is also required. The modulation amplitude used has to be significantly less than the half - width of the narrowest line so that peak height distortion does not occur. Since the peak - to - peak linewidth of NMPH^{\dagger} is about 0.2 G, and in the quantum yield experiment the

magnetic field is fixed at the peak of the ESR signal; very slight fluctuations in magnetic field will cause a large error in the quantum yield obtained. Besides, it is quite impossible to determine the relation between the area of the strongest line and the area of an unsplit signal due to the complexity of the spectrum. In this work, the signal was overmodulated so that the whole spectrum could be used in place of the strongest line and the area under the absorption curve was used instead of peak - to - peak amplitude in the calculation of the concentration of the unknown. It has been shown (69) that overmodulation does not result in a significant error in the evaluation of the area under the absorption curve.

In the quantum yield experiment, the krypton laser was aligned so that the laser beam passed through the centre of the cavity. The ESR spectra of NMPH⁺ were stored on the CAT. Peak - to - peak amplitudes of the signals ($2\Delta Y'$) were measured in terms of the number of the counts in the CAT, and areas under the entire absorption curve were determined by double integration using a PDP 10 computer (see Section 3.4.3). It was found that there is a linear relation between the area and the peak - to - peak amplitude. The slope S of the straight line was determined by the least squares method.

$$\text{Area} = S \cdot (\Delta Y') \quad (4.17)$$

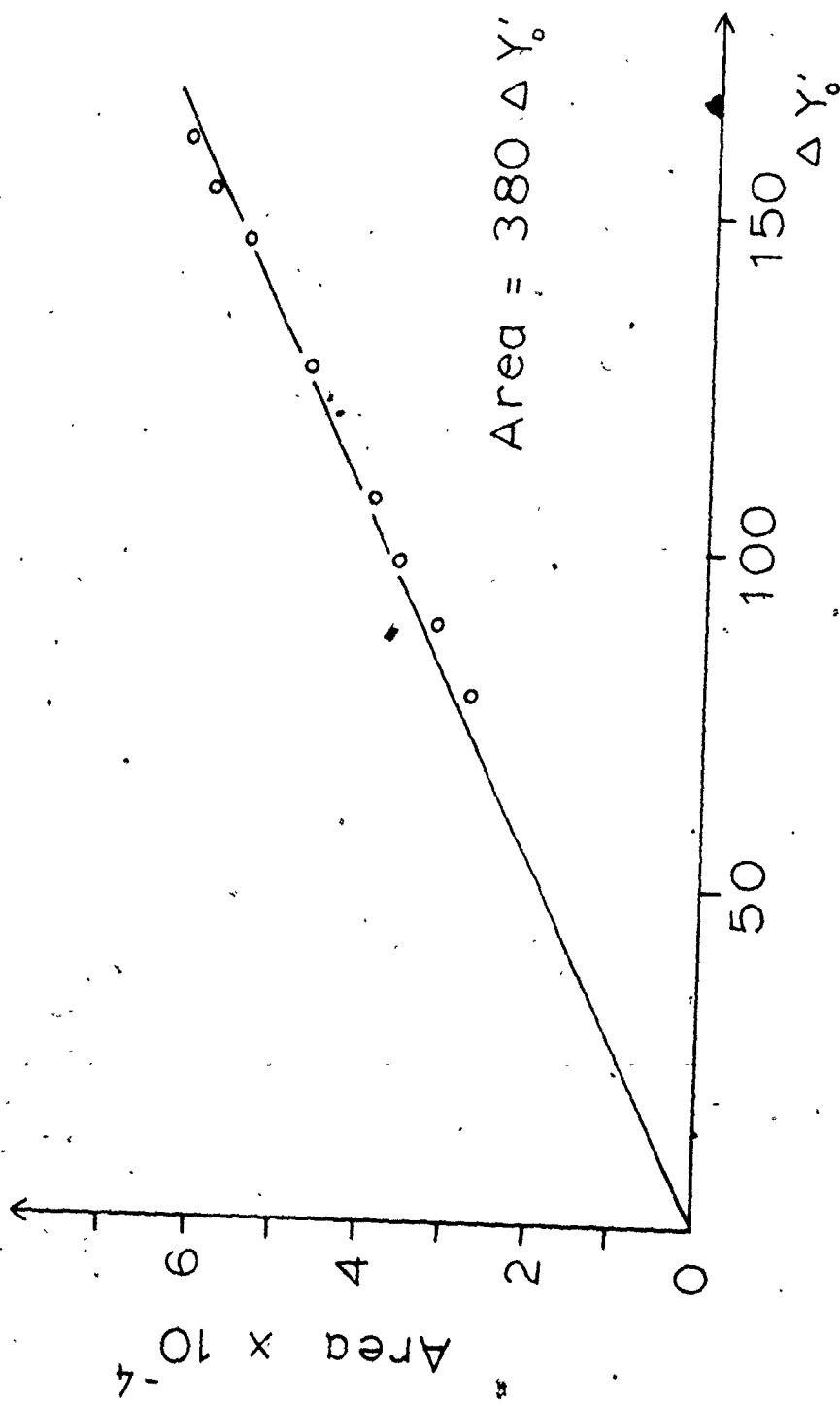
Fig. 4.11 shows that S is equal to 380 ± 4 when the settings of the ESR spectrometer were: scan range, 100 G; modulation amplitude, 16 G; scan time, 2 minutes; time constant, 0.1 s and microwave power, 4 mW. S is equal to 158 ± 1 when the settings were: scan range, 200 G;

Figure 4.11

The Relation between the Area under the Absorption Curve and the Peak-to-Peak Amplitude of the ESR Signal.

Modulation amplitude 16 G, time constant 0.1 s,
scan time 2 min., microwave power 4 mW.

Handwritten scribble or signature at the top left of the page.



modulation amplitude, 4 G; scan time, 4 minutes; time constant, 0.3 s and microwave power 10 mW. In both cases, the correlation coefficients between Area and $\Delta Y'$ are larger than 0.999. The Second setting is the optimal condition for the NMPH⁺ ESR signal, that is, the signal - to - noise ratio is highest. Under these conditions no power saturation is observed and the ESR signal is overmodulated so that only a broad peak is observed.

A 9.7×10^{-5} M solution of 4-hydroxy-2,2,6,6-tetramethylpiperidine-1-oxyl was used as the standard. The ESR spectra were stored on the CAT and the areas were found by double integration. In this case the standard was uniformly distributed in the cell while NMPH⁺ which was generated by the irradiation of a laser beam was concentrated at the centre of the sample cell. The field modulation intensity along the vertical axis of the sample is a maximum at the centre of the cavity and a minimum at the top and bottom of the cavity. It has been found by careful measurement that the signal amplitude ($\Delta Y'$) received from a sample with uniformly distributed spins along the vertical axis is 0.50 times the signal amplitude obtainable from the same number of spins concentrated at the cavity centre ($\Delta Y'_0$) (70):

$$\Delta Y' = (0.50 \pm 0.03) \Delta Y'_0 \quad (4.18)$$

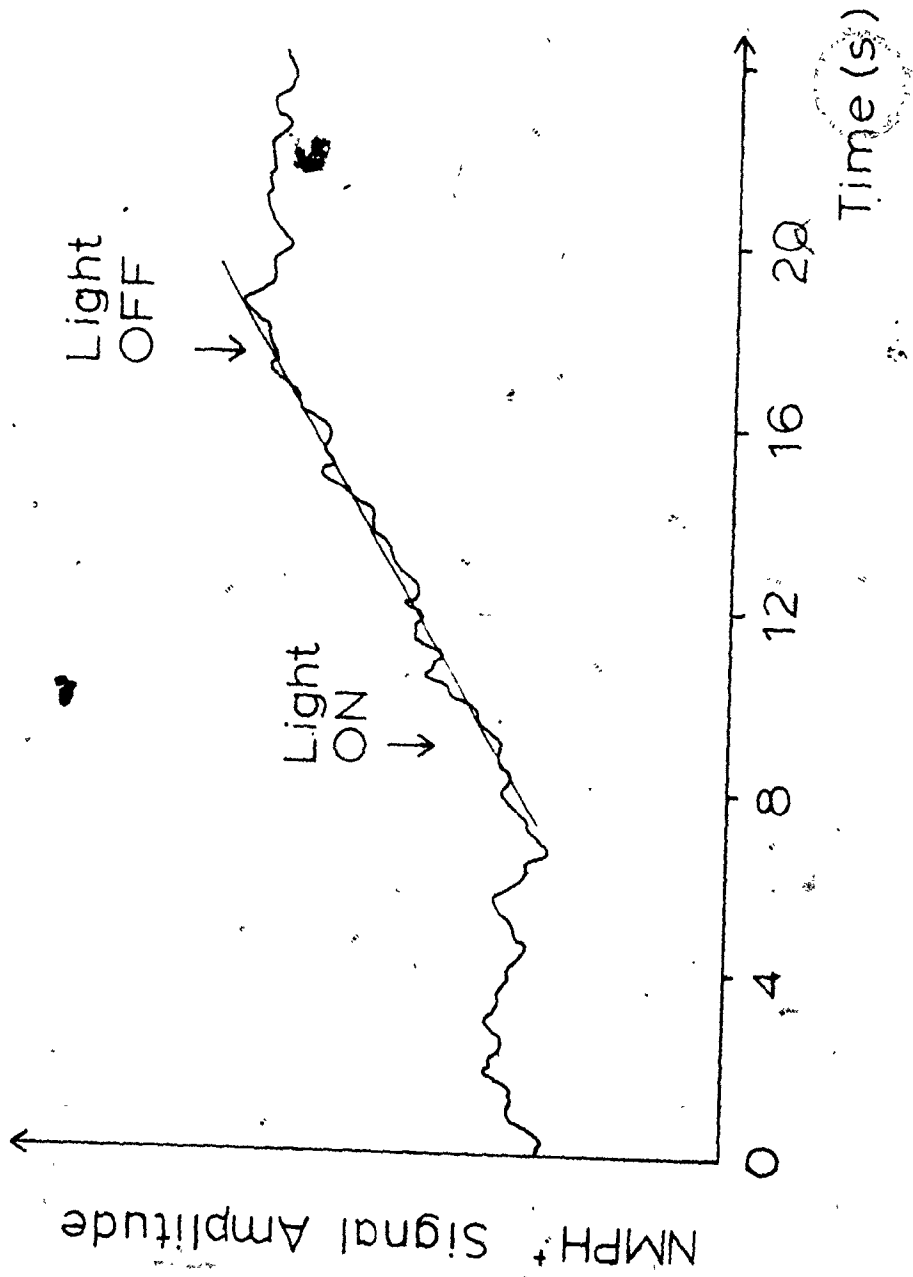
where the subscript 0 indicates the spins being concentrated at the cavity centre.

The time dependent ESR signal at constant magnetic field and at the peak of the NMPH⁺ signal was recorded and the output data were stored on the CAT. Fig. 4.12 shows the change of ESR signal amplitude with time. During the quantum yield experiments the laser beam was

Figure 4.12

A Typical Trace Obtained in the Quantum Yield
Determination Experiment.

Modulation amplitude 16 G, time constant 0.1 s,
microwave power 4 mW.



cut off after 8 s by a shutter to avoid heating up the sensor of the radiometer. The slope of the line shown in Fig. 4.12, $d(\Delta Y_0)/dt$, was determined by the least squares method. The radicals are concentrated at the centre of the cavity so Eq. 4.18 was then used to convert $d(\Delta Y_0)/dt$ to $d(\Delta Y')/dt$. Using Eq. 4.17 the factor was then changed to $d(\text{Area})/dt$. The ESR spectrum of a nitroxide standard of known concentration was recorded using the same modulation amplitude, incident microwave power, solvent and sample cell and at the same temperature as that used in the quantum yield experiment. Thus all the criteria in Section 3.4.1 were met. Using Eq. 3.3, the factor $d(\text{Area})/dt$ was converted to $d[\text{NMPH}^{\cdot+}]/dt$. The factor R in Eq. 3.3 was set to 1 for both standard and $\text{NMPH}^{\cdot+}$ because whole spectra were used in the double integration. S is 1/2 for both cases. The g factor of $\text{NMPH}^{\cdot+}$ was found to be 2.0035 and the g factor of the nitroxide standard is 2.0060. The g factor standard used was α, α -diphenyl- β -picrylhydrazyl (DPPH) with g factor 2.0037 ± 0.0002 (71). The method used was described in Section 3.4.2.

In order to ensure that the light intensity remained constant throughout the sample cell, the absorbance of the sample was kept below 0.1 ($\approx 1 \times 10^{-3}$ M).

The fraction of light absorbed B was determined using the following equation which is a simplified approximate formula derived by considering the effects of multiple reflection at the surfaces of a flat cell (the sample cell)(57):

$$B = 1 - t - (1 + t^2) \left(\frac{1 - t_0}{1 + t_0} \right) \quad (4.19)$$

where $t = I/I_{\infty}$, $t_0 = I_0/I_{\infty}$, I is the transmitted light intensity through the sample cuvette containing the sample, and I_0 is the transmitted light intensity through a similar cuvette containing solvent only. I_{∞} is the light intensity with no cuvette. I , I_0 and I_{∞} were measured by a radiometer and recorded by a Varian G2000 strip chart recorder.

The quantum yield of NMPH^{\dagger} in pH 7 buffer at 476.2 nm is equal to $(d[\text{NMPH}^{\dagger}]/dt)/(B I_{\infty})$ and was found to be 0.29 ± 0.03 . Table 4.2 summarizes the results. Table 4.3 shows the uncertainties in the measurements. These errors are the average of the percentage standard deviations obtained in various measurements.

The quantum yields for the formation of NMPH^{\dagger} at various pH values were determined relative to that obtained at pH 7 at constant NMP^+ concentration. 5×10^{-3} M phosphate buffer, 5×10^{-3} M phthalate buffer and hydrochloric acid solutions were used as the solvent for pH above 5.5, pH between 3 to 5.5 and pH < 3 respectively. All samples were purged with nitrogen gas. The light source was the 472.7 nm line of an argon laser. The magnetic field was set at the peak of the NMPH^{\dagger} signal. The changes of ESR signal amplitude with time for various solutions were recorded. The initial change of ESR signal amplitude was measured and then compared to that obtained in a pH 7 solution. The relative quantum yield is directly proportional to the initial slope. The result is shown in Fig. 4.13 which shows that at pH 3, the quantum yield is 1.1. According to the proposed mechanism on page 63 the maximum quantum yield of the formation of NMPH^{\dagger} would be 2, that is, for every photon absorbed,

Table 4.2

Summary of the Results in the Quantum Yield Experiments at $\lambda = 476.2$ nm.

Run*	No. of Trials	S	B	I_{∞} (E_s^{-1})	$d[NMPH^{\ddagger}]/dt$ (M_s^{-1})	$\phi_{NMPH^{\ddagger}}$
1	4	380	0.32 ± 0.01	$(1.80 \pm 0.05) \times 10^{-9}$	$(1.65 \pm 0.07) \times 10^{-10}$	0.29
2	5	158	0.129 ± 0.010	$(4.64 \pm 0.21) \times 10^{-10}$	$(1.79 \pm 0.08) \times 10^{-11}$	0.30
3	4	158	0.130 ± 0.012	$(3.94 \pm 0.10) \times 10^{-10}$	$(1.40 \pm 0.08) \times 10^{-11}$	0.28
4	5	158	0.116 ± 0.007	$(5.29 \pm 0.18) \times 10^{-10}$	$(1.69 \pm 0.15) \times 10^{-11}$	0.28

For run 1 modulation amplitude was 16 G and microwave power was 4 mW while for runs 2 to 4 modulation amplitude was 4 G and microwave power was 10 mW.

For the definition of the symbols please refer to the text.

* All experiments were carried out at room temperature.

Table 4.3

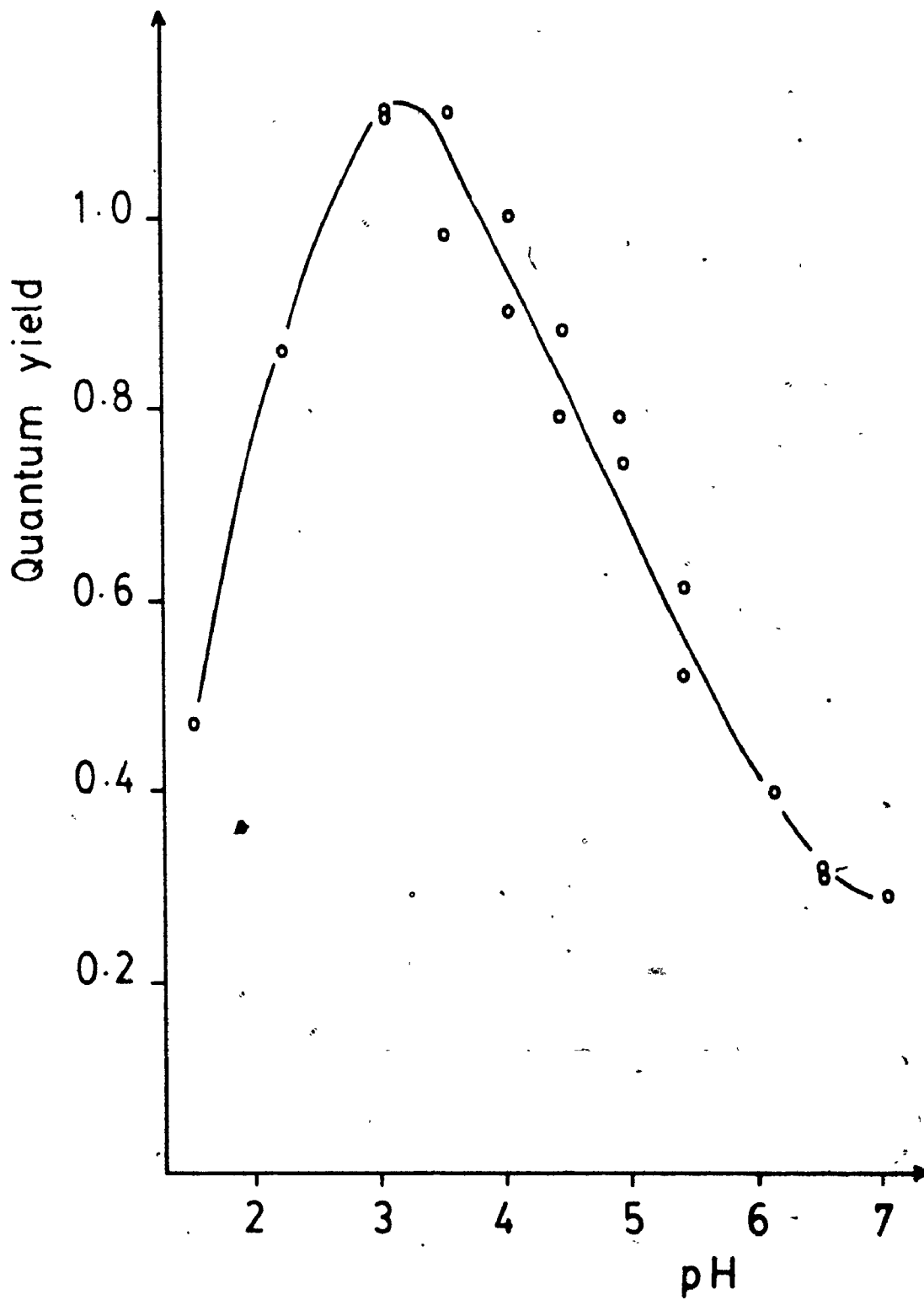
Summary of the Uncertainties in the Quantum
Yield Measurements

Standard deviation from	
Measurement of B	6.5 %
Intensity measurement	3.3 %
Slope measurement	5.8 %
Eq. 4.18	6.0 %
Estimated instrumental error	
Calibration with standard and retuning the spectrometer	2.0 %
From the radiometer	2.0 %
	<hr/>
Square root of sum of squares of the above	11.4 %

Figure 4.13

The pH Dependence of the Quantum Yield
of the Formation of $\text{NMPH}^{\cdot+}$

$\phi = 0.29$ at pH 7 was used as the reference point
in calculating the quantum yield at other pH's



2 molecules of NMPH^+ should be formed, if all photons absorbed result in the formation of the observed products.

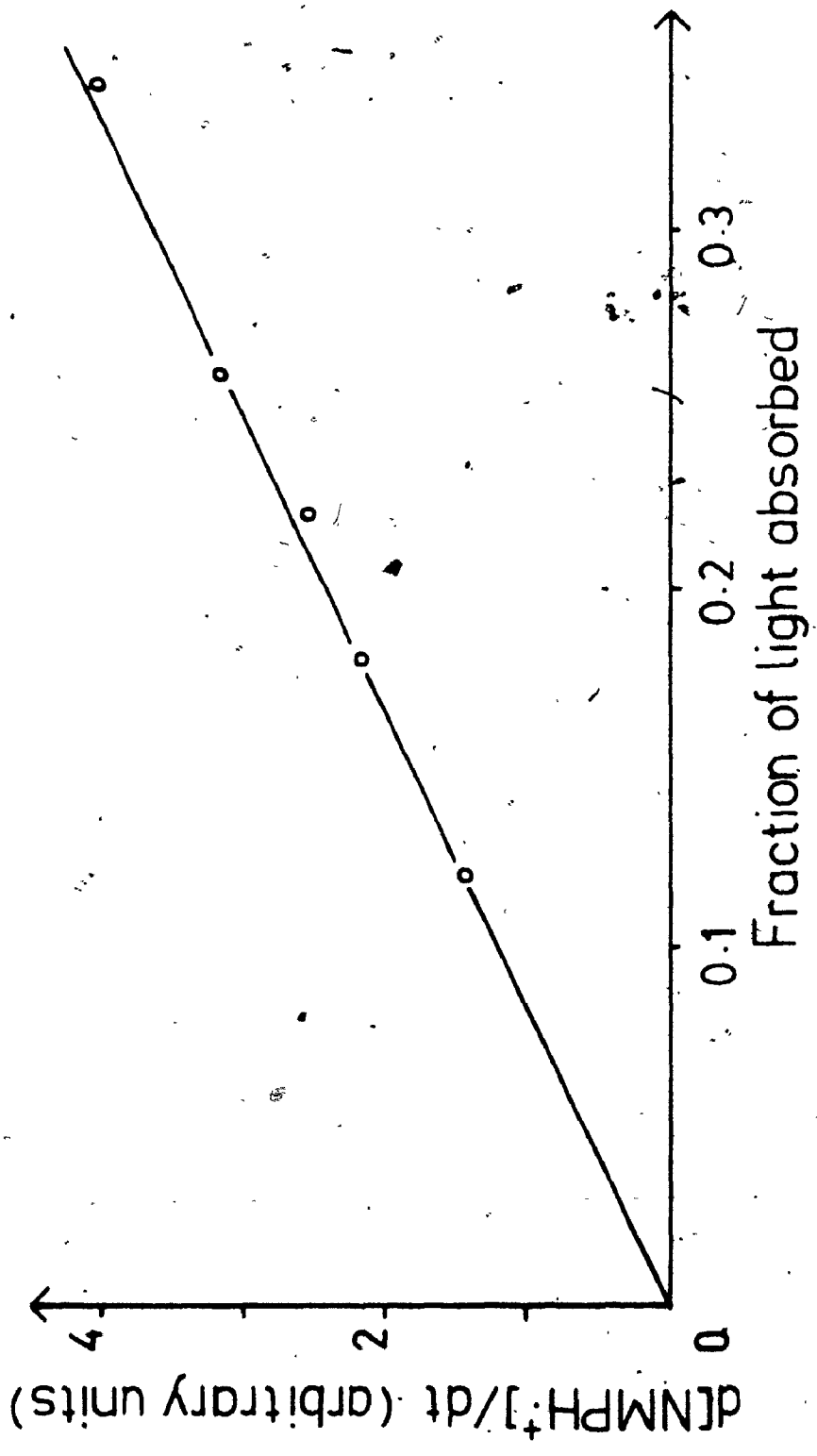
A similar experiment at pH 3 was carried out for various NMP^+ concentrations. Again the absorbance of the sample was kept below 0.2 so that less than 40 % of light was absorbed. It was found that there is a linear relation between the initial change in the ESR signal and the fraction of light absorbed by the sample (Fig. 4.14) which was calculated from the concentration of NMP^+ . But when the absorbance of NMP^+ sample is higher than 0.3 (more than 50 % of light is absorbed), the points obtained started to deviate from linearity probably due to nonuniformity in light intensity across the sample cell. The result means that the quantum yield for the formation of NMPH^+ is independent of the concentration of NMP^+ .



Figure 4.14

The Relation between the Initial Change in ESR Signal
and the Fraction of Light Absorbed by NMP^+ at pH 3.

Modulation amplitude 4 G, time constant 0.3 s, scan
time 1 min., microwave power 10 mW.



4.4 FLUORESCENCE AND REDOX BEHAVIOUR OF NMP^+

4.4.1 Fluorescence Behaviour

The fluorescence emission spectrum of NMP^+ in water shows a broad peak at 525 nm (Fig. 4.15). The excitation spectrum is virtually a mirror image of the optical absorption spectrum. The fluorescence intensity decreased very quickly while the excitation wavelength was set at 385 nm. Hence, the excitation wavelength was set at 360 nm where the drop is slower and the emission wavelength was fixed at 525 nm. The time dependence of the fluorescence intensity at 525 nm was measured. The initial fluorescence intensities at various pH values were then obtained by extrapolation to zero time. Fig. 4.16 shows the pH dependence of the fluorescence intensity. The intensity starts to drop around pH 4 and falls sharply as the pH is decreased below 3.

4.4.2 Fluorescence Quantum Yield

Eq. 3.14 in Section 3.6 was used to determine the fluorescence quantum yield. The standard used was quinine sulfate. The equation used is only good for dilute solutions (absorbance less than 0.05). Due to the low fluorescence yield of NMP^+ and sensitivity of the fluorimeter, the optical density of NMP^+ solution used was around 0.3. The fluorescence quantum yield was estimated to be 0.5 % in water. Because of the high absorbance of the solution, there is an incident light intensity gradient across the cell, and the measured fluorescence intensity is therefore somewhat underestimated so the figure of 0.5 % fluorescence yield should be considered as a lower limit, but probably is not higher than 1 %.

Figure 4.15

The Fluorescence Spectrum of NMP^+ in Water .

Excitation wavelength 360 ± 4 nm,

emission wavelength 525 ± 4 nm,

$[\text{NMP}^+] = 10^{-5}$ M.

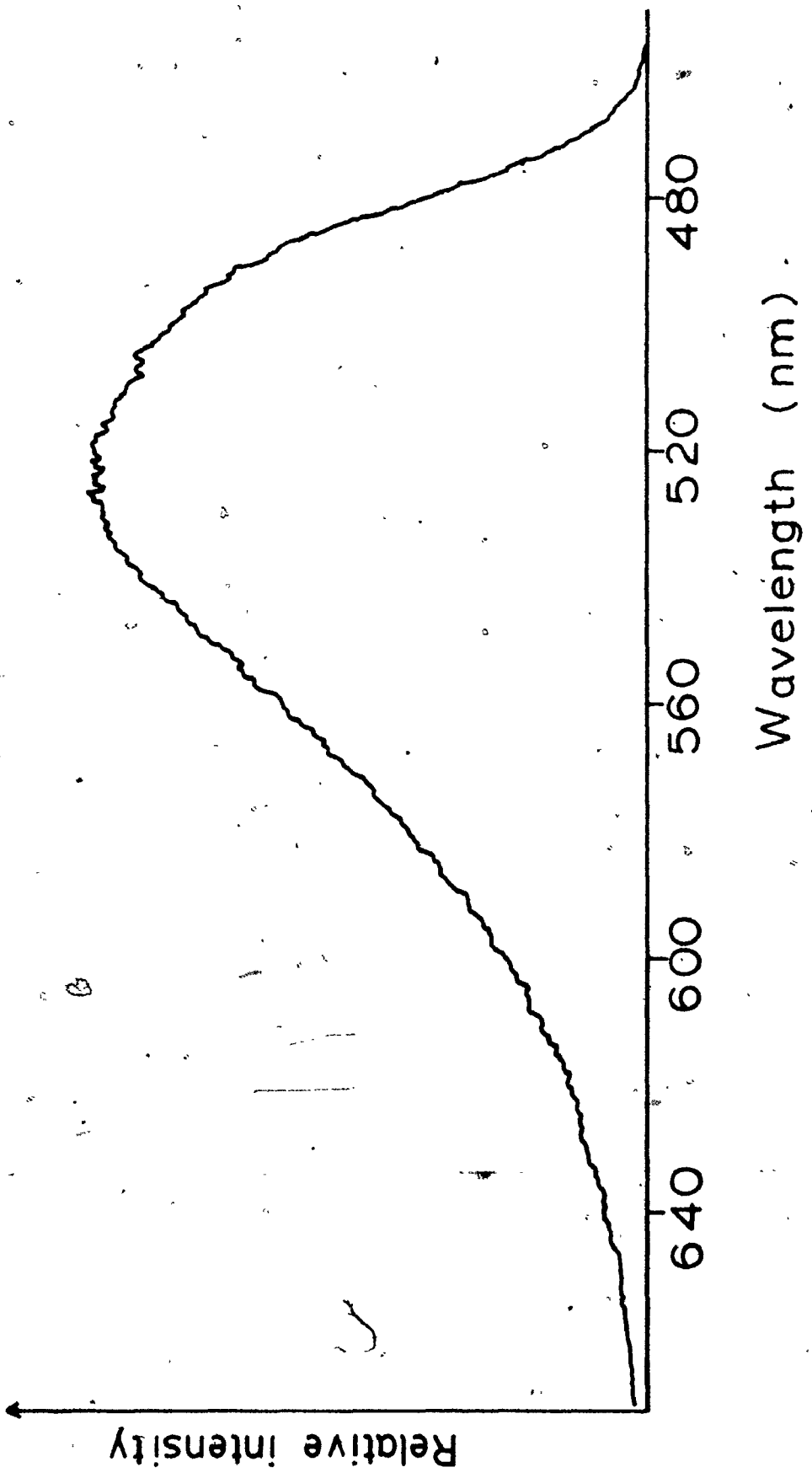
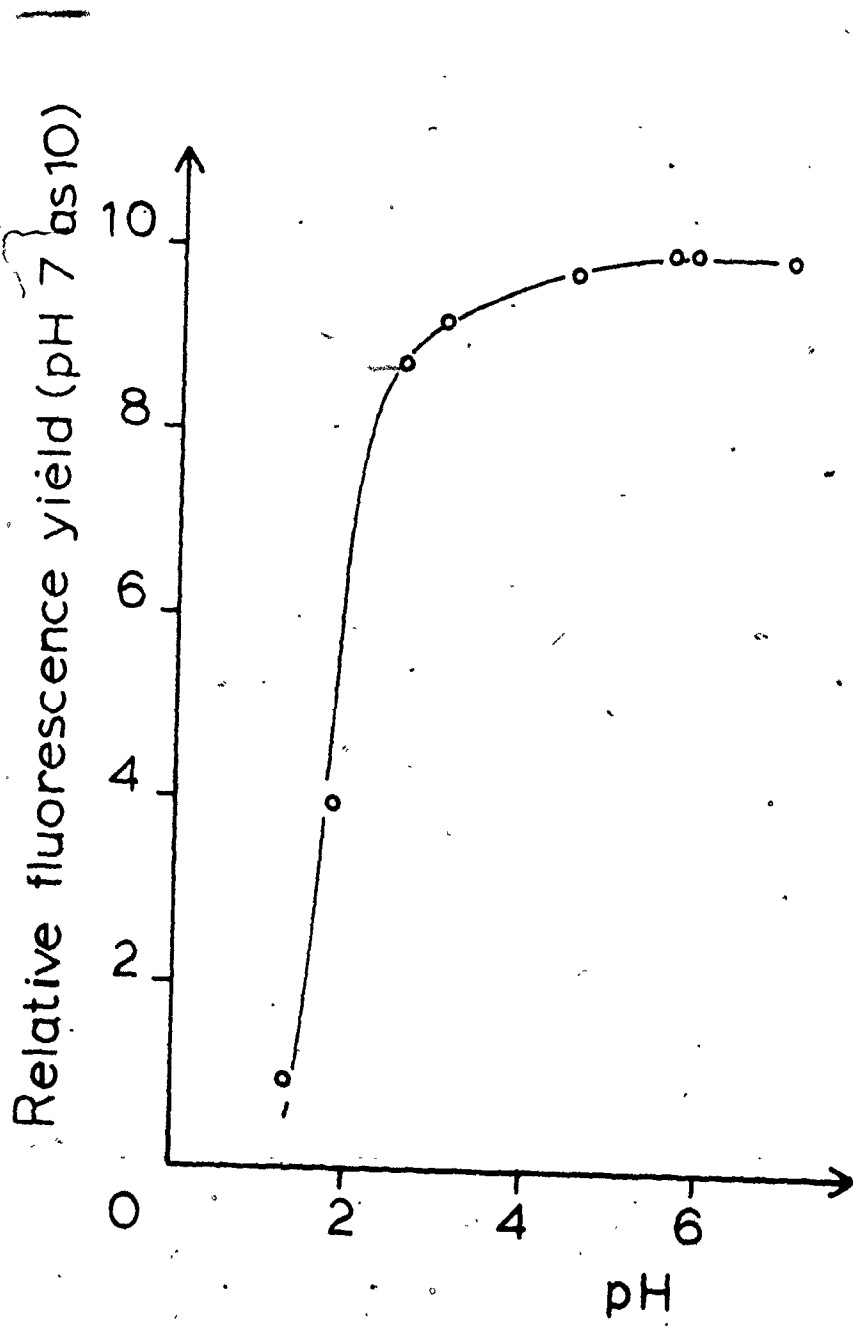


Figure 4.16

The Effect of pH on the Initial Fluorescence Yield
of NMP^+ Compared to that in Solution of pH 7.

Excitation wavelength 360 ± 4 nm,
emission wavelength 525 ± 4 nm,
 $[\text{NMP}^+] = 10^{-5}$ M.



4.4.3 Reactions Involving the Singlet State

Using the flash photolysis ESR technique with the magnetic field set at the peak of the $\text{NMPH}^{\cdot+}$ signal, the radical concentration formed after a flash was found to be same as in nitrogen - purged, air - saturated and oxygen - saturated aqueous solutions even though the decay rate of $\text{NMPH}^{\cdot+}$ is faster in the oxygenated solution. Since oxygen is a ground state triplet and a triplet quencher, and the formation of $\text{NMPH}^{\cdot+}$ is not affected by the presence of oxygen, this means that the reactive species is in a singlet state as suggested by Reaction 4.1. The fluorescence yields of a nitrogen - purged sample and an air - saturated sample are very similar, indicating that oxygen is not quenching the excited singlet state.

The rate of formation of $\text{NMPH}^{\cdot+}$ was measured at different light intensities by placing a neutral density filter in front of a krypton laser beam. The plot of the rate of the formation of $\text{NMPH}^{\cdot+}$ versus light intensity gives a straight line (Fig. 4.17) and so we conclude that the excitation process involves only one photon. The rate of formation of $\text{NMPH}^{\cdot+}$ at constant incident light intensity measured by ESR spectroscopy is also found to be proportional to the concentration of NMP^+ in solution (Fig. 4.18). Also recall that Fig. 4.14 shows that the quantum yield of the formation of $\text{NMPH}^{\cdot+}$ only depends on the fraction of light absorbed, further indicating this photochemical reaction is a one - photon process as shown in Reaction 4.1.

Fig. 4.16 shows the pH dependence of the fluorescence yield. It starts to drop off around pH 4. Rubaszewska and

Figure 4.17

The Relation between the Rate of Formation of
 NMPH^+ and the Light Intensity.

Modulation amplitude 4 G, time constant 0.3 s,
microwave power 5 mW.

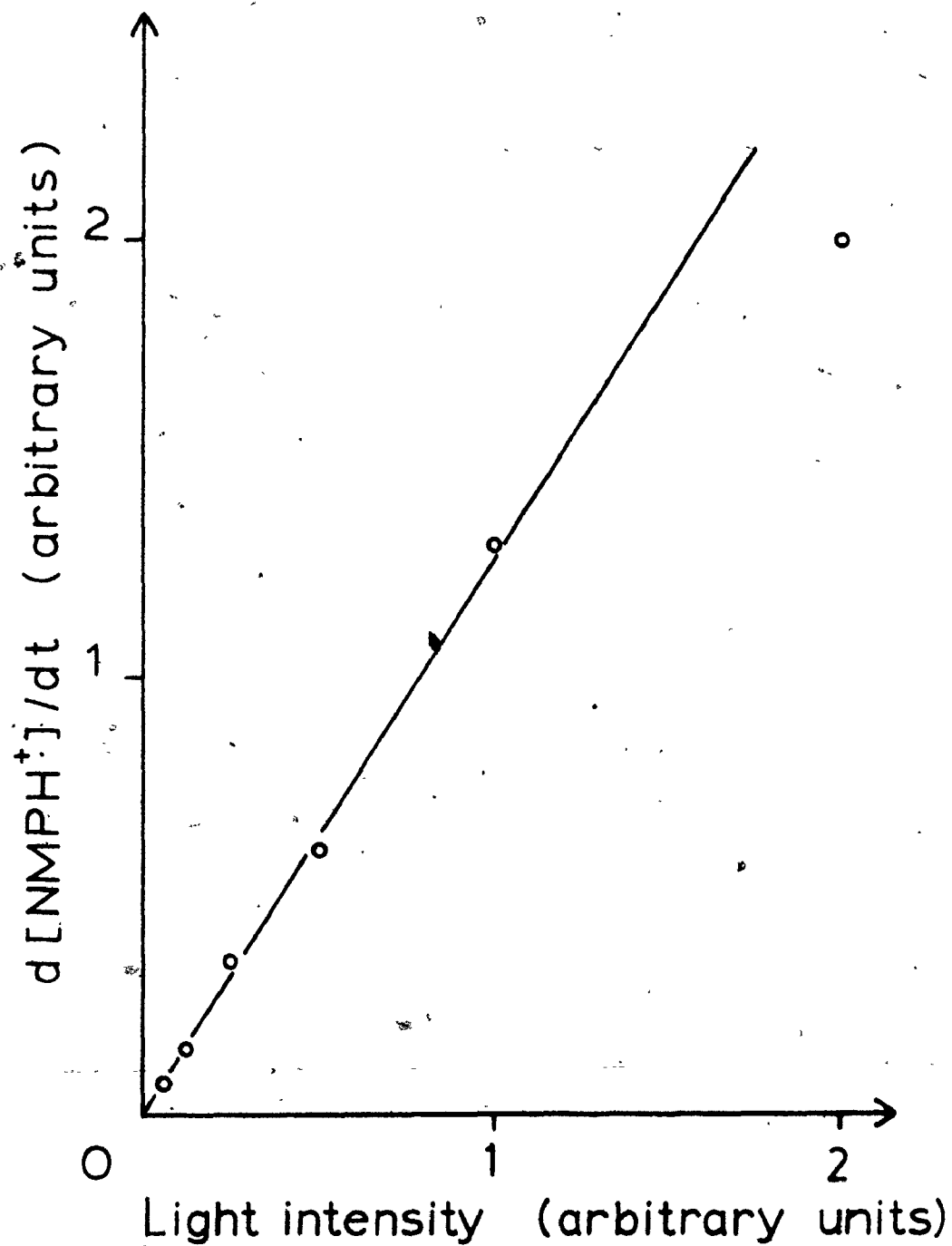
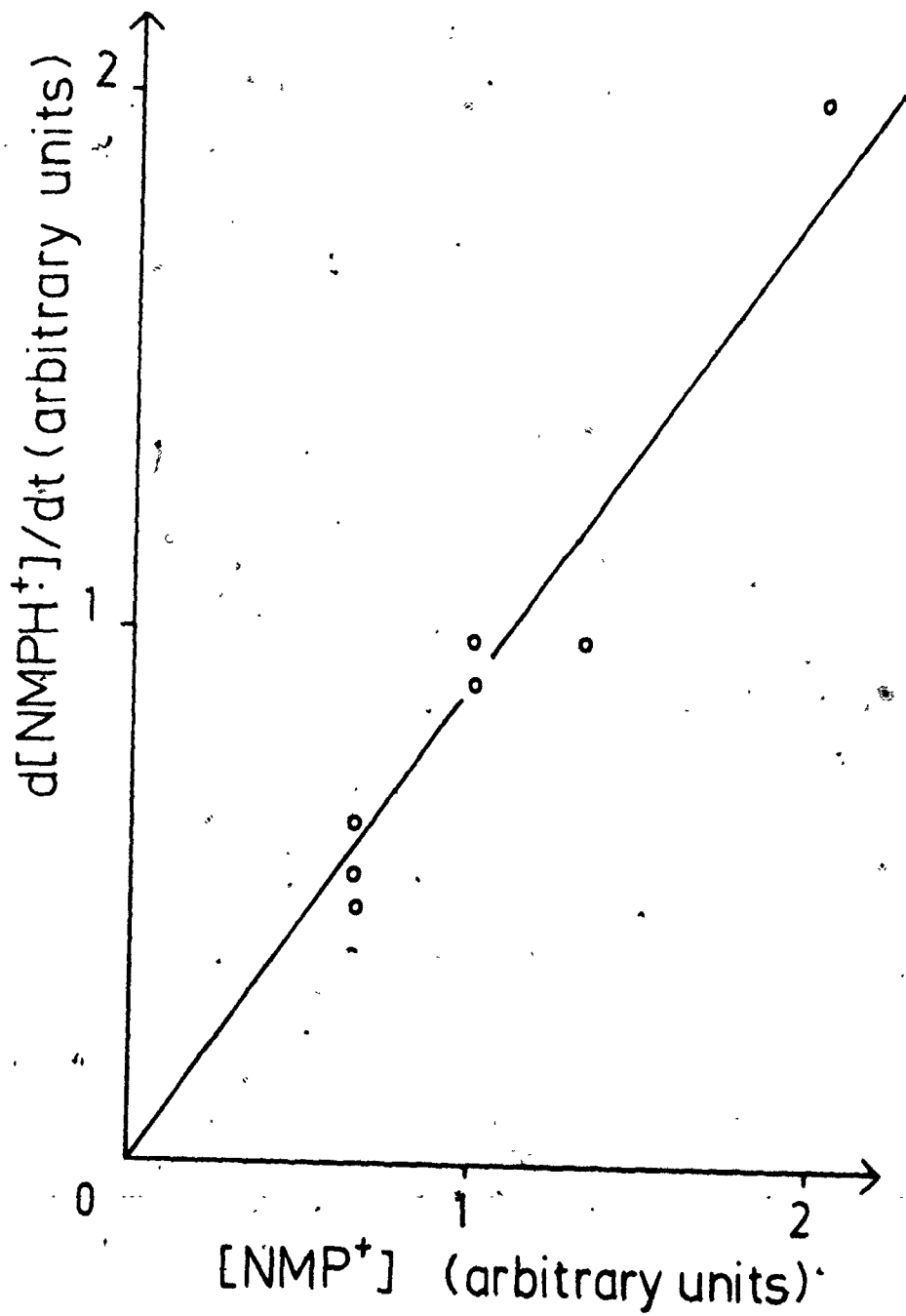


Figure 4.18

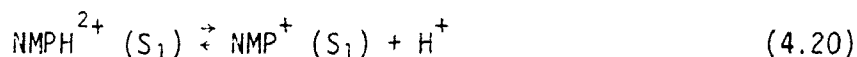
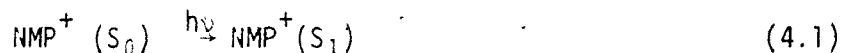
The Relation between the Rate of Formation of NMPH^+
and the Concentration of NMP^+ .

Modulation amplitude 4 G, time constant 0.3 s,
microwave power 5 mW.



5

Grabowski (25) reported that the pK_a value of the excited protonated NMP^+ ($NMPH^{2+}(S_1)$) is 3.3, that is at pH 3.3, the concentration of the unprotonated excited NMP^+ and the protonated excited NMP^+ are the same.



The excited protonated NMP^+ is the predominant species at pH below 3.3. The drop off of the fluorescence yield at 525 nm matches the drop off of the quantum yield of $NMPH^+$ (Fig. 4.13) at pH below 4. It would thus appear that $NMPH^{2+}(S_1)$ is non-fluorescent and photochemically inactive. The reactive species in this system is probably the excited unprotonated species, that is $NMP^+(S_1)$. The fluorescence yield and quantum yield at pH 2.3 are not equal to one-tenth of the yields at pH 3.3 where at equilibrium the concentration of $NMP^+(S_1)$ is only one-tenth of that of $NMPH^{2+}(S_1)$. This indicates that the protonation of $NMP^+(S_1)$ which requires the reaction of two cations is very slow compared to the rate of reactions involving $NMP^+(S_1)$. From the above results we conclude that $NMP^+(S_1)$ is the photochemically active state.

4.4.4 Redox Behaviour

Both NMP^+ and PYH^+ have been shown to undergo two separate one-electron reductions at pH values lower than 7. In order to establish the thermodynamically allowed reactions for the NMP^+ and pyocyanine systems, the redox potentials of NMP^+ at various pH's were determined. The redox behaviour of pyocyanine has been studied by Friedheim and Michaelis (42).

Potentiometric titration (Section 3.5) of NMP^+ in buffers at pH 2, 3 and 7 were carried out using chromous chloride as the reducing agent. The solution was purged with nitrogen throughout the experiment. The volume of chromous chloride consumed was less than 2 ml which is rather small when compared to the total volume of the solution (~ 100 ml). Fig. 4.19, 4.20 and 4.21 show plots of the potential E versus $\log(x/(u-x))$ at pH 2, 3 and 7 respectively; u is the amount of reductant used up at the end point of titration and x is the amount of reductant used. The potentials of NMP^+ at various pH values were determined from the intercepts of these straight lines. The number of electrons involved in the reduction steps were determined from the slopes of these lines.

Table 4.4 summarizes the results in various pH buffers. At low pH, two one - electron reduction steps are well separated. Hence, two end - points are obtained, and thus two different lines arise with same values of $x/(u-x)$. While at pH 7 two one - electron curves overlap and the titration curve becomes like that of a compound with only one two - electron step. The experimental slope values are considerably higher than the theoretical ones. Probably this is due to the error in $x/(u-x)$.

The formal potentials of pyocyanine (42) in various pH buffers are also shown in Table 4.4. From the potentials of NMP^+ and PYH^+ at pH 3, it can be shown that Reaction 4.8 is thermodynamically allowed.

Figure 4.19

The Potentiometric Titration of NMP^+ at pH 2.

Chromous chloride was used as the reducing agent.

u is the amount of reductant used up at the end point of titration and x is the amount of reductant used.

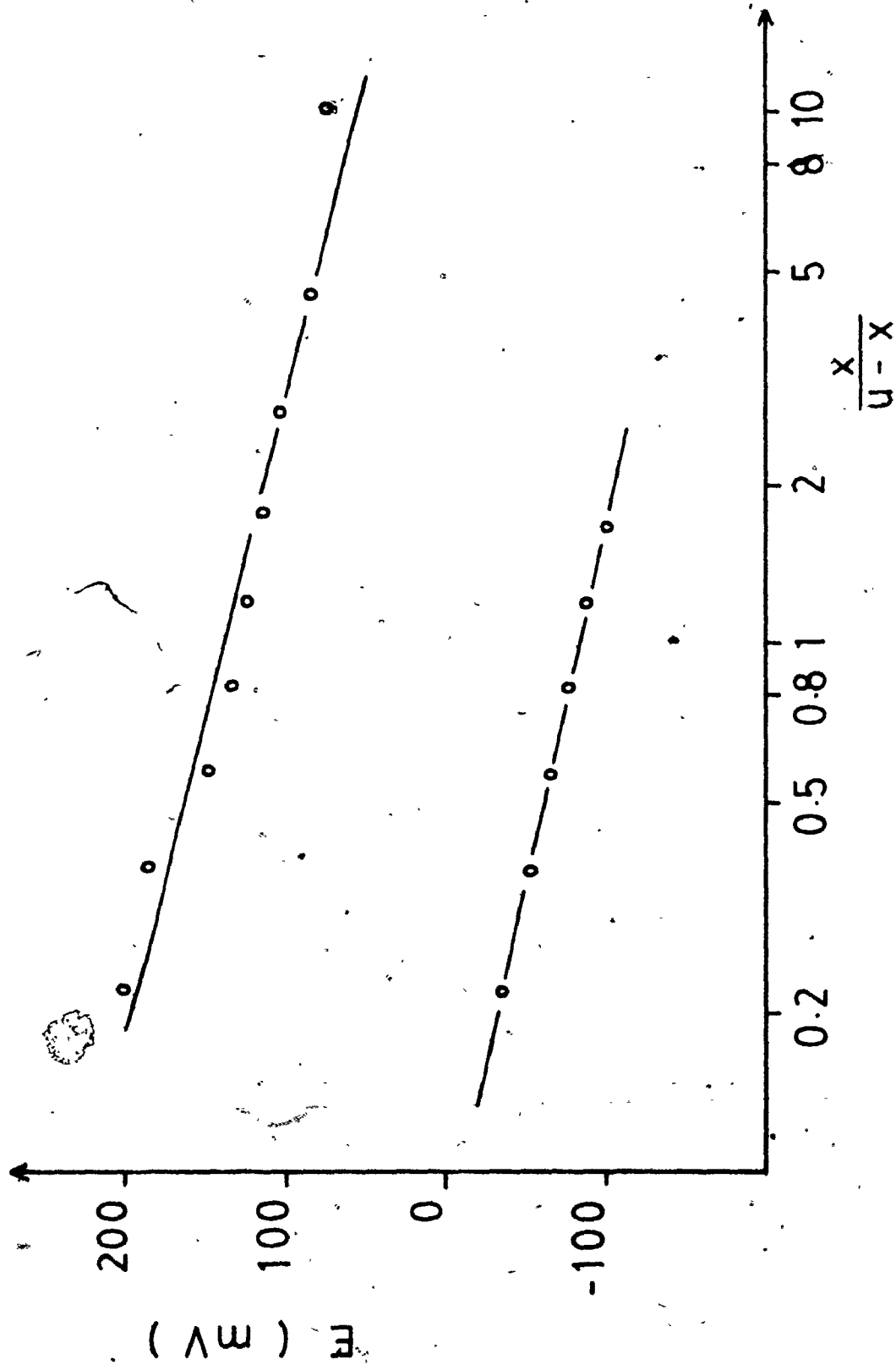


Figure 4.20

The Potentiometric Titration of NMP^+ at pH 3.

Chromous chloride was used as the reducing agent

u is the amount of reductant used up at the end point of titration and x is the amount of reductant used.

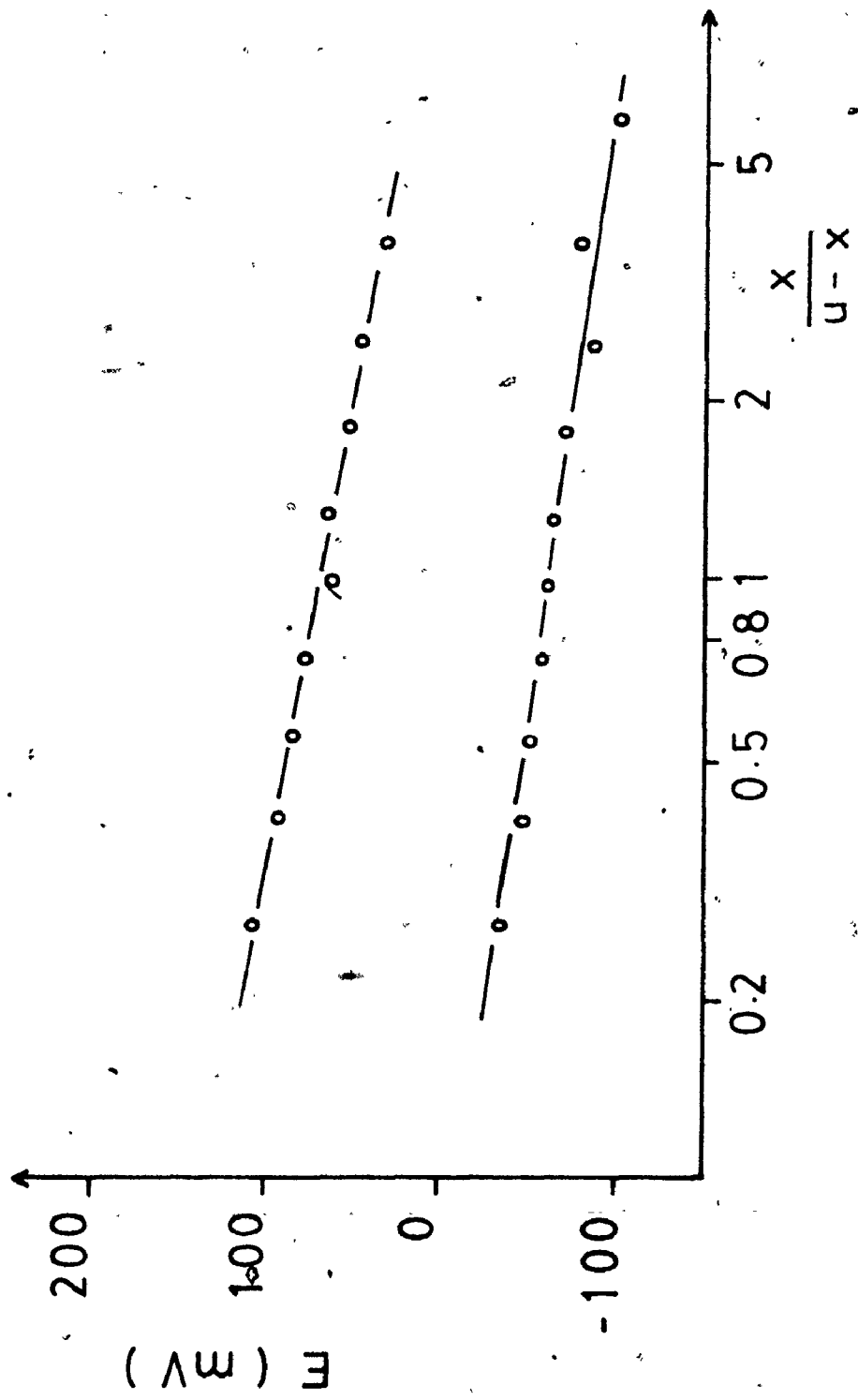


Figure 4.21

The Potentiometric Titration of NMP^+ at pH 7.

Chromous chloride was used as the reducing agent.

u is the amount of reductant used up at the end point of titration and x is the amount of reductant used.

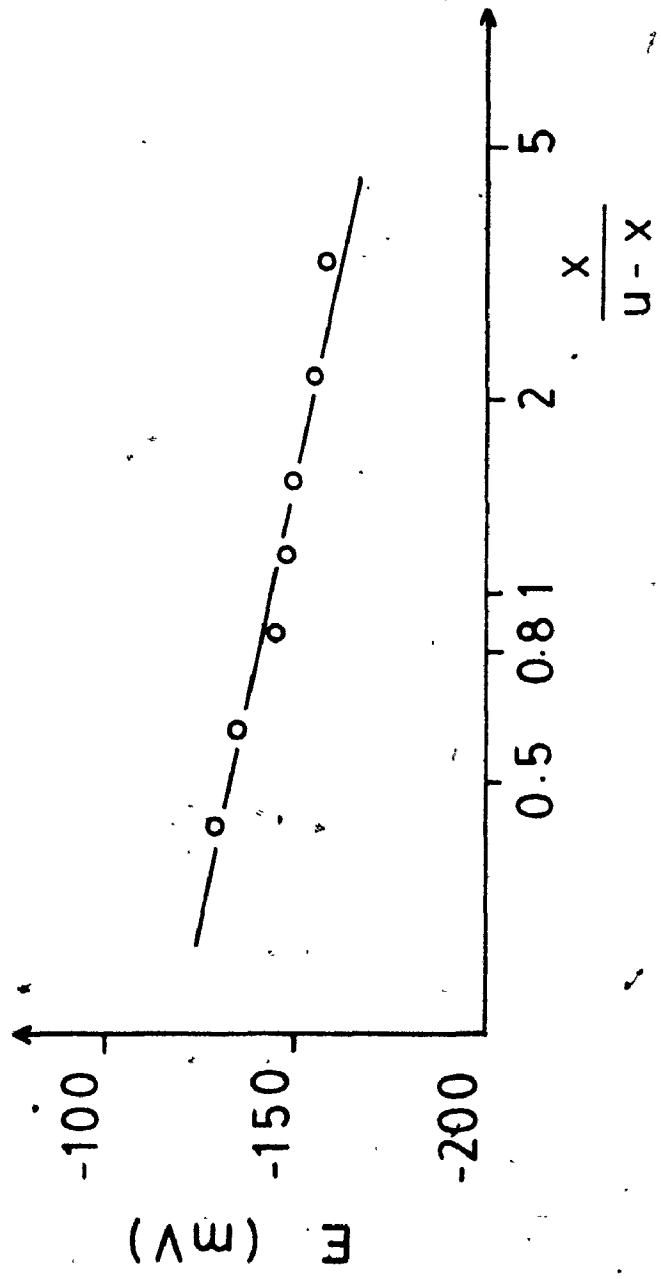


Table 4.4

The Apparent Reduction Potentials of NMP^+ at Various pH's

pH	slope ³	NMP^+		PY ⁴	
		E_1 (V)	E_2 (V)	E_1 (V)	E_2 (V)
2	-0.083 ± 0.008	0.38 ± 0.03		0.262	
	-0.072 ± 0.002		0.16 ± 0.01		0.097
3	-0.064 ± 0.002	0.31 ± 0.01		0.207	
	-0.049 ± 0.003		0.18 ± 0.01		0.097
7 ⁵	-0.034 ± 0.003	0.099 ± 0.007		-0.34	

$$^1 E_1 = E_1^0 - 0.059 \text{ pH}$$

$$E_2 = E_2^0$$

E_1^0 and E_2^0 are the apparent potentials at pH 0. E_1 depends on the pH of the solution while E_2 does not.

² All potentials are referred to the standard hydrogen electrode.

³ For a one-electron reduction step, slope should be -0.059 while for a two-electron reduction step, slope should be -0.030 . If the activities of all species are used in the calculation.

⁴ Obtained from Ref. 42.

⁵ A two-electron reduction.

4.5 OPTICAL FLASH PHOTOLYSIS

The final products of this photochemical reaction have already been identified as NMPH^+ and PYH^+ and their optical absorption maxima are known. The formation of these products can thus be followed using the optical flash photolysis technique, which can also be used to detect the formation of other intermediate species formed in the system. The kinetics of formation of NMPH^+ and pyocyanine were monitored at 443 nm and 525 nm respectively at pH 3, even though both NMP^\bullet and PYH^+ absorb at 525 nm and NMPH^+ , PYH^+ and NMP^+ all absorb at 443 nm. Nevertheless, PYH^+ and NMPH^+ are the species that absorb most strongly at 525 nm and 443 nm respectively at pH 3.

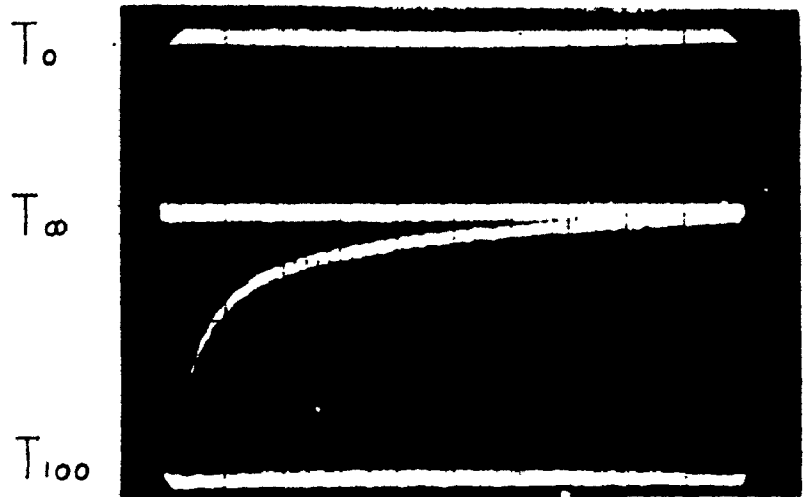
4.5.1 Rate Constant Determination

A 10^{-5} M NMPMS solution in 5×10^{-3} M phthalate buffer at pH 3 was nitrogen purged for at least fifteen minutes. It was found that there were no significant differences in the rise kinetics between a nitrogen purged and a vacuum degassed sample. Nitrogen purged samples were used for all the experiments unless otherwise stated. Typical traces at 443 nm and 525 nm are shown in Fig. 4.22. Fig. 4.23 and Fig. 4.24 show the $\log(A_\infty - A)$ plot as a function of time at 443 nm and 525 nm respectively, where A is the absorbance at time t and A_∞ is the absorbance about two seconds after the firing of the photolysis flash lamp. (The duration of the photolysis flash lamp is about 75 μs). The slope of the straight line of $\log(A_\infty - A)$ versus time was determined using the weighted least squares method and is equal to $-k/2.303$ where k is the rate constant of the reaction. Since there is a linear relation between

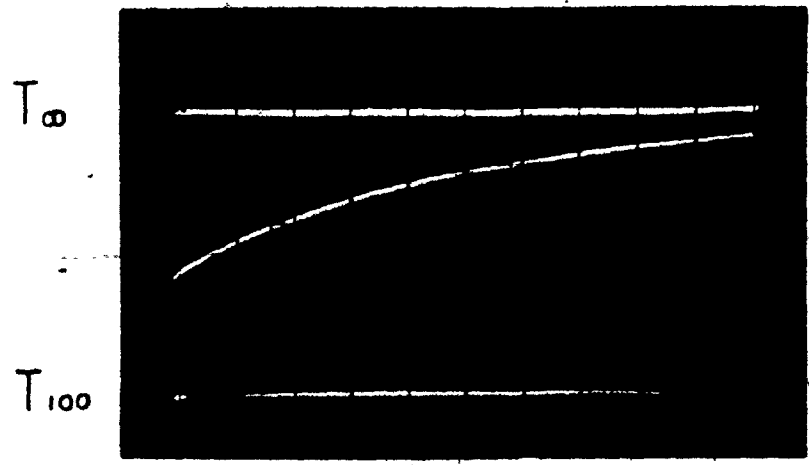
Figure 4.22

The Original Traces Obtained in the Optical Flash
Photolysis at 443 nm and 525 nm.





1ms full scale 443 nm



50 ms full scale 525 nm

Figure 4.23

The First Order Kinetics Plot Measured
at 443 nm at pH 3.

This is a semi-log plot, $[NMP^+] = 10^{-5}$ M.

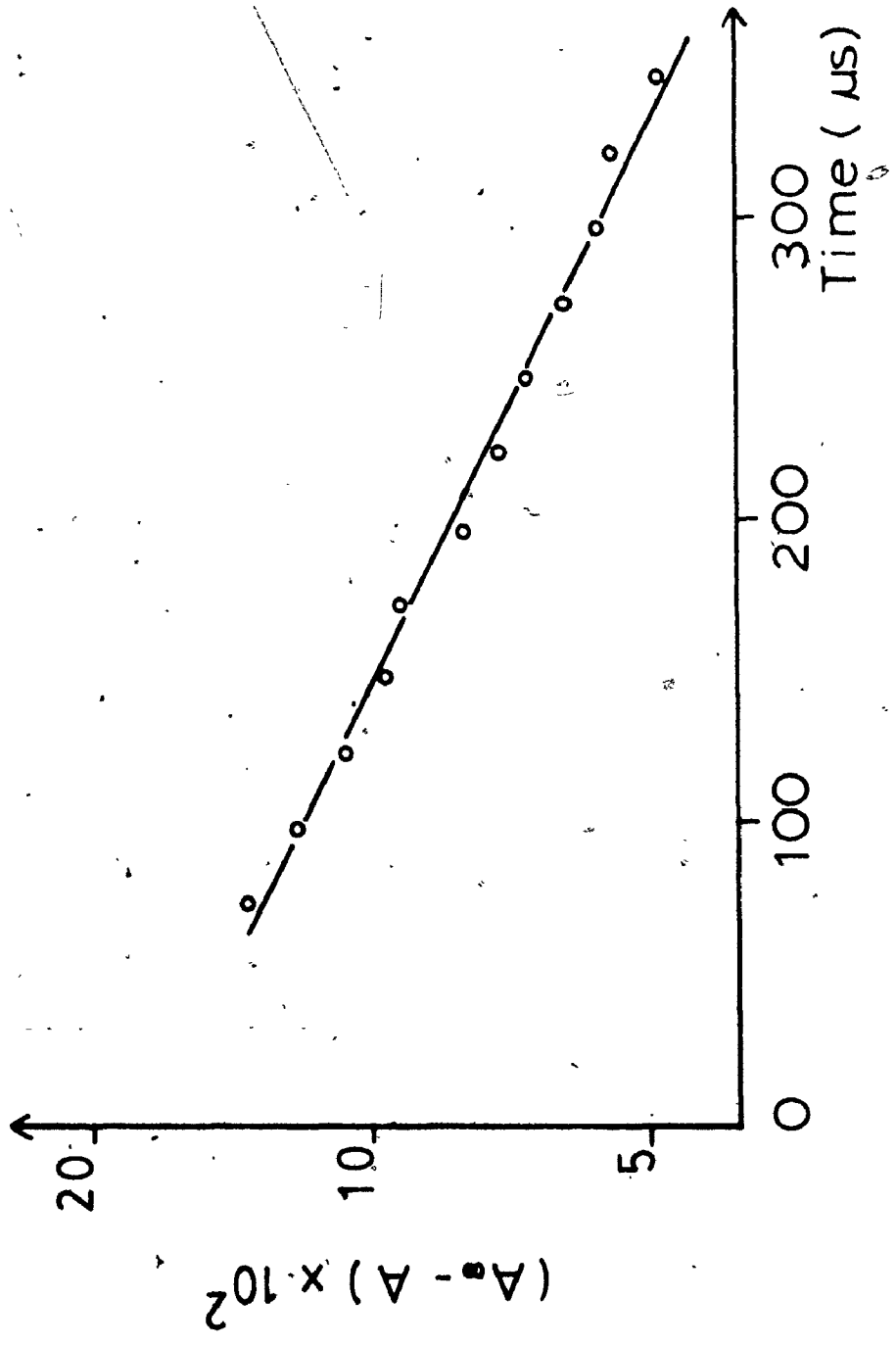
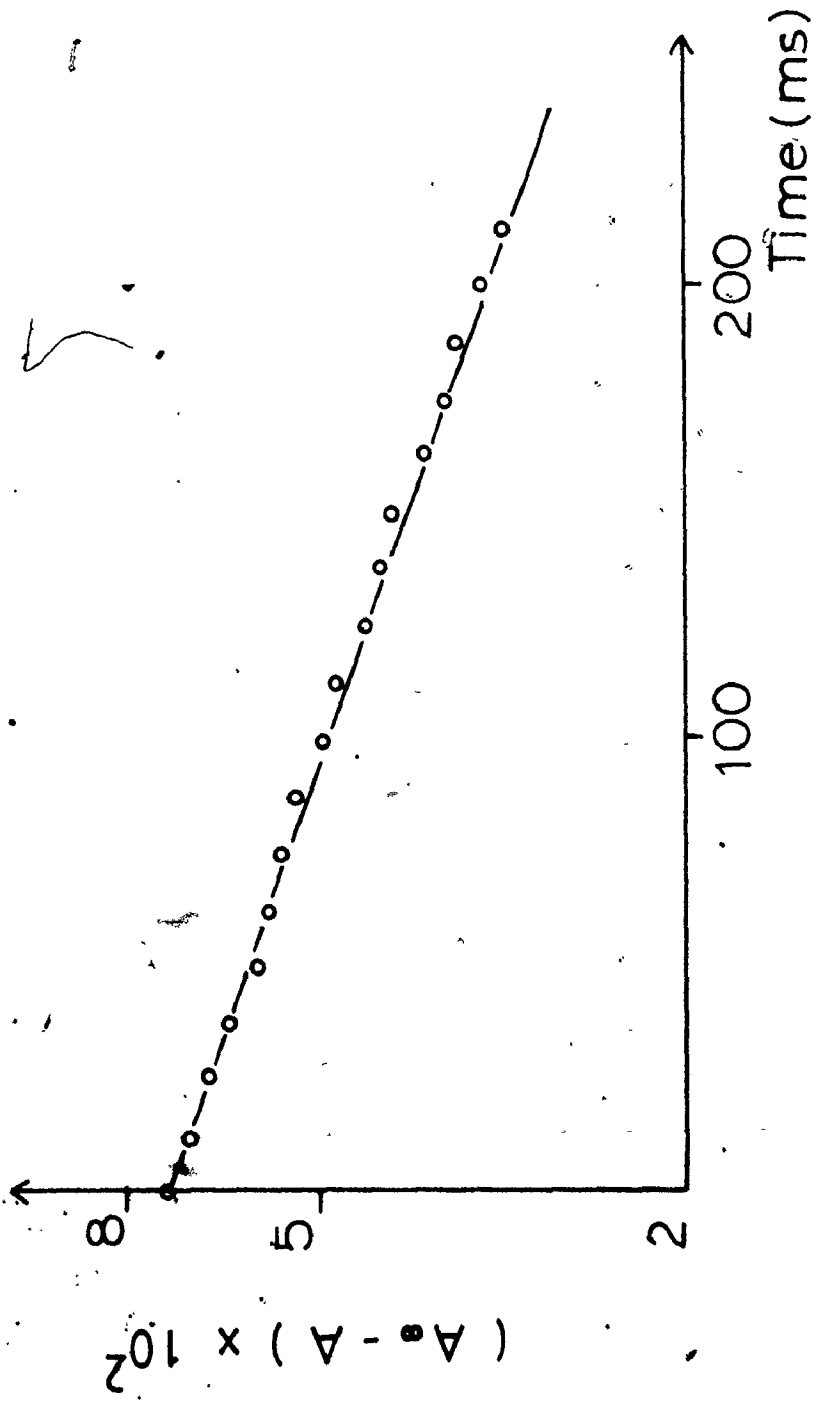


Figure 4.24

The First Order Kinetics Plot Measured
at 525 nm at pH 3

This is a semi-log plot, $[NMP^+] = 10^{-5}$ M.



$\log (A_{\infty} - A)$ and time, this suggests that the reaction is either first order or pseudo first order. Similar experiments were carried out at various NMP^+ concentrations at pH 3. It was found that both rate constants are proportional to the concentration of NMP^+ ; hence, both reactions are pseudo first order. In other words, the reaction is a second order reaction and the concentration of one of the reactants (namely, NMP^+) is considerably larger than the other. From Fig. 4.25 and 4.26, second order rate constants (k_5 and k_8), which are equal to the slopes of the straight lines, were found to be $(7.7 \pm 1.1) \times 10^8 \text{ M}^{-1} \text{ s}^{-1}$ and $(5.8 \pm 0.9) \times 10^6 \text{ M}^{-1} \text{ s}^{-1}$ for the formation of NMPH^+ and pyocyanine (Reaction 4.8) at pH 3 respectively. It will be shown in Section 4.5.2 and Section 4.10 that $\text{NMP}\cdot$ is formed first and is followed by fast protonation to give NMPH^+ . The above rate constant for the formation of NMPH^+ is actually the rate constant for Reaction 4.5. The chronological order of appearance of NMPH^+ and PYH^+ suggests that Reactions 4.5 and 4.7 proceed before Reaction 4.8.

It was found that the kinetics monitored at 433 nm are complex. First there is a fast rise which is then followed by a slow decay. The slope of the plot, $\log (A_{\infty} - A)$ versus time, of the fast rise portion was compared to that at 443 nm of the same NMP^+ concentration at pH 3 (Fig. 4.27). This shows that both straight lines have the same slope within experimental error, that is, the rate constants of the formation of this species and that of NMPH^+ are the same. The first order rate constant of the slow decay at 433 nm is close to that of the formation of pyocyanine at 525 nm

Figure 4.25

The Effect of the Concentration of NMP^+ on the Pseudo
First Order Rate Constant of Reaction 4.5 Measured at
443 nm and at pH 3.

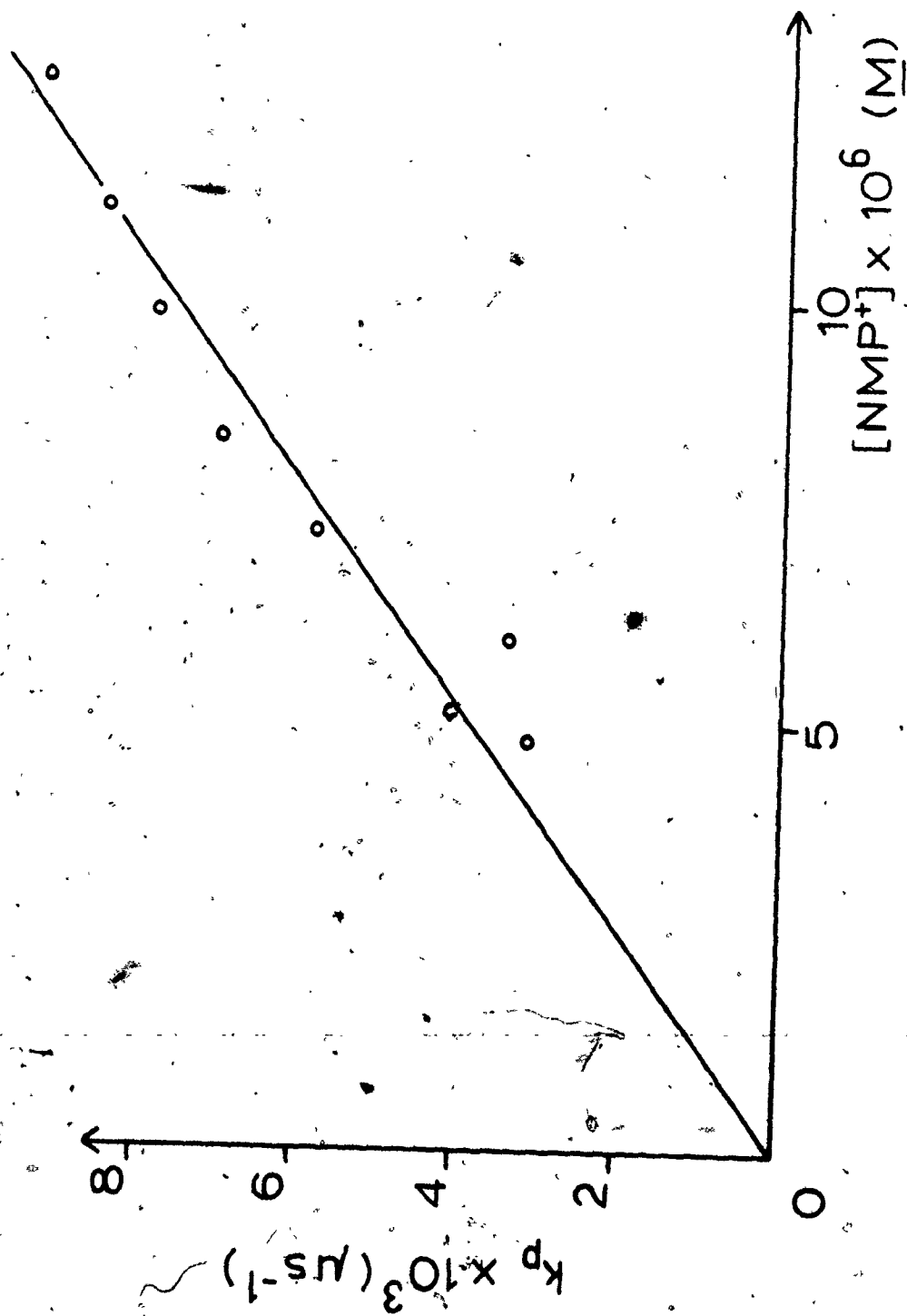


Figure 4.26

The Effect of the Concentration of NMP^+ on the Pseudo
First Order Rate Constant of Reaction 4.8 Measured at
525 nm and at pH 3.

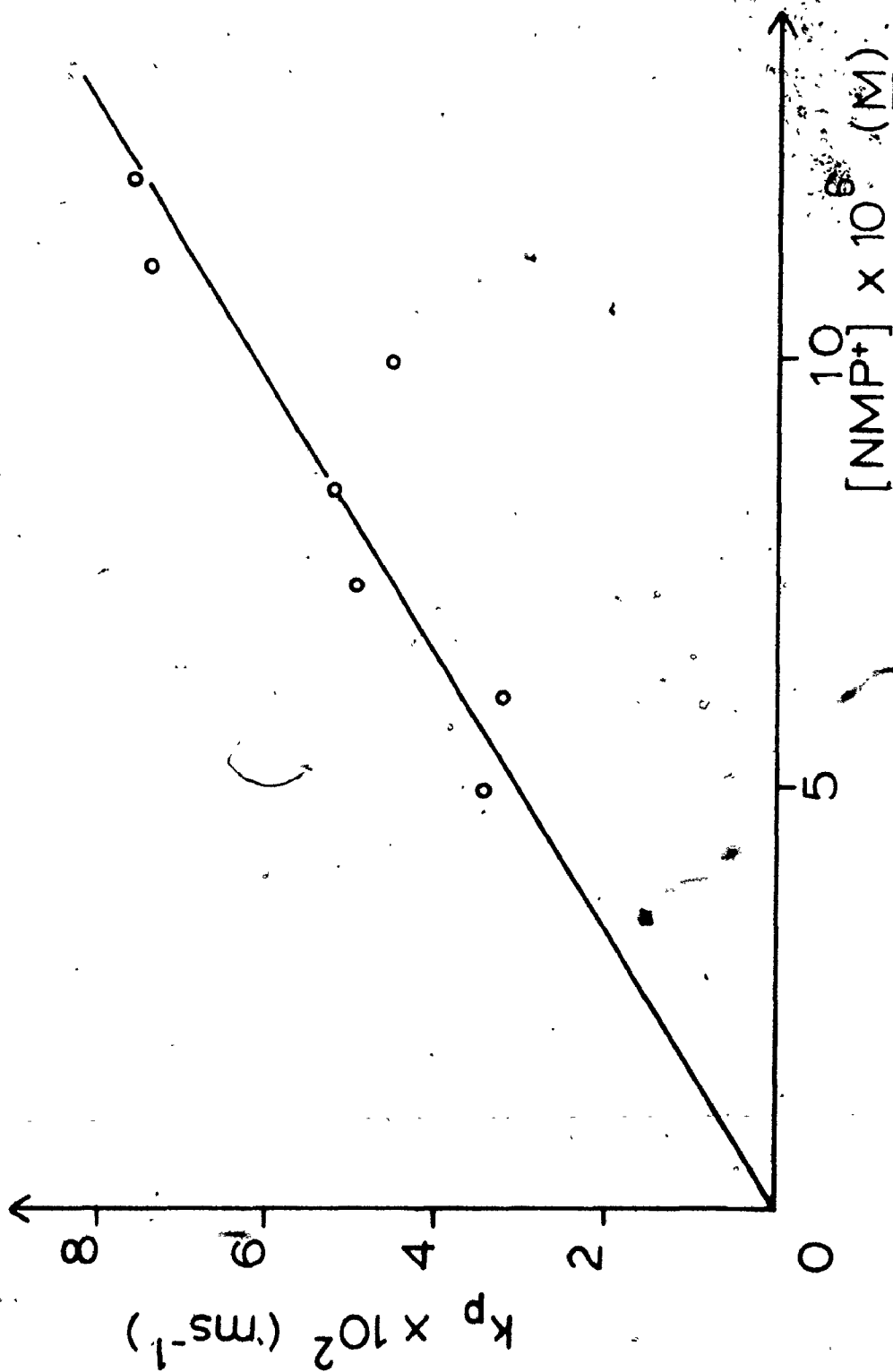
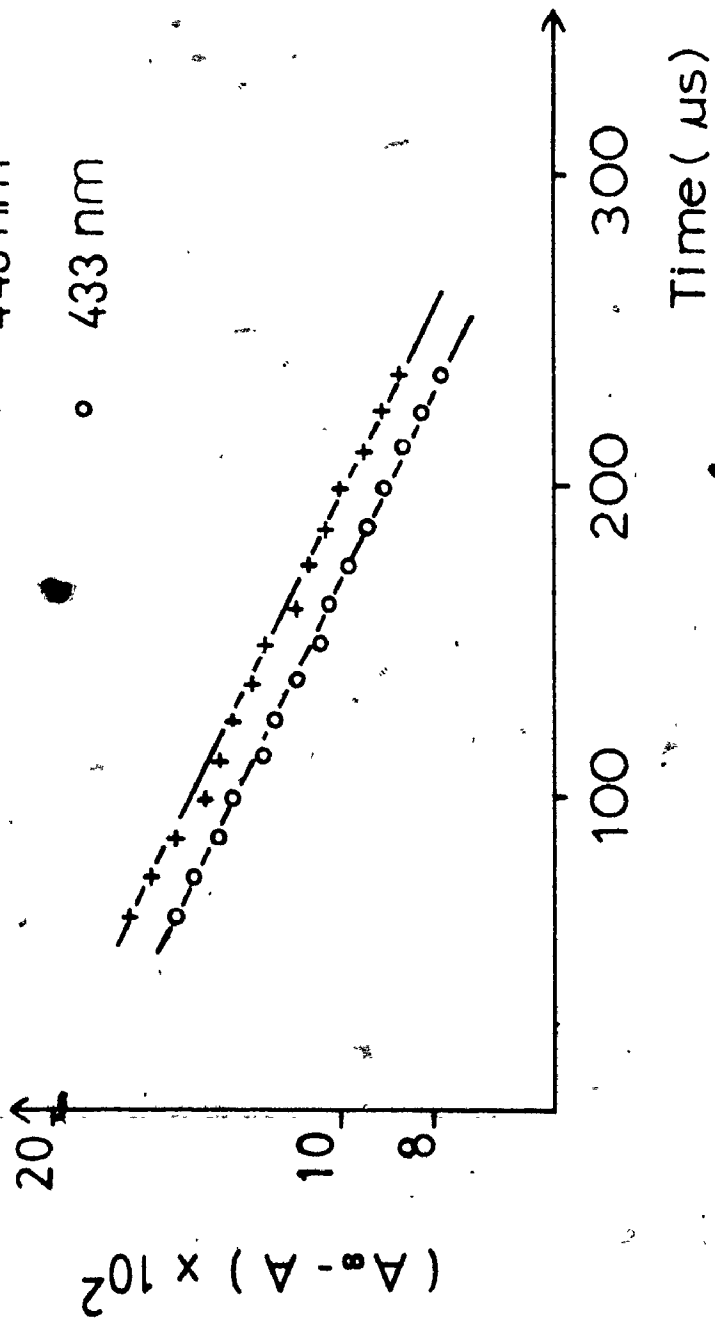


Figure 4.27

The Comparison of Rise Kinetics at 443 nm
and 433 nm at pH 3.

This is a semi-log plot; $[NMP^+] = 10^{-5}$ M.



at pH 3 (Fig. 4.28). Zaugg (14) reported that semireduced pyocyanine (PYH_2^+) absorbs at 433 nm. Thus we propose that PYH_2^+ is formed in Reaction 4.5, and then reacts with NMP^+ to give PYH^+ (Reaction 4.8), since the rise time of PYH_2^+ is the same as that of NMPH^+ and its decay matches the rise of PYH^+ . These results also suggest that protonation (Reaction 4.7) at pH 3 is fast so that the rise kinetics of NMPH^+ matches that of PYH_2^+ . It has been shown in Section 4.4.4 that Reaction 4.8 is allowed thermodynamically.

The kinetics were monitored from 320 nm to 680 nm at pH 3 in 10 nm intervals to search for a species with a decay time similar to the rise time of the formation of NMPH^+ but the search was unsuccessful. Especially in the region between 350 nm and 400 nm, any information would be masked by the bleaching of the ground state NMP^+ which has a strong absorption peak at 385 nm.

4.5.2 A Transient Species at 525 nm

In the pH dependence experiments (see Section 4.6), a transient species was found accidentally around 525 nm which started to decay right after the firing of the photolysis lamp. The rate of decay is faster than the rate of formation of PYH^+ which is in the millisecond region. The initial signal intensity (absorbance) of the transient increases as the pH of the solution increases (Fig. 4.29) which is different from the behaviour of the pyocyanine absorbance (Fig. 4.37). Fig. 4.30 shows that the decay kinetics at pH 4.75 in the log (A) versus time plot is biphasic. When the same reaction was carried out without nitrogen purging, the fast decay

Figure 4.28

The Comparison of the Rise Kinetics at 525 nm and
the Decay kinetics at 433 nm at pH 3.

These are semi-log plots; $[NMP^+] = 10^{-5}$ M.

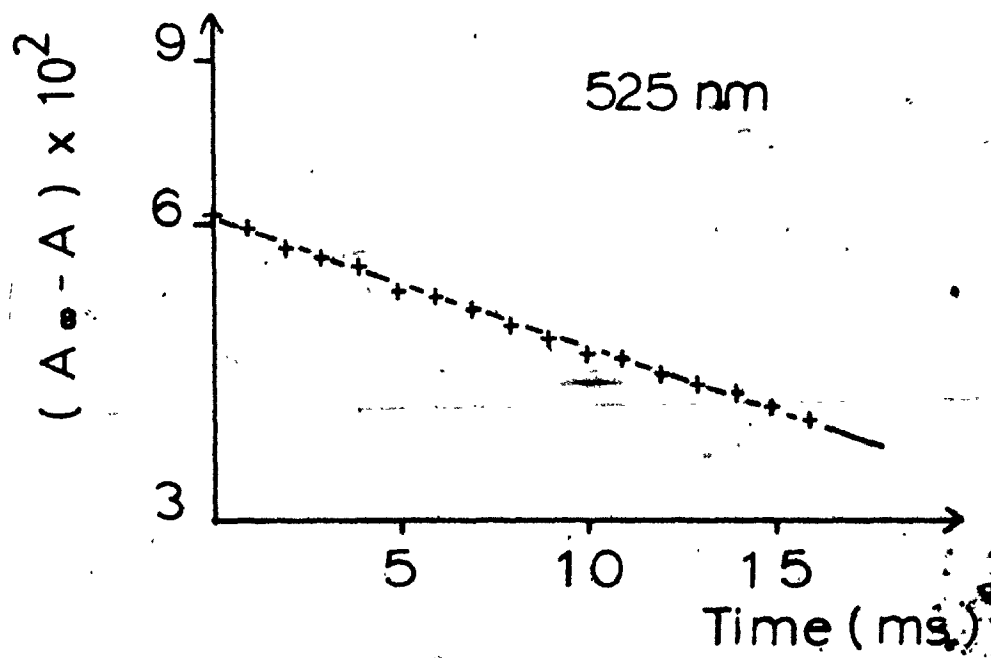
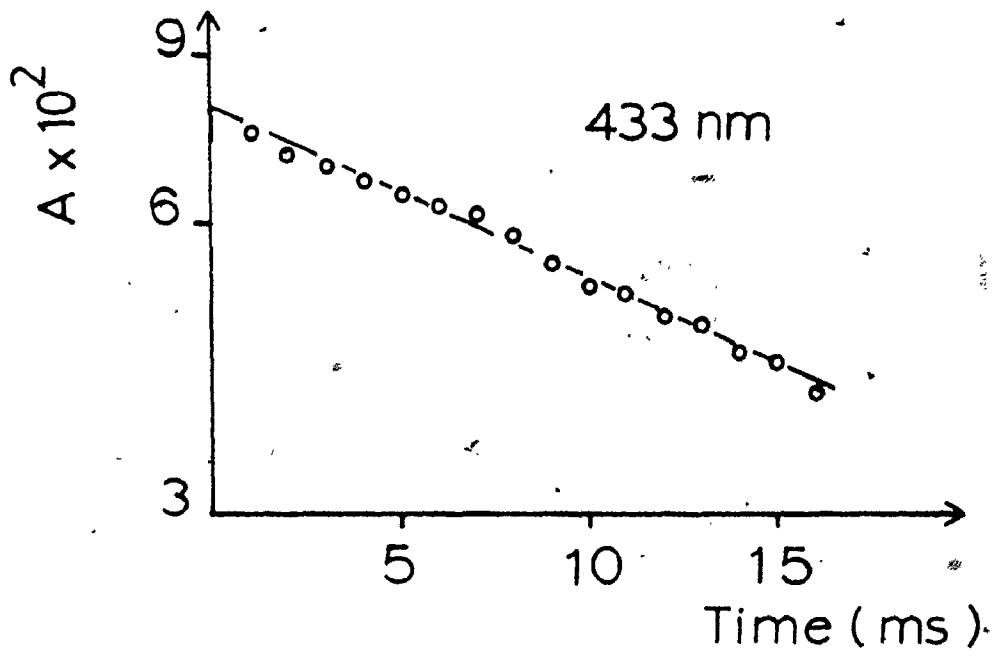


Figure 4.29

The Effect of pH on the Maximum Yield of the
Fast Decay Transient Detected at 525 nm.

$$[\text{NMP}^+] = 10^{-5} \text{ M.}$$

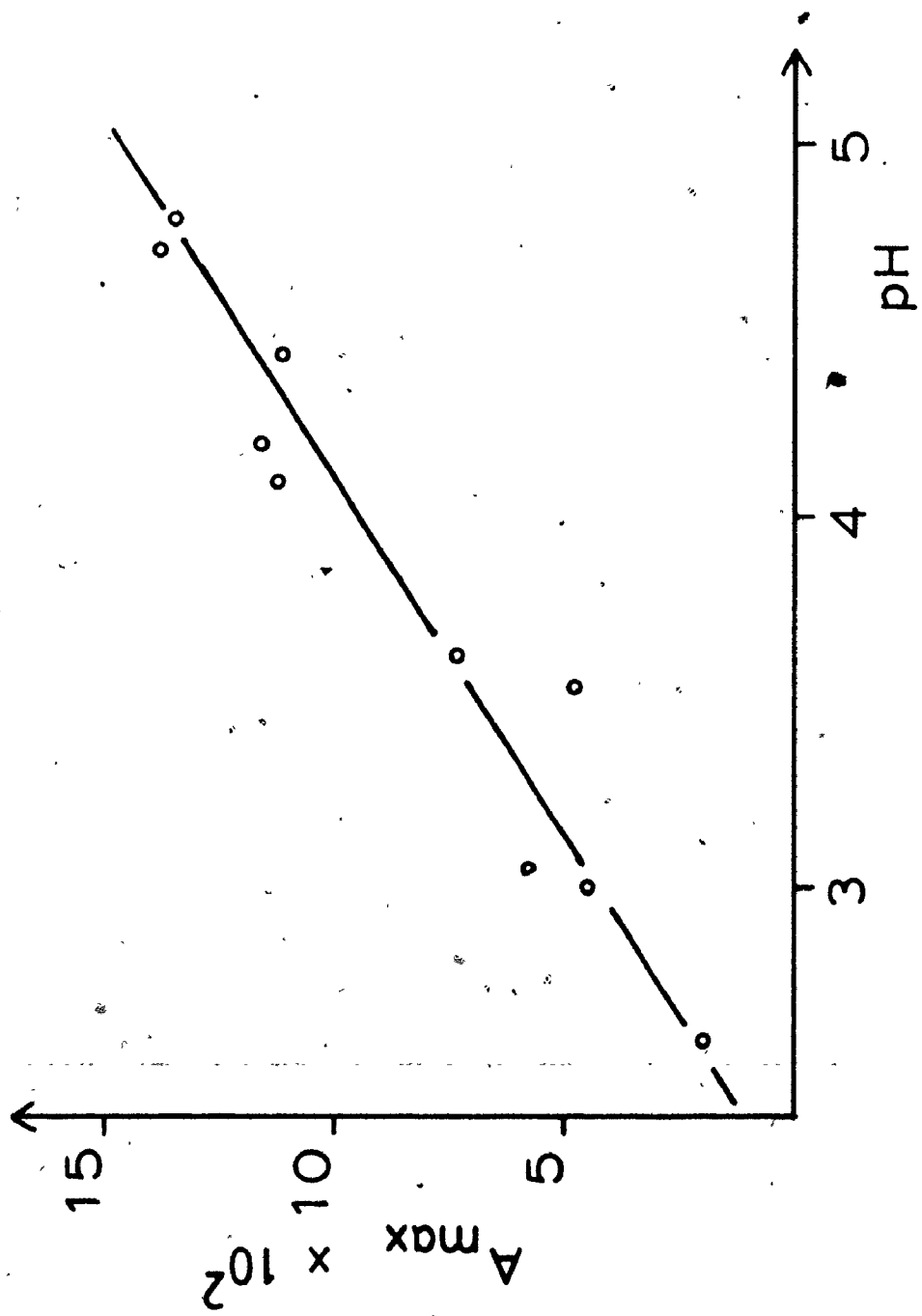
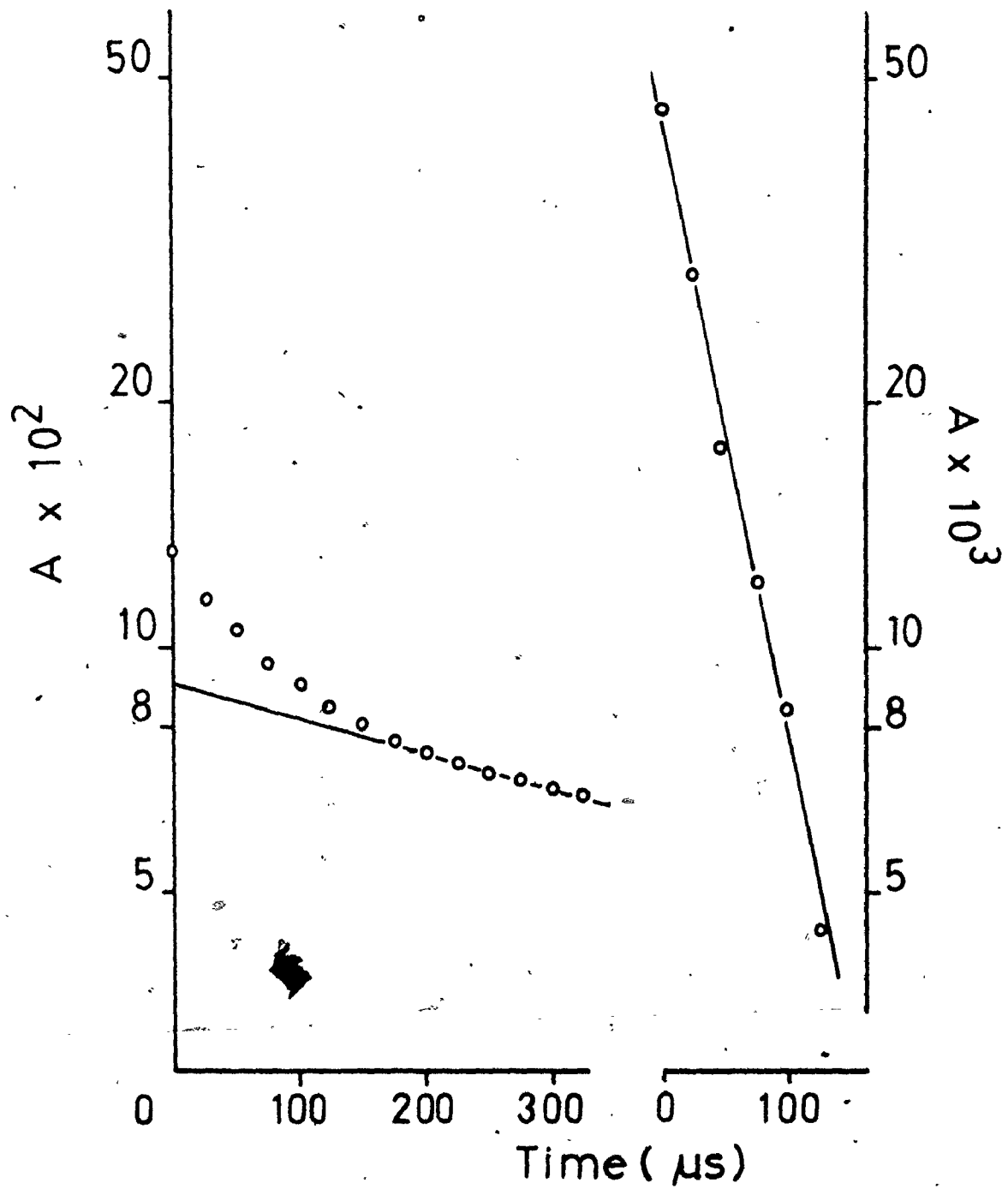


Figure 4.30

The Transient Observed at 525 nm (left) and the Decay Kinetics of the Fast Decay Component (right).

The rate constant of the slow decay was determined using the data at longer time scale. The contribution from the slow portion was subtracted from the data in the short time region. These values were then replotted at the right and used to determine the rate constant of the fast decay.



portion disappeared. The reaction is a first order one, that is, the $\log(A)$ versus time plot gives a straight line. This suggests that the biphasic character of the decay kinetics at 525 nm is due to the presence of two species.

The contribution from the slow portion was subtracted from the data before the rate constant of the fast decay portion was calculated. It was found that both the rate constants of the fast decay portion and the slow decay portion are independent of the concentration of NMP^+ (Fig. 4.31). Thus, the transient is not the intermediate X because the decay of X should depend on the concentration of NMP^+ . The rate constants of both decays were determined in various pH buffer solutions. The signal amplitude became very small below pH 7.5 and hence measurements were not possible below this pH. Fig. 4.32 shows that the rate constant of the fast portion of the transient is independent of the concentration of the hydronium ion.

The fast decay transient is quenched by air. It has been shown in Section 4.4.3 that the fluorescence yield of NMP^+ is not affected by the presence of air. The fast decay component probably arises from the triplet state of NMP^+ which returns to ground state of NMP^+ (Reaction 4.3) either by phosphorescence or by radiationless decay. If the reaction is a first order reaction then the rate constant (k_3) will be about $2 \times 10^4 \text{ s}^{-1}$.

Since the formation of PYH^+ at 525 nm is much slower than the fast decay, it can be neglected in the determination of the

Figure 4.31

The Effect of the Concentration of NMP^+ on the Rate
Constants of Both Fast and Slow Decay Transients

Measured at 525 nm at pH 4.8.

$$[\text{NMP}^+] = 10^{-5} \text{ M.}$$

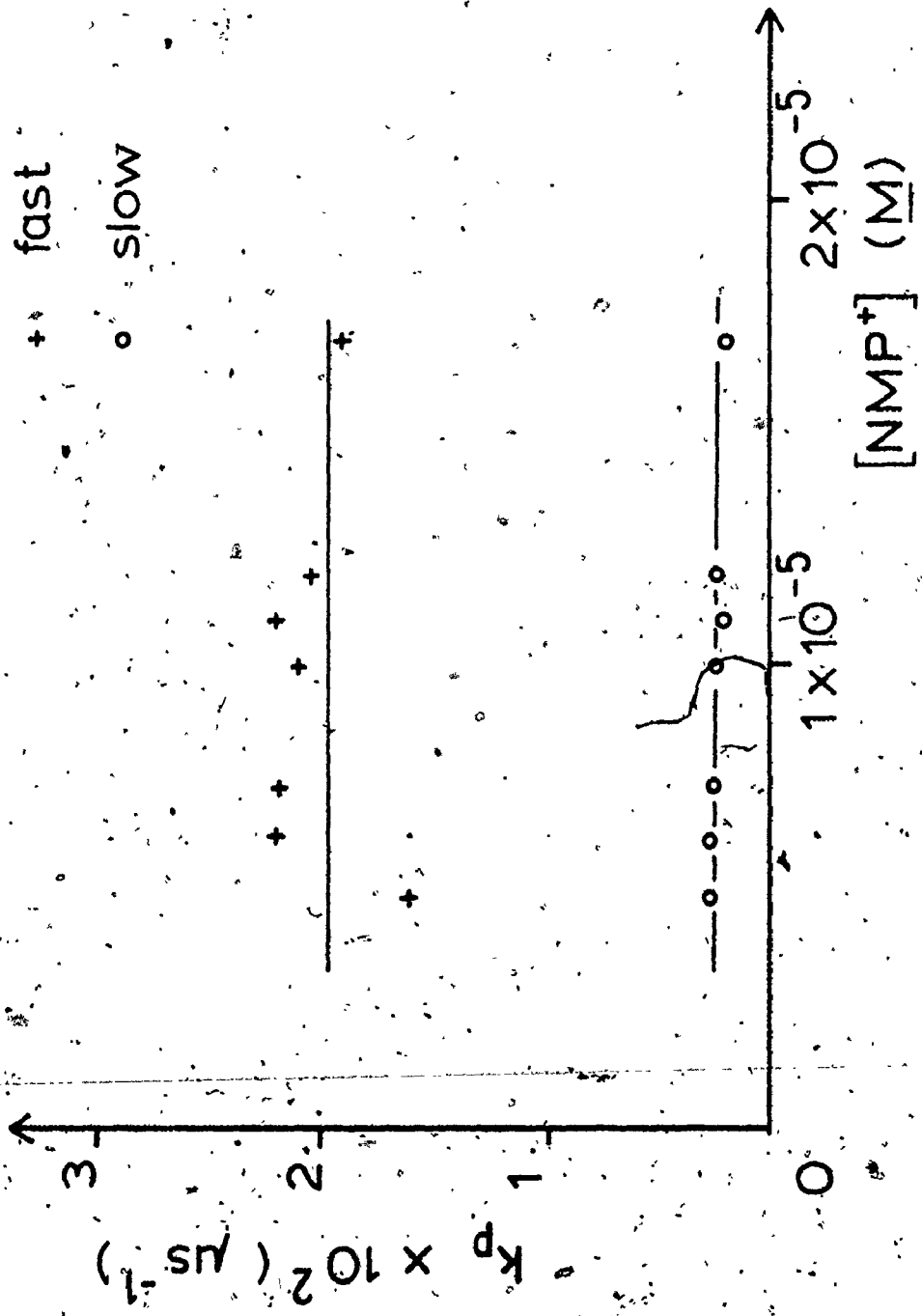
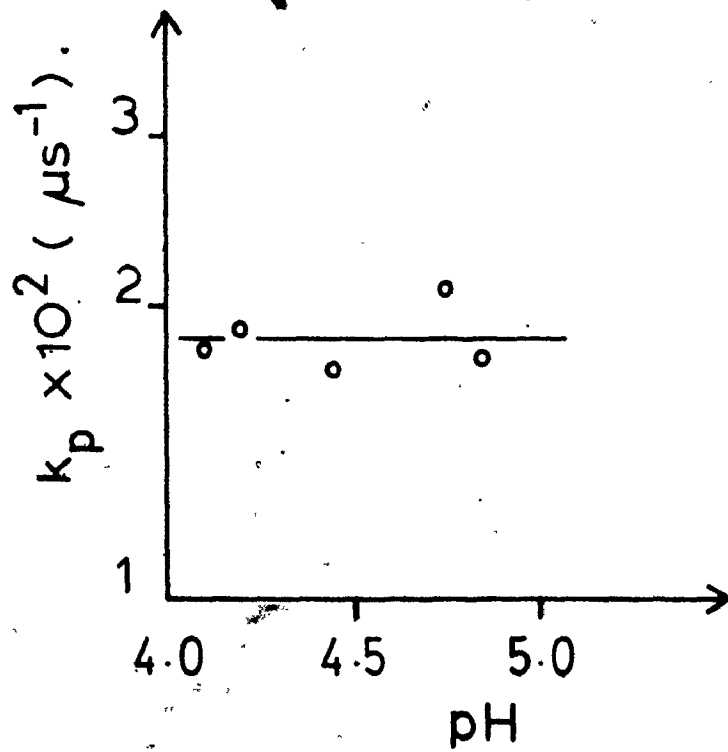


Figure 4.32

The Effect of pH on the Rate Constant of the Fast
Decay Transient Detected at 525 nm.

$$[\text{NMP}^+] = 10^{-5} \text{ M.}$$



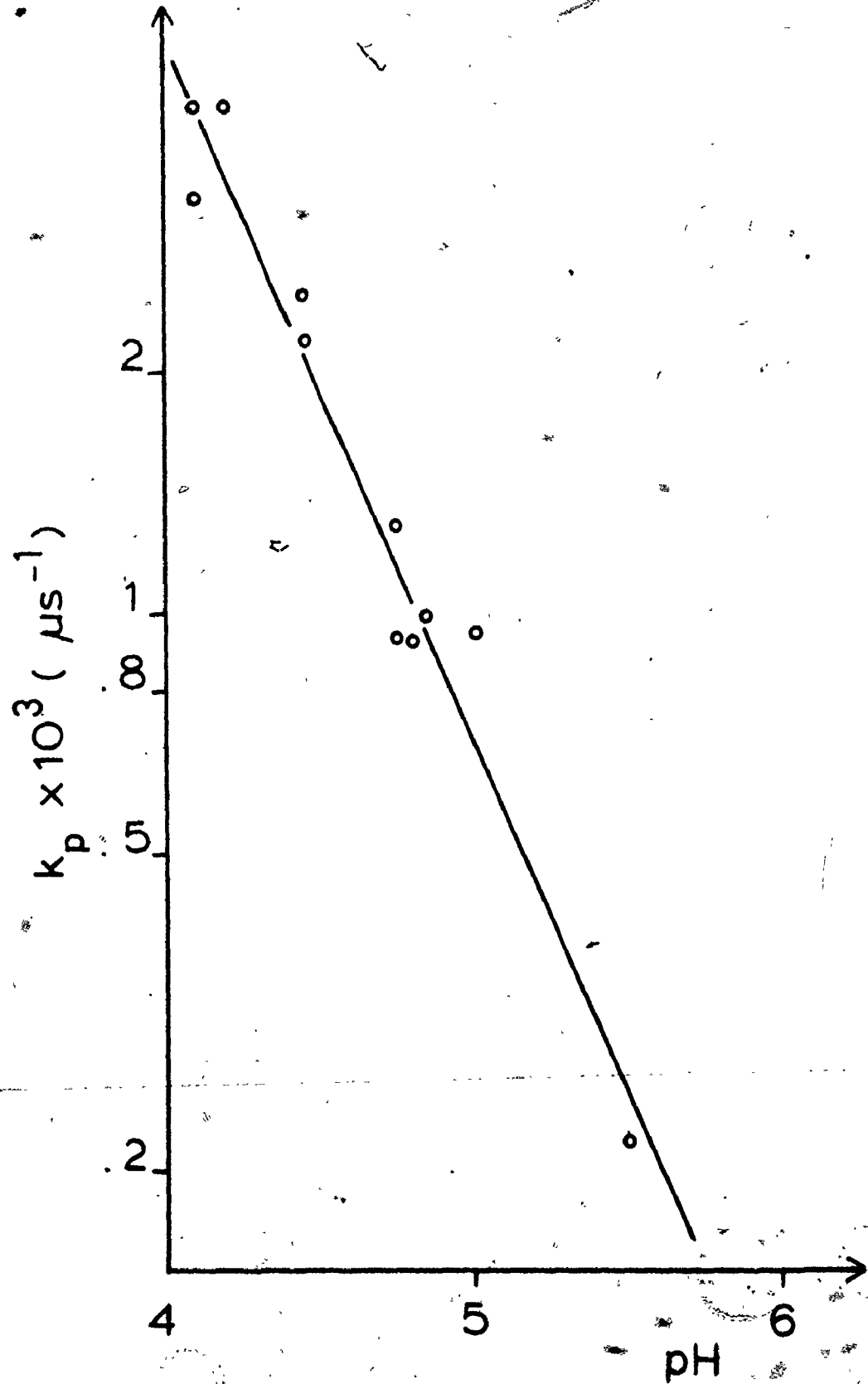
fast rate constant. Even though the formation of PYH^+ is also slower than the slow decay at pH 3.5, nevertheless this term can no longer be neglected in the calculation of the rate constant of the slow decay transient at higher pH. The pH dependence of the slow decay rate constant was investigated in air - saturated solutions. Under this condition, the fast decay disappears and the contribution from the formation of PYH^+ is small within 150 μs after the firing of the photolysis lamp, hence, more points can be obtained for the calculation without taking into account the contribution from the formation of PYH^+ .

Fig. 4.33 shows a plot of \log (rate constant of the slow decay) versus the pH. The slope of the straight line is -0.88 ± 0.06 which is close to -1 . This suggests that the reaction is an approach to an acid - base equilibrium. The reaction is actually a second order reaction where the hydronium ion concentration is constant. The second order rate constant is equal to the average value of $k_p/[\text{H}_3\text{O}^+]$, $(6.6 \pm 1.4) \times 10^7 \text{ M}^{-1} \text{ s}^{-1}$.

PYH^+ and $\text{NMP}\cdot$ are the only species among all the known products and intermediates that absorb strongly around 525 nm. Since the acid - base reaction occurs at an earlier time than the formation of PYH^+ , $\text{NMP}\cdot$ is probably the species that is involved in the reaction. Reaction 4.7 requires that the pseudo first order rate constant k_p be independent of the concentration of NMP^+ and proportional to the concentration of hydronium ion. These requirements agree with the experimental observations of the slow decay at 525 nm. We thus propose that $\text{NMP}\cdot$ is formed first and then

Figure 4.33

The pH Dependence of the Pseudo First Order Rate
Constant for the Slow Decay Transient Reaction 4.7
Observed at 525 nm.



protonated to give NMPH^+ (Reaction 4.7).

4.6 pH DEPENDENCE OF THE RATE CONSTANTS AND THE YIELD

Reactions 4.5 and 4.8 do not involve H_3O^+ so that the pseudo first order rate constants of these two reactions should not depend on pH. The pseudo first order rate constants of the formation of $NMPH^+$ and PYH^+ in 5×10^{-3} M phthalate buffer solutions at various pH's were determined as described in Section 4.5.1. The results are shown in Fig. 4.34 and 4.35. It was found that the rate constant for the formation of $NMPH^+$ at pH 3 is almost twice the value at pH 5 while the concentration of hydronium ion at pH 3 is a hundred times higher than that at pH 5. In other words, H_3O^+ is not involved as a direct reactant in the formation of either $NMPH^+$ or PYH^+ as in Reaction 4.5 and 4.8. Similarly, the yields of $NMPH^+$ and pyocyanine are relatively insensitive to the pH of the solutions from pH 2 to pH 5 (Fig. 4.36 and 4.37), that is, the yield does not change by tenfold when the pH is changed by one pH unit.

Both Fig. 4.36 and 4.37 show a maximum at pH around 3 and at pH about 5 the yields drop to ~50 % of that at pH 3. This behaviour is very similar to the pH dependence of the quantum yield of the formation of $NMPH^+$ (Fig. 4.13) and the pH dependence of the pseudo first order rate constant of Reaction 4.5 (Fig. 4.34). But the pseudo first order rate constant of Reaction 4.8 behaves quite differently.

Since the fluorescence yield (Fig. 4.16) does not depend on the pH of the solution for pH >3 and only $NMPH^+$ (not $NMPH$) is observed as a final product at pH 7, the yield of $NMPH^+$ and pyocyanine

Figure 4.34

The Effect of pH on the Pseudo First Order Rate
Constant of Reaction 4.5 Measured at 443 nm.

$$[\text{NMP}^+] = 10^{-5} \text{ M.}$$

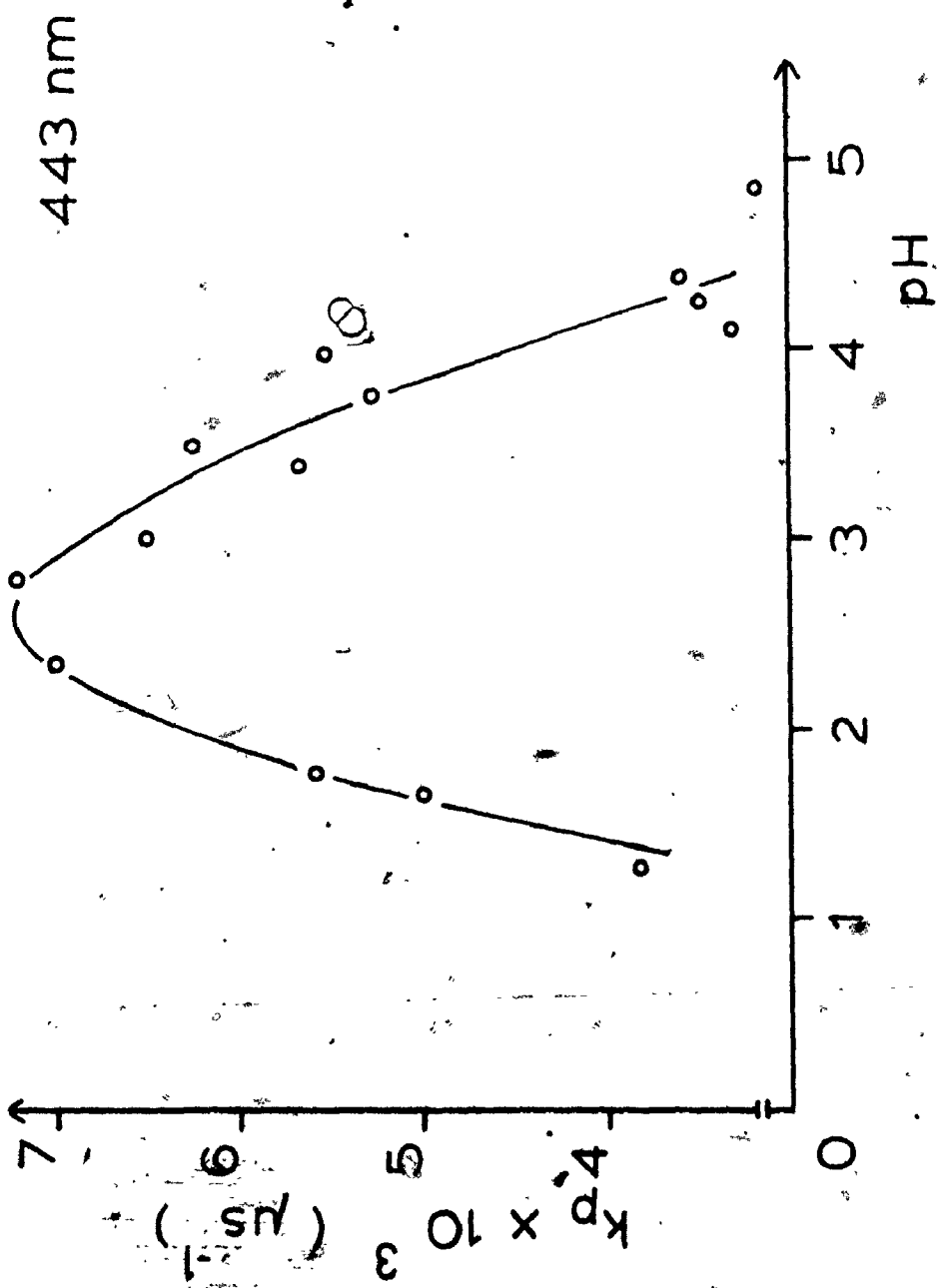


Figure 4.35

The Effect of pH on the Pseudo First Order Rate
Constant for the Formation of Pyocyanine

Measured at 525 nm.

$$[\text{NMP}^+] = 10^{-5} \text{ M.}$$

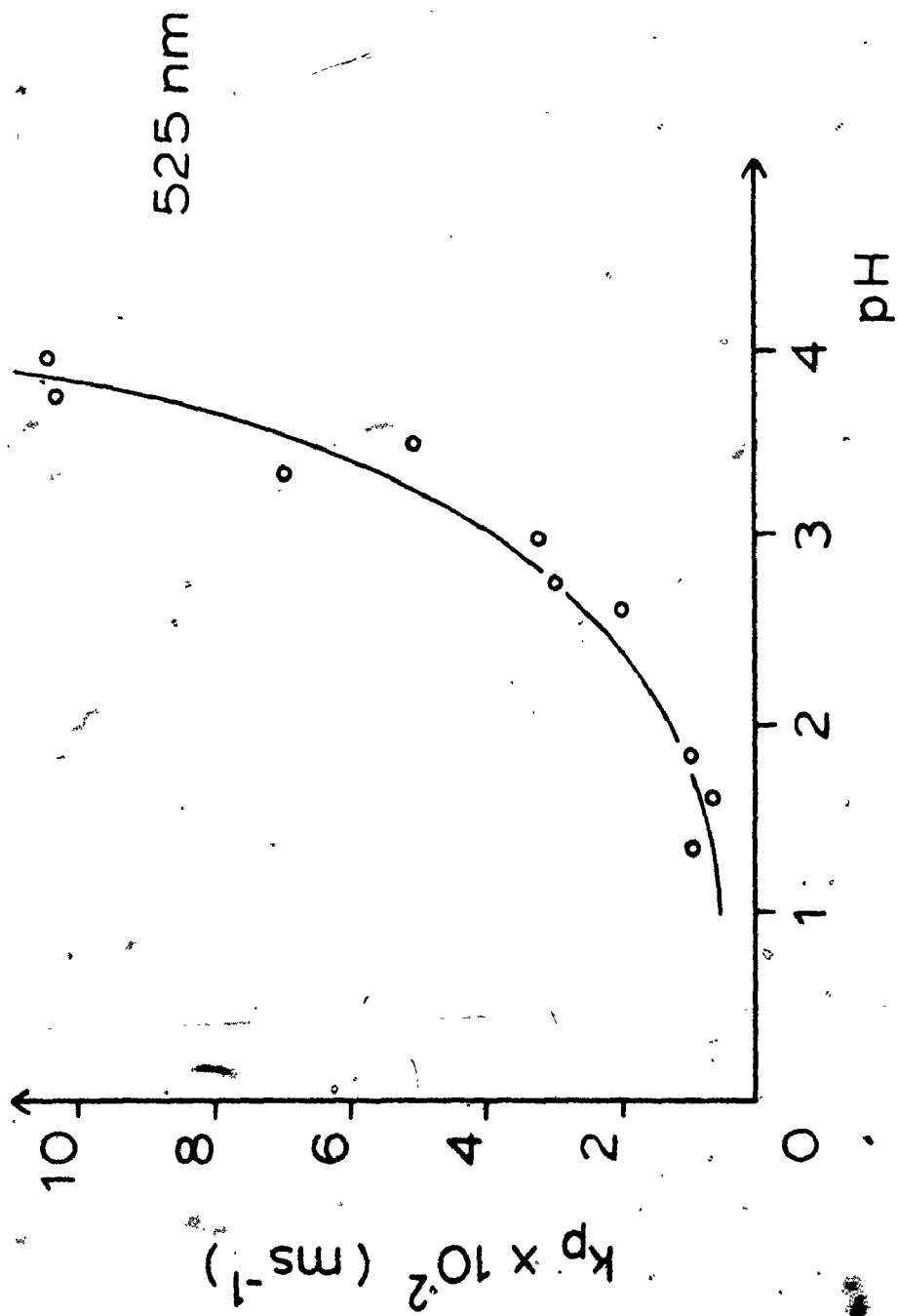


Figure 4.36

The Effect of pH on the Ultimate Yield of NMP^+

Measured at 443 nm

$$[\text{NMP}^+] = 10^{-5} \text{ M.}$$

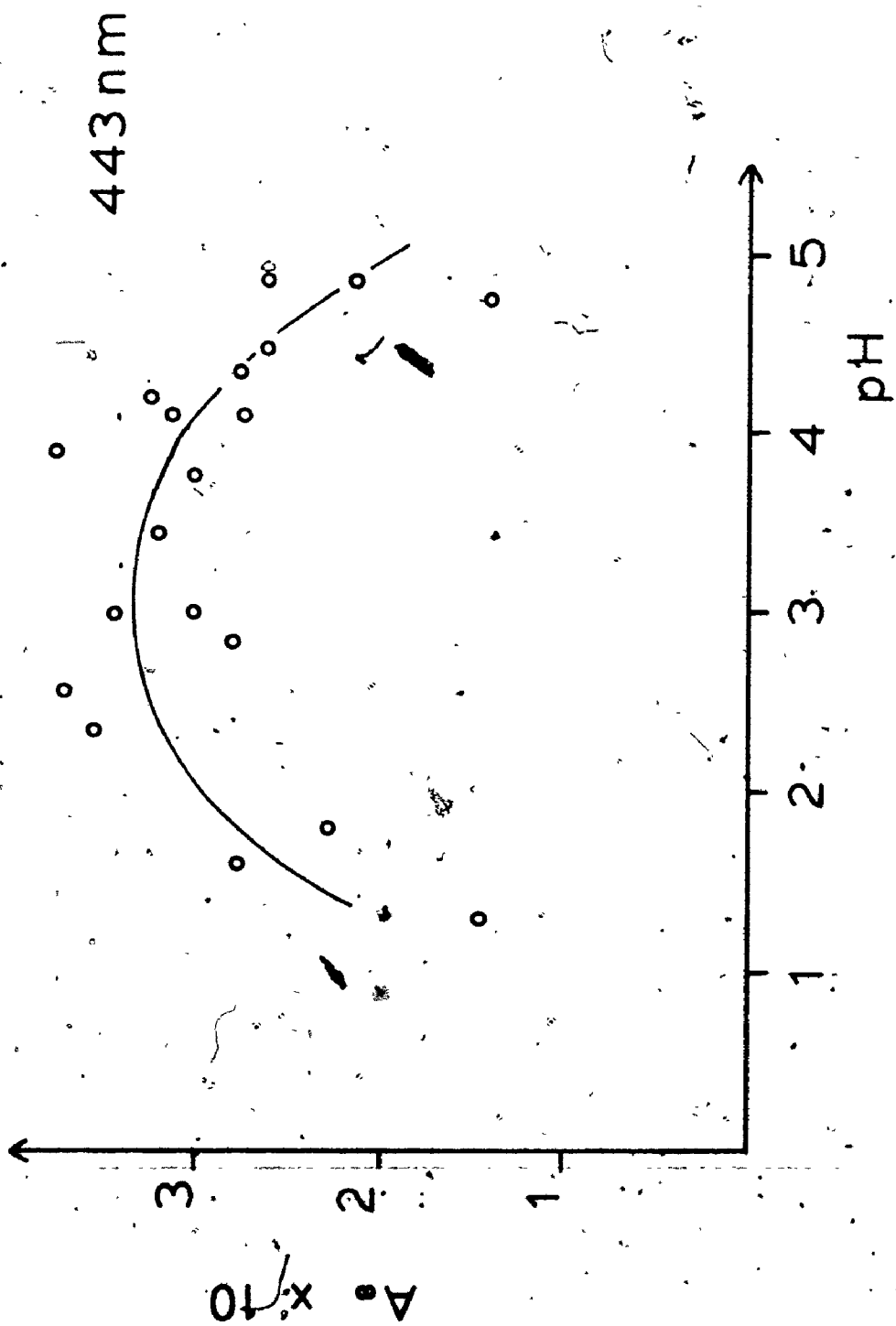
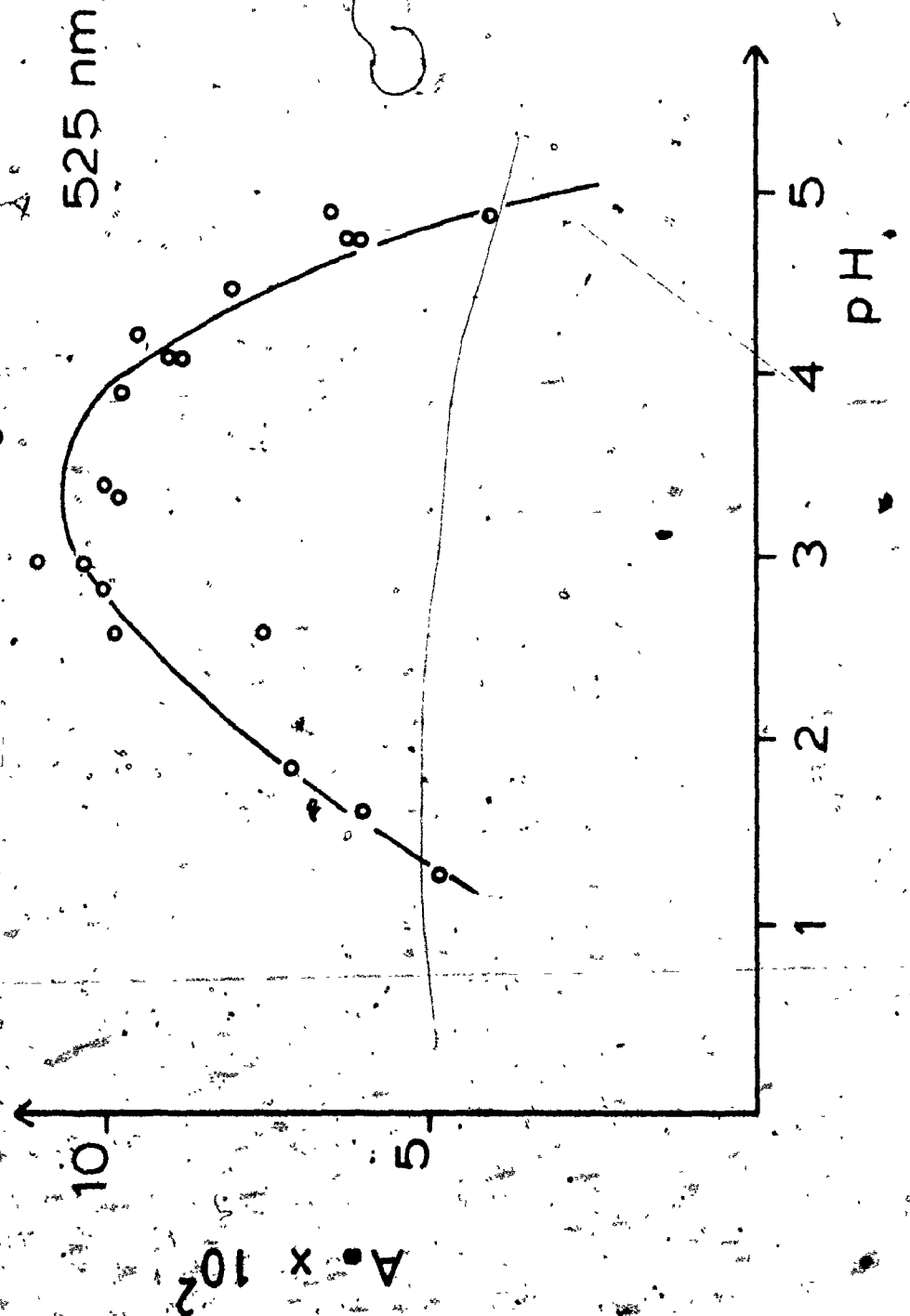


Figure 4.37

The Effect of pH on the Ultimate Yield of Pyocyanine

Measured at 525 nm.

$[NMP^+] = 10^{-5} \text{ M.}$



should not depend on pH for pH between 3 and 7. In the following sections several reactions will be discussed to account for the fact that there is a small but real pH effect.

4.6.1 Disproportionation of NMPH^+ and NMP^+

Zaugg (14) reported that semireduced NMP^+ undergoes disproportionation to form NMP^+ and NMPH and that semireduced NMP^+ is readily regenerated when such a solution is again made acidic and can also be formed when NMPH is added to an acid solution of NMP^+ . This suggests that a disproportionation equilibrium exists which can be written as Reactions 4.11 and 4.12 on page 63. Zaugg (14) also reported that most of the semireduced NMP^+ species undergo the disproportionation reaction at pH 7.5 to 8 in aqueous solution.

An experiment was set up to determine whether the decrease in the NMPH^+ yield at high pH was due to disproportionation or just a deprotonation reaction. NMPH^+ oxalate salt was prepared as reported by Takagi *et al.* (30). It was then dissolved in about 100 ml of 4×10^{-2} M pH 3 phthalate buffer. Concentrated sodium hydroxide solution was used to adjust the pH of the solution. The solution was purged with nitrogen throughout the experiment. In the case of the disproportionation reaction (Reaction 4.11)

$$K_{11} = \frac{[\text{NMP}^+][\text{NMPH}][\text{H}^+]}{[\text{NMPH}^+]^2} \quad (4.21)$$

$$\log \frac{2A}{A_0 - A} = -0.5 \text{ pH} + 0.5 \text{ p}K_{11} \quad (4.22)$$

where A_0 is the initial absorbance at 443 nm and A is the absorbance at 443 nm measured at various pH values, $\text{p}K_{11}$ is

the negative logarithm of the equilibrium constant for the disproportionation and the initial concentrations of NMP^+ and NMPH^+ are zero. For the deprotonation reaction,

$$\log \frac{A}{A_0 - A} = \text{pH} + \text{p}K_a \quad (4.23)$$

where $\text{p}K_a$ value was reported to be 5.7 (25) or 6.8 (27). Fig. 4.38 shows that there is a linear relation between $\log (2 \cdot A / (A_0 - A))$ and pH. It was found that the slope is equal -0.6 ± 0.1 and the intercept is 3.8 ± 0.2 . These results suggest that NMPH^+ disproportionates as the pH increases (Reaction 4.11). But we still cannot rule out the possibility that deprotonation is followed by the disproportionation of NMP^\bullet (Reaction 4.12) which also gives the same overall reaction as Reaction 4.11. The $\text{p}K_{11}$ value for the disproportionation was found to be 7.6. This value agrees with Zaugg's observation, that is, most of NMPH^+ underwent disproportionation at pH 7.5 to 8 in aqueous solution. Besides, the second derivative ESR spectrum of the light induced species generated at pH 7 is exactly the same as that of NMPH^+ at pH 3. Hence, at pH 7 any equilibrium concentration of NMP^\bullet cannot be greater than about 10 % of that of NMPH^+ . The cause of the discrepancy between this observation and the reported $\text{p}K_a$ value of NMPH^+ is not clear.

In order to determine whether disproportionation is important in the present work, the conversion factor α , defined as $[\text{NMPH}]/[\text{NMPH}^+]_0$, was calculated. $[\text{NMPH}^+]_0$ is the initial concentration of NMPH^+ , $[\text{NMPH}]$ is the concentration of NMPH .

The results are shown in Table 4.5. The quantum yield experiments

Figure 4.38

The pH Dependence of the Factor $(2 A / (A_0 - A))$.

A is the absorbance measured at 443 nm,

A_0 is the initial absorbance at 443 nm.

$$\frac{2 \cdot A}{A_0 - A}$$

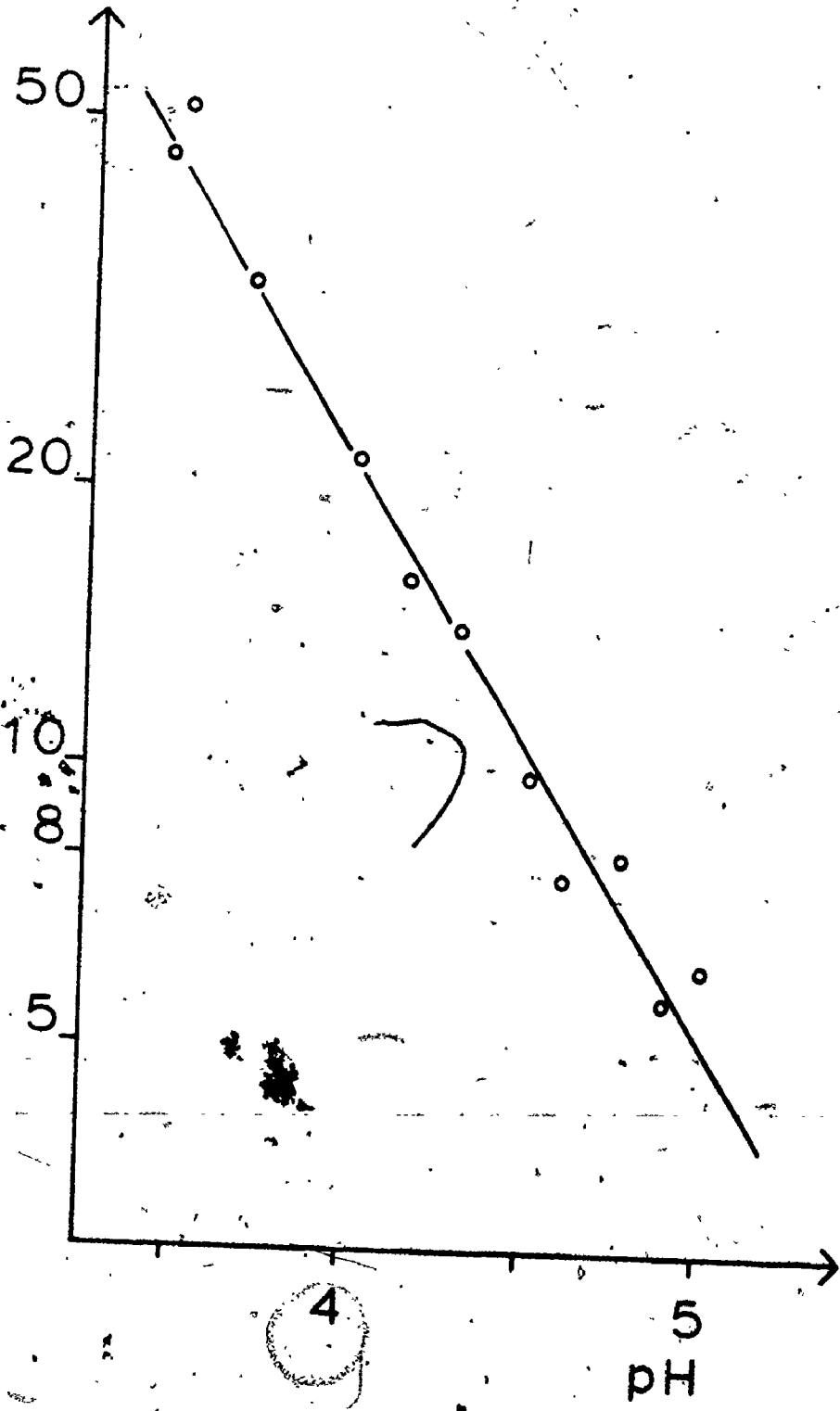
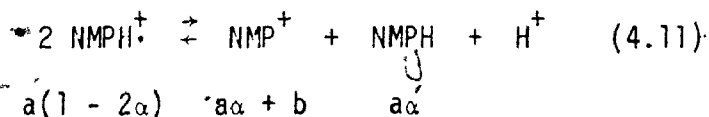


Table 4.5

The Conversion Factor of The Disproportionation Reaction



$$K_{11} = \frac{(a\alpha + b)(a\alpha)[\text{H}^+]}{(a(1 - 2\alpha))^2}$$

[H ⁺]	α			
	b = 0	b = 10 ⁻⁶ M	b = 10 ⁻⁵ M	b = 10 ⁻⁴ M
10 ⁻⁹	0.455	0.450	0.423	0.319
10 ⁻⁸	0.380	0.369	0.302	0.133
10 ⁻⁷	0.250	0.228	0.125	0.0228
10 ⁻⁶	0.120	0.089	0.0224	0.0025
10 ⁻⁵	0.0455	0.0194	0.0025	0.00025
10 ⁻⁴	0.0154	0.0024	0.0003	
10 ⁻³	0.0050	0.00025		

a Initial concentration of NMPH⁺, a = 10⁻⁵ M
in this calculation

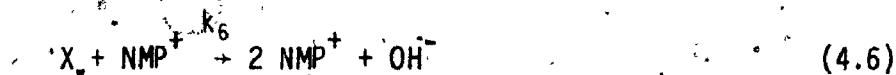
b Initial concentration of NMP⁺

Conversion factor defined as the concentration
of NMPH when initial concentration of NMPH⁺
is 1M

were carried out at and below pH 7 and such that the concentration of NMP^+ was considerably higher than the concentration of NMPH^+ formed ($b > a$). Under these conditions the results in Table 4.5 indicate that disproportionation is not important in the present system (α is very small). Besides, the drop in the conversion factor is very small from pH 3 to 5 and it does not match the drop in quantum yield versus pH (Fig. 4.13). Thus the drop in quantum yield versus pH cannot be attributed to disproportionation.

4.6.2 Competitive Reactions Involving Intermediate X.

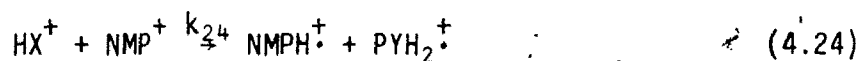
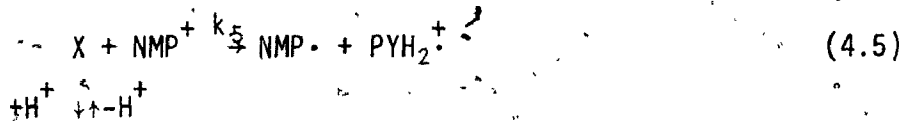
Fig. 4.33 indicates that at $\text{pH} > 3$, the rate constant for the formation of $\text{NMP}\cdot$ (k_5) is not directly proportional to the concentration of hydronium ion. A possible explanation is that k_5 is linearly dependent on the concentration of the hydronium ion, that is, $k_5 = k_5' + k_5'' [\text{H}_3\text{O}^+]$, as the concentration of hydronium ion increases, k_5 increases. The plot of k_5 versus $[\text{H}_3\text{O}^+]$, which is not shown here, indicates a possible linear relation between them. Since the quantum yield of NMPH^+ decreases as pH increases (for $\text{pH} > 3$), there must be a competitive reaction involving X. As k_5 decreases, the competitive reaction becomes more important, hence, the yields drop at $\text{pH} > 3$. This competitive reaction may not be a unimolecular reaction since if it were the quantum yield of $\text{NMP}\cdot$ should depend on the concentration of NMP^+ . A possible bimolecular competitive reaction is



This reaction involves the same reactants as Reaction 4.5, that is, in the transition state, the activated complex can follow either

Reaction 4.5 or 4.6. If k_6 were independent of pH, as pH increases, k_5/k_6 would decrease and the quantum yield of NMPH^+ would decrease for $\text{pH} > 3$, in the same way as k_5 . But it seems that the drop in quantum yield is slower than k_5 . Probably k_6 is also a function of the concentration of hydronium ion, so that the quantum yield of NMPH^+ decreases for $\text{pH} > 3$.

At $\text{pH} < 3$, the yield of NMP^+ (S_1) decreases (see Section 4.4.3) while the photochemically inactive NMPH^{2+} (S_1) predominates. Hence, the quantum yield of NMPH^+ decreases. Fig. 4.34 also indicates that the rate constant for the formation of NMPH^+ or $\text{NMP}\cdot$ decreases as the pH is lowered. A possible explanation is



At low pH (< 3), HX^+ dominates and possibly $k_{24} = k'_{24} + k''_{24}/[\text{H}_3\text{O}^+]$, so as $[\text{H}_3\text{O}^+]$ increases, k_{24} decreases. Hence the pseudo first order rate constant observed at 443 nm decreases as pH decreases ($\text{pH} < 3$).

In summary, at $\text{pH} > 3$, possibly Reaction 4.5 dominates, the rate constant for the formation of $\text{NMP}\cdot$ follows the relation $k_5 + k_5'' [\text{H}_3\text{O}^+]$ and due to the competitive reaction (Reaction 4.6) the yield of NMPH^+ drops as pH increases. At $\text{pH} < 3$, Reaction 4.24 dominates, the rate constant for the formation of NMPH^+ follows $k'_{24} + k''_{24}/[\text{H}_3\text{O}^+]$ and due to the drop in the concentration of NMP^+ (S_1), the quantum yield of NMPH^+ decreases as pH decreases. Hence both the rate constant observed at 443 nm (Fig. 4.33) and the quantum

yield of the formation of NMPH^+ (Fig. 4.12) versus pH follow bell-shaped curves.

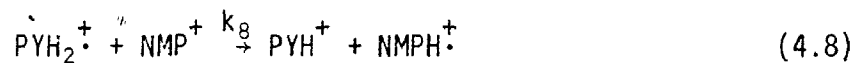
The fluorescence yield is small (Section 4.4.2), yet the maximum quantum yield of NMPH^+ obtained is only half of the maximum possible value of 2. This can be explained by the presence of Reaction 4.6 which consumes the intermediate X, the formation of a triplet state which is photochemically inactive and the formation of NMPH^{2+} (S_1) which is also photochemically inactive at pH < 3.

4.6.3 Reaction of PYH_2^+

Reaction 4.8 suggests that PYH_2^+ is oxidized by NMP^+ to give PYH^+ and NMPH^+ . Fig. 4.22 shows that NMPH^+ reaches a steady state concentration after about 0.5 ms while it takes PYH^+ about 60 ms to rise to its final concentration; hence the formation of NMPH^+ and of PYH^+ (Reaction 4.8) seem to be independent processes. However, the absorption change at 443 nm corresponds to the net change in absorption. One has to account for the formation of PYH^+ and NMPH^+ and at the same time, the depletion of NMP^+ and PYH_2^+ at this wavelength. It was found that the sum of the molar absorption coefficients of NMP^+ ($2.8 \times 10^3 \text{ M}^{-1} \text{ cm}^{-1}$) and PYH_2^+ ($7.2 \times 10^3 \text{ M}^{-1} \text{ cm}^{-1}$) and the sum of the molar absorption coefficients of NMPH^+ ($1.1 \times 10^4 \text{ M}^{-1} \text{ cm}^{-1}$) and PYH^+ ($9.7 \times 10^2 \text{ M}^{-1} \text{ cm}^{-1}$) at 443 nm are about the same. Hence, no change in absorption at 443 nm after 0.5 ms should be observed.

Voriskova (44) reported that the pK_a value of PYH_2^+ is 5.63 in aqueous solution. This pK_a value is within the pH range of the experiments, so the equilibrium between the protonated and unprotonated species may affect the rate of the formation of PYH^+ .

Thus the formation of pyocyanine can be rewritten as



PYH^\bullet is the semireduced pyocyanine neutral radical. Then the pseudo first order rate constant k_p for the formation of pyocyanine becomes

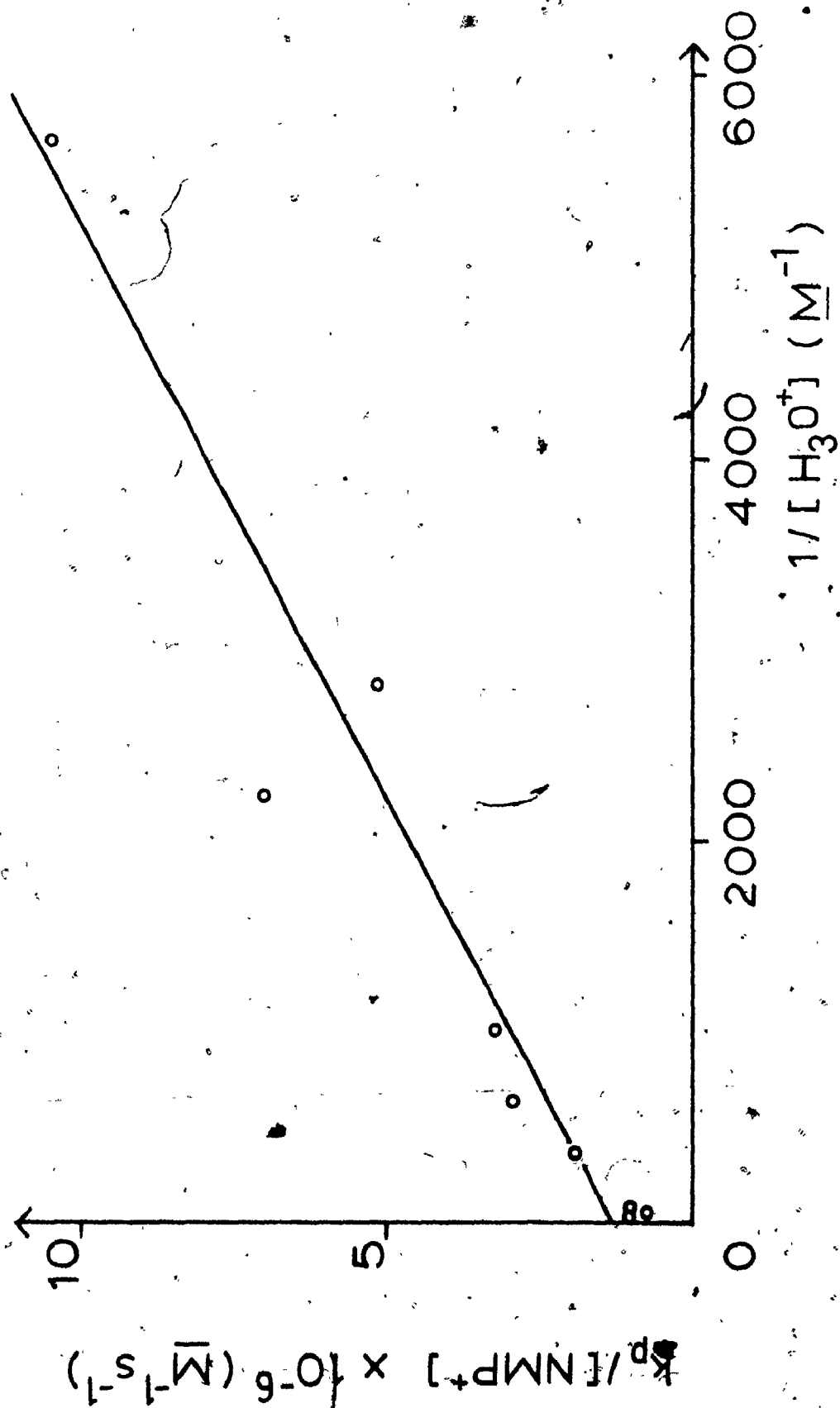
$$k_p = (k_8 + k_9 K_{10} / [\text{H}_3\text{O}^+]) [\text{NMP}^+] \quad (4.25)$$

where K_{10} is the equilibrium constant of semireduced pyocyanine and can be calculated from the reported $\text{p}K_a$ value of PYH_2^+ . If this is the case, then the plot of $k_p / [\text{NMP}^+]$ versus $1 / [\text{H}_3\text{O}^+]$ should be a straight line. The intercept is equal to k_8 and the slope is equal to $k_9 K_{10}$. Fig. 4.39 shows that there is indeed a linear relation between $k_p / [\text{NMP}^+]$ and $1 / [\text{H}_3\text{O}^+]$. k_8 and k_9 were found to be $1 \times 10^6 \text{ M}^{-1} \text{ s}^{-1}$ and $7 \times 10^8 \text{ M}^{-1} \text{ s}^{-1}$ respectively. At low pH, the reaction between PYH_2^+ and NMP^+ is predominant and the rate of the formation of PYH^+ is slow. As pH increases, the second term in the above equation becomes significant. Hence the rate of the formation of pyocyanine increases.

Figure 4.39

A Plot of $1/[H_3O^+]$ versus the Ratio of the Pseudo First Order Rate Constant Measured at 525 nm to the Concentration of NMP^+ .

$$[NMP^+] = 10^{-5} \text{ M.}$$



4.7 THE STOICHIOMETRIC RATIO OF NMPH^+ AND PYH^+

The overall reaction (Reaction 4.13) requires that the stoichiometric ratio of NMPH^+ and PYH^+ be 2. The following experiments were set up to determine this ratio.

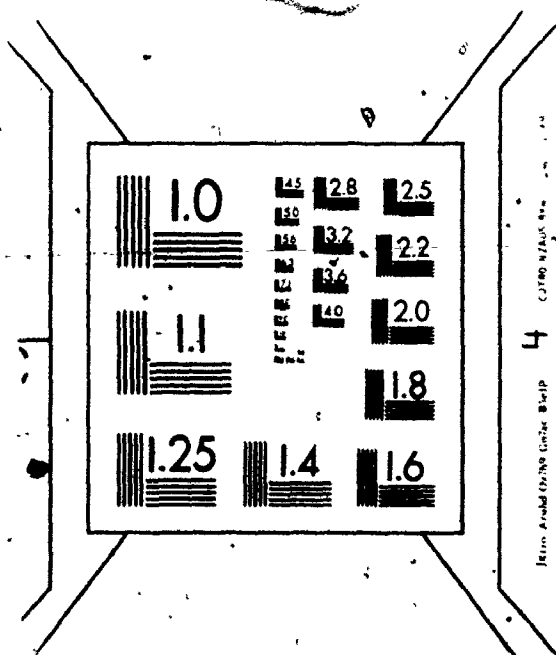
An experiment was planned to measure the ratio of the yield of NMPH^+ to PYH^+ at pH 3 simultaneously, where the concentration of NMPH^+ was to be measured by ESR, and the concentration of PYH^+ was to be measured by visible spectrometry. Because of the small absorption coefficient of the absorption peak of PYH^+ at 525 nm (a typical value of absorbance obtained is less than 0.1), large errors are likely to occur in the determination of this ratio. This experiment was therefore abandoned.

An attempt was made to neutralize the pH 3 solution using sodium hydroxide. The concentration of PYH^+ was determined from the absorption spectrum at 310 nm where absorption coefficient of PY at this wavelength is $2.9 \times 10^4 \text{ M}^{-1} \text{ cm}^{-1}$. It was found that the ratio was 1.1. It is impossible to estimate the error involved in this method due to the following reasons. Since the shape of the titration curve (pH versus the volume of base/acid added) is S shaped, a slight excess of base will cause the pH of the solution jump to ~9. McIlwain (24) reported that in aqueous alkaline solution NMP^+ decomposes even in the absence of air to phenazine, NMPH and formaldehyde. The concentration of NMP^+ was about $4 \times 10^{-4} \text{ M}$ and the concentration of the PYH^+ formed is less than 10^{-4} M . A small decomposition of NMP^+ will produce a considerable

3

3

OF/DE



amount of NMPH. NMPH has a broad optical absorption peak at 332 nm. Although its absorption coefficient at 310 nm is about one sixth of that of PY at that wavelength, it will still interfere with the measurement of the absorption peak of PY at 310 nm because of its high concentration. It was found that at the end of the experiment the concentration of NMP^+ and NMPH^+ were comparable, so from Table 4.5 the conversion factor α was found to be 0.12 at pH 7. Hence, NMPH could be formed by the disproportionation of NMPH^+ , NMPH will again interfere with the measurement. Thus due to the interference of NMPH, the determination of the ratio by the above method may be considerably in error on the low side. Thus another experiment was set up.

From the values of A_{∞} at both 443 nm and 525 nm which were obtained from optical flash photolysis results at pH 3, one finds that the ratio of NMPH^+ formed per flash to PYH^+ formed is 1.4. The A_{∞} at 443 nm corresponds to the net change in absorbance and is equal to the difference of the absorbance of NMPH^+ formed and that of NMP^+ depleted at that wavelength (the contribution of PYH^+ is negligible). The concentration of NMP^+ depleted is equal to the sum of the concentration of NMPH^+ and PYH^+ . The concentration of PYH^+ can be calculated directly from A_{∞} at 525 nm, so we have two simultaneous equations in two unknowns. In the optical flash photolysis experiments; very dilute solutions (10^{-5} M) were used. Even when a 19.5 cm long cell is used, the absorbances obtained at 443 nm and 525 nm are always less than 0.3. The standard deviation of the stoichiometric ratio obtained after solving the equations is fairly large (at least 15 %).

The final method devised was as follows. An NMP^+ solution in pH 3 hydrochloric acid was placed in an anaerobic absorption cell. The optical absorbances at 443 nm and 385 nm were measured at various irradiation times. The change in absorbance at 385 nm is considerably larger than that at 443 nm, thus the error in the measurement is smaller at 385 nm. The following equations were used to find the concentrations of NMPH^+ and PYH^+ at various irradiation times.

$$A(385 \text{ nm}) = \epsilon_1[\text{NMP}^+] + \epsilon_2[\text{NMPH}^+] + \epsilon_3[\text{PYH}^+] \quad (4.26)$$

$$A(443 \text{ nm}) = \epsilon_1'[\text{NMP}^+] + \epsilon_2'[\text{NMPH}^+] + \epsilon_3'[\text{PYH}^+] \quad (4.27)$$

$$[\text{NMP}^+] = [\text{NMP}^+]_0 - [\text{NMPH}^+] - [\text{PYH}^+] \quad (4.28)$$

where $[\text{NMP}^+]_0$ is the initial concentration of NMP^+ , ϵ_1 , ϵ_2 , ϵ_3 and ϵ_1' , ϵ_2' , ϵ_3' are the molar absorption coefficients of NMP^+ , NMPH^+ and PYH^+ at 385 nm and 443 nm respectively. It was found that the stoichiometric ratio of NMPH^+ and PYH^+ is 2.2 ± 0.4 after three independent runs and a total of twenty measurements. This further supports the proposed mechanism which requires the ratio to be 2.

4.8 EFFECT OF ADDED AGENTS

4.8.1 Addition of Spin Traps

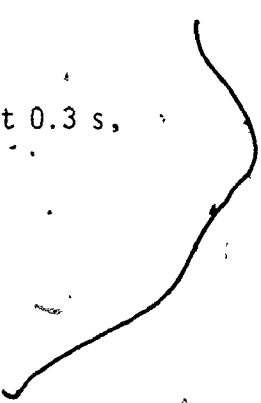
By adding 5,5-dimethyl-1-pyrroline-1-oxide (DMPO) (final concentration 10^{-2} M) to a NMP^+ solution, a spin adduct, whose ESR spectrum has a 1 : 2 : 2 : 1 quartet pattern, is formed immediately after the light is turned on. The spin adduct starts to decay after 2 to 3 minutes of steady illumination. Experiments were also carried out in NMP^+ - H_2O and NMP^+ - D_2O using phenyl-t-butyl-nitron, PBN, (saturated solution) as the spin trap. About a 20 % narrowing of spin adduct linewidth in D_2O solution was observed. The ESR spectrum of the DMPO spin adduct is shown in Fig. 4.40a. The background signal is due to the presence of NMPH^+ . The spectra of the spin adduct are identical to the ESR signals obtained from UV photolysis of a 1 % H_2O_2 solution in the presence of DMPO (Fig. 4.40b) and PBN. Harbour et al. (72) have shown that $\cdot\text{OH}$ radical is the main product from the UV photolysis of a 1 % hydrogen peroxide solution, while both $\cdot\text{OH}$ and HO_2 radicals are formed at higher concentrations of hydrogen peroxide. Table 4.6 shows the comparison of the hyperfine splitting constants of the spin adduct in the present system and that of the $\cdot\text{OH}$ radical. These results indicate that either the hydroxyl radical or a radical similar to it is formed in the system.

The relation between the peak - to - peak amplitude and the area under the ESR absorption curve of the $\cdot\text{OH}$ spin adduct using PBN as the spin trap was determined. The method was described in Section 4.3. This factor was used later in the determination of the ratio of the spin adduct to NMPH^+ formed. A nitrogen purged NMP^+ and PBN

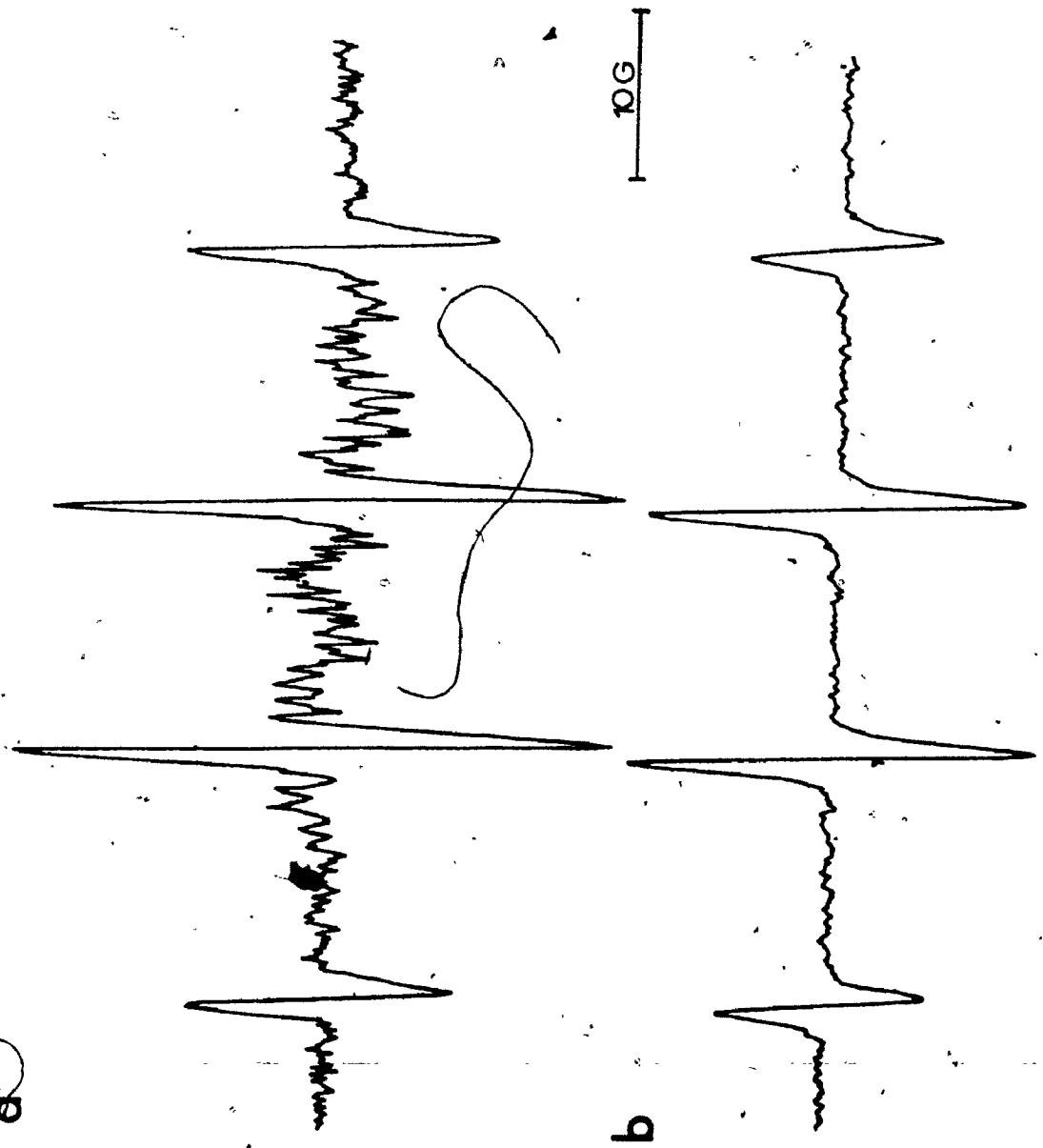
Figure 4.40

The First Derivative ESR Spectrum Obtained after
Irradiation of (a) NMP^+ ; (b) 1 % H_2O_2 Solution
Both in the Presence of DMPO.

Modulation amplitude 0.5 G, time constant 0.3 s,
scan time 4 min., microwave power 10 mW.



20



b

Table 4.6

The Comparison of Hyperfine Splitting Constants of Spin Adducts Formed in NMP^+ to that of $\cdot\text{OH}$ -Radical Spin Adducts Using DMPO and PBN as the Spin Traps

	PBN	DMPO
From Ref. 72	$a^{\text{N}} = 15.3 \text{ G}$	$a^{\text{N}} = 14.9 \text{ G}$
	$a_{\beta}^{\text{H}} = 2.70 \text{ G}$	$a_{\beta}^{\text{H}} = 14.9 \text{ G}$
		$a_{\gamma}^{\text{H}} = 0.61 \text{ G}$
		$a_{\gamma}^{\text{H}} = 0.25 \text{ G}$
From this work	$a^{\text{N}} = 15.4 \pm 0.2 \text{ G}$	$a^{\text{N}} = 15.1 \pm 0.2 \text{ G}$
	$a_{\beta}^{\text{H}} = 2.74 \pm 0.05 \text{ G}$	$a_{\beta}^{\text{H}} = 15.1 \pm 0.2 \text{ G}$

sample was studied using FPESR technique. The magnetic field was set at the first low field line of the spin adduct, which is near the tail part of the $\text{NMPH}^{\cdot+}$ signal. From the change in peak - to - peak amplitude per flash, which was mainly due to the spin adduct, the area under the absorption curve was then calculated using the factor determined above. The area under the absorption curve of the $\text{NMPH}^{\cdot+}$ formed per flash was also found by the difference in area under the absorption curve before and several minutes after a flash. (By that time most of spin adduct decayed and double integration of the whole spectrum gave the area of $\text{NMPH}^{\cdot+}$). The ratio of the spin adduct to $\text{NMPH}^{\cdot+}$ formed per flash was found to be about 0.52 ± 0.05 . This result indicates that PBN only trapped about 66 % of the intermediate X formed because in the reaction between PBN and X only one $\text{NMPH}^{\cdot+}$ is formed while in the absence of PBN two $\text{NMPH}^{\cdot+}$ are formed per X formed.

4.8.2 Effect of Other Solutes

- a. Formate buffer: Formic acid is highly reactive with the $\cdot\text{OH}$ radical because an α hydrogen is available in this molecule. The yield of the formation of $\text{PYH}^{\cdot+}$ drops considerably in pH 3 sodium formate - formic acid buffer. Fig. 4.41 shows the yield of $\text{PYH}^{\cdot+}$ at various concentrations of formate buffer solutions. There must be an additional reaction involving formate and the intermediate X.

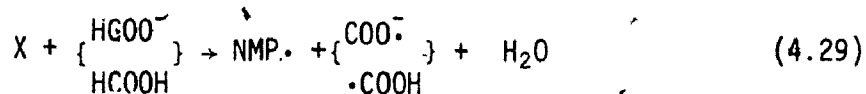
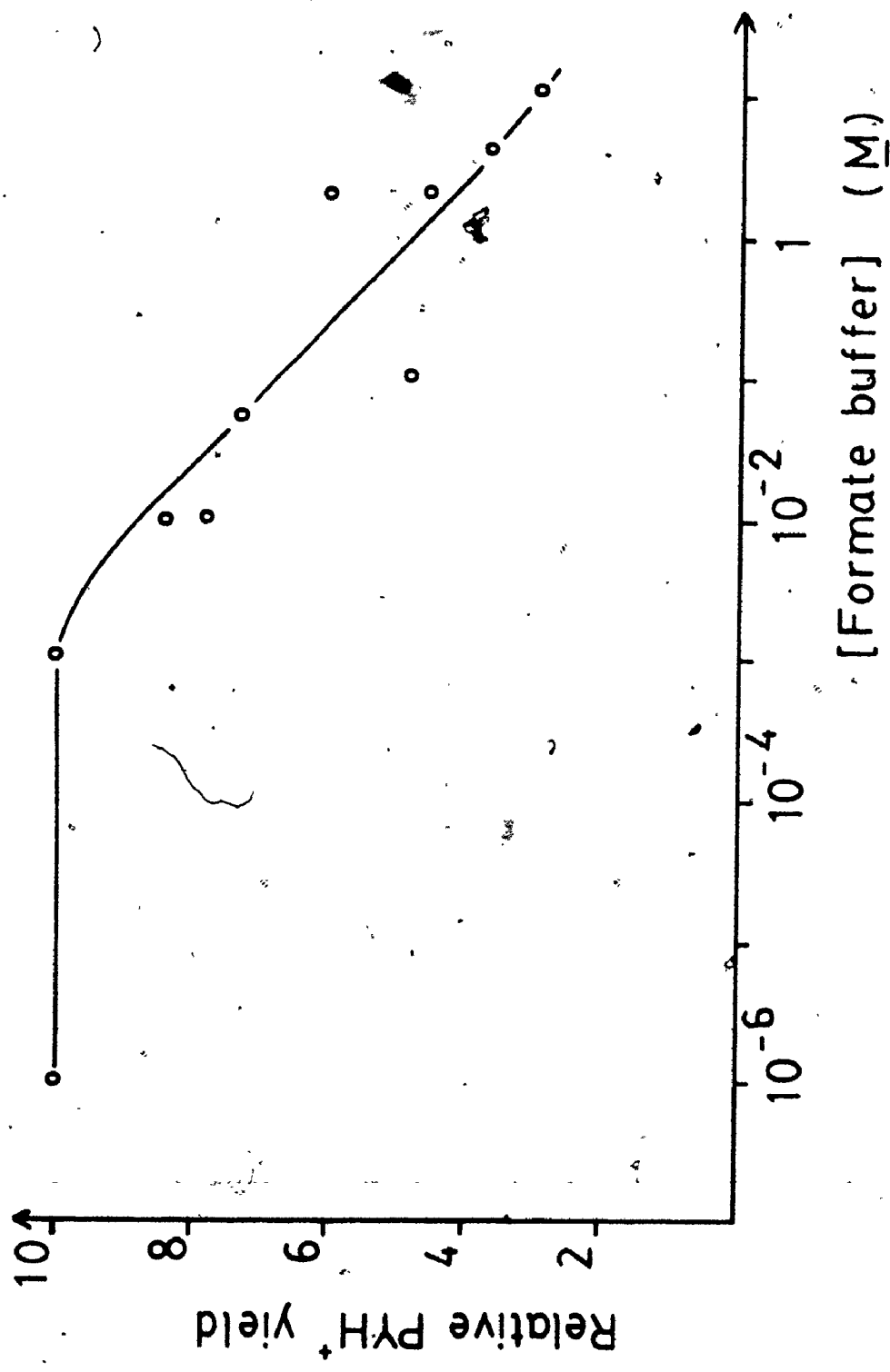


Figure 4.41

The Effect of the Concentration of Formate Buffer
on the Yield of Pyocyanine Compared to that
in 10^{-6} M Formate Buffer.



When the rate of Reaction 4.5 and this competitive reaction are the same, the yield of PYH^+ would be half of that in the absence of formate. It was found that in the presence of 0.8 M formate, the yield is only half of that in a pH 3 hydrochloric acid solution. The rate constant of the reaction between the intermediate and formate at pH 3 was found to be about $5 \times 10^3 \text{ M}^{-1} \text{ s}^{-1}$. It has been reported that the rate constant for the reaction of $\cdot\text{OH}$ with formic acid at pH 1 is $7.5 \times 10^7 \text{ M}^{-1} \text{ s}^{-1}$ (73). This suggests that the intermediate behaves like an $\cdot\text{OH}$ radical but is very much less reactive than $\cdot\text{OH}$. The rates of the formation of NMPH^+ which are measured by ESR in pH 3 hydrochloric acid and 10^{-1} M pH 3 formate buffer are very similar under steady - state illumination. Formic acid or formate probably reacts with the precursor to form NMPH^+ so that the yield of NMPH^+ remains the same while the yield of pyocyanine decreases.

- b. Acetate buffer: The rate constant for the reaction of $\cdot\text{OH}$ with acetic acid at pH 1 has been reported to be $1.4 \times 10^7 \text{ M}^{-1} \text{ s}^{-1}$ (73). The authors (73) also indicate that it is very unlikely that the $\cdot\text{OH}$ reacts at the carboxyl group either by H atom abstraction or by addition. The possible site of attack is at the $-\text{CH}_3$ position. When NMP^+ was added to various concentrations of sodium acetate - acetic acid pH 7 buffer, the formation of PY after illumination (which was determined optically at 310 nm) decreased as the concentration of acetate increased. It was

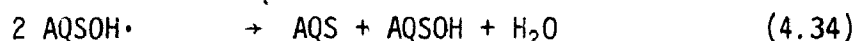
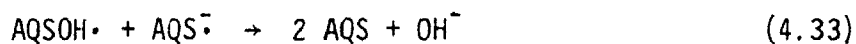
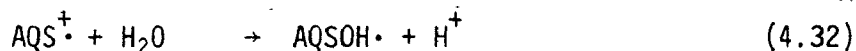
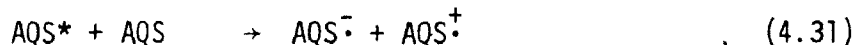
found that a 0.4 M acetate buffer could lower the yield of PY to 50 % of that of a NMP^+ sample in a 4×10^{-4} M acetate buffer. The rate constant k_5 at pH 7 was estimated from the pH dependence of the rate constant to be about $10^8 \text{ M}^{-1} \text{ s}^{-1}$. The rate constant of the reaction between the intermediate and acetate at pH 7 was estimated to be about $3 \times 10^3 \text{ M}^{-1} \text{ s}^{-1}$. Acetate, an .OH quencher, can again reduce the yield of PY. It further suggests that the intermediate X involved in the reaction is a strong oxidant.

- c. Iron salts: When iron (III) was added to an NMP^+ solution in 0.05 M sulfuric acid solution, the concentration of iron (II) increased after irradiation. The concentration of iron (II) was determined by the optical absorbance at 510 nm after the addition of 1,10-phenanthroline. Using FPESR, the addition of iron (II) has no effect on the stability of NMPH^+ formed in a pH 3 hydrochloric acid solution except for the first few flashes. But in the presence of iron (III), the NMPH^+ signal decays right after the flash. As the concentration of iron(III) is increased, the amount of NMPH^+ remaining after the decay decreases. These results suggest that NMPH^+ can reduce iron (III) to iron (II), thus causing the reduction of NMPH^+ signal after flashing. This reaction is thermodynamically allowed. The presence of iron (III) impurity in the iron (II) sample probably causes the decay of the NMPH^+ ESR signal during the first few flashes and the reduction of iron (III) to iron (II), thus increasing the concentration of iron (II) after irradiation.

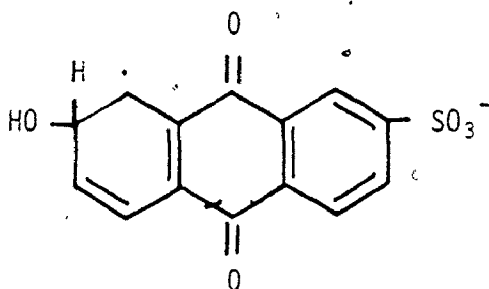
4.9 THE NATURE OF THE INTERMEDIATE X

When DMPO was added to a sodium 9,10-anthraquinone-2-sulfonate aqueous solution, the ESR spectrum of the spin adduct was found to be similar to that obtained in the NMP⁺ system. Probably the intermediates in the two systems have some similar characteristics.

Clark and Stonehill (74, 75) suggested two mechanisms for the photohydroxylation of 9,10-anthraquinone-2-sulfonate anion (AQS) in aerobic aqueous solution. These mechanisms involve an ·OH radical and a species equivalent to the ·OH adduct of AQS. Recently, Burchill *et al.* (76) showed that 1 volume % of isopropanol could quench the hydroxylation of AQS when the solution was γ irradiated. Charlton *et al.* (77) reported that even in the presence of 10 volume % of isopropanol the photohydroxylation reaction still occurred. The authors suggested that ·OH radical was not involved in this reaction. They further suggested the following mechanism which involves the formation of a radical pair and the addition of water to the cation radical to form another intermediate:



The proposed structure of the intermediate (AQSOH•) is



Clark and Stonehill (78) also recently reported that free •OH was not an intermediate in AQS system. They based this contention on the effects of several •OH scavengers and the effects of high OH⁻ concentration on hydroxylation yield in γ radiolysis and photolysis.

Dekker et al. (79) suggested that the primary step of the photohydroxylation of 7,8-dimethylalloxazine was the addition of water to the excited singlet state, because the reaction proceeded under aerobic conditions where the triplet was efficiently quenched by oxygen. Durren et al. (80) suggested that this stable primary photoproduct is LOH₃⁺ (Fig. 4.42). They proposed that it then further reacts with another molecule of 7,8-dimethylalloxazine to form LO and LH₃⁺ (Fig. 4.42). The reaction is a two - electron reduction reaction. They found that this reaction is a pseudo first order reaction and the bimolecular rate constant was $1.4 \times 10^9 \text{ M}^{-1} \text{ s}^{-1}$.

We propose that the formation of the intermediate in the NMP⁺ reaction involves the addition of solvent water to the excited

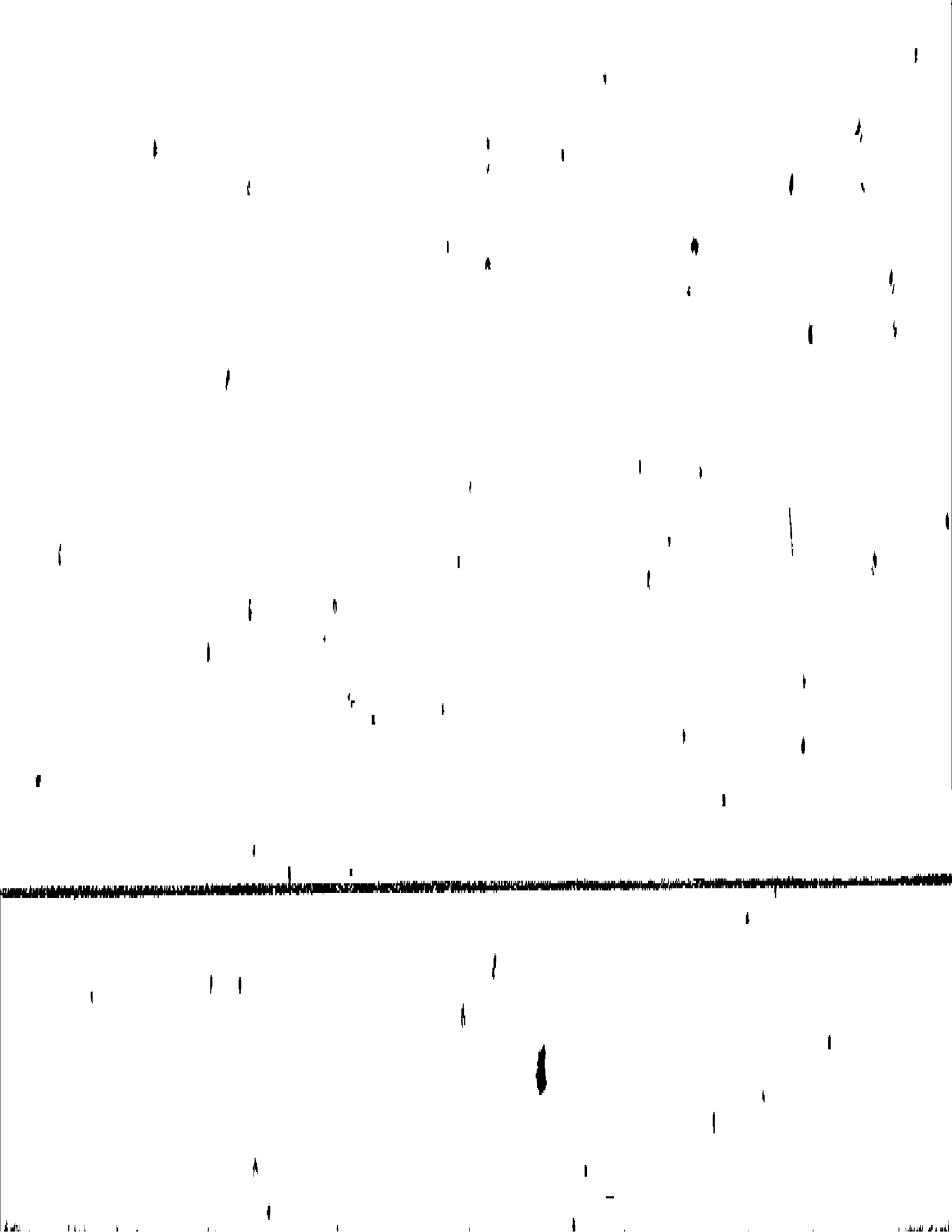
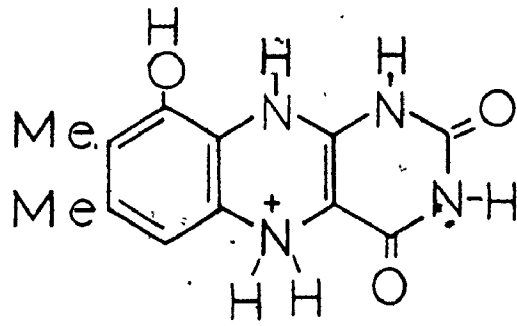
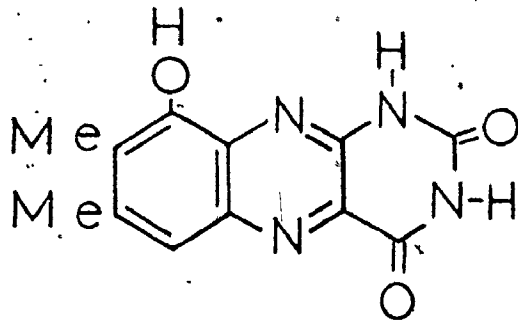


Figure 4.42

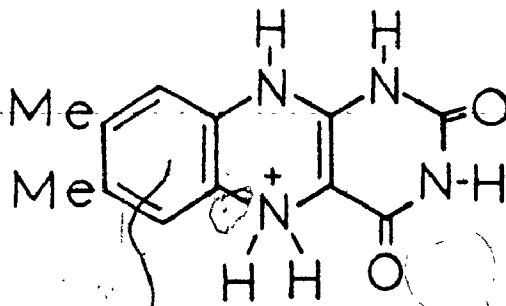
Structures of Various Species Involved in the
Photohydroxylation of 7,8-Dimethylalloxazine.



LOH_3^+

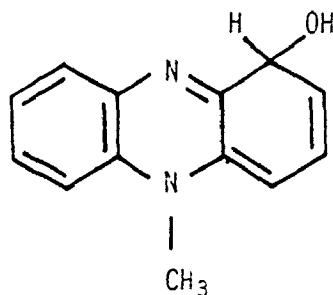


LO



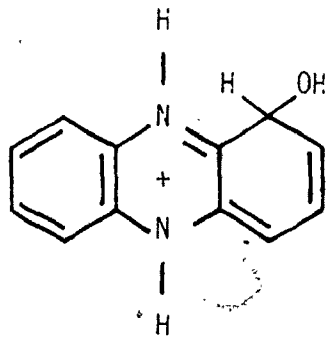
LH_3^+

state. The structure proposed for X is



This structure is very similar to that proposed by Wake *et al.* (40) for the photochemical reaction of phenazine in acidic solution.

The structure of their proposed intermediate is



The mechanism of the phenazine reaction is shown on Fig. 2.3. The structure of the proposed intermediate in AQS, phenazine and NMP⁺ systems all involve a hydrogen atom and a hydroxyl group attached to a carbon. This unit may then serve as either an electron donor or an $\cdot\text{OH}$ donor.

The $\cdot\text{OH}$ scavengers such as formate and acetate are capable of decreasing the yield of pyocyanine. Furthermore, the $\cdot\text{OH}$ spin adduct is formed after the addition of a spin trap. Thus, it would appear that the intermediate X is either an $\cdot\text{OH}$ radical donor or at least a very strong oxidant. The intermediate then reacts with

another molecule of NMP^+ to give $\text{NMP}\cdot$, and PYH_2^+ , the second order rate constant being $7.7 \times 10^8 \text{ M}^{-1} \text{ s}^{-1}$ at pH 3 which is comparable to the rate constant of the 2-electron reduction reaction in the 7,8-dimethylalloxazine system.

4.10 KINETIC SIMULATIONS

The following rate laws for Reactions 4.5 and 4.7 were set up.

$$\frac{d[\text{NMP}\cdot]}{dt} = k_5[\text{X}][\text{NMP}^+] - k_7[\text{NMP}\cdot][\text{H}^+] \quad (4.35)$$

$$\frac{d[\text{NMPH}^+]}{dt} = k_7[\text{NMP}\cdot][\text{H}^+] \quad (4.36)$$

The coupled differential equations were solved by numerical integration (81). The rise of PYH^+ is slower than the formation of NMPH^+ and was neglected in this calculation which only covered the first millisecond after photolysis. From Section 4.5.2, the second order rate constant (k_7) of Reaction 4.7 was estimated to be $6.6 \times 10^7 \text{ M}^{-1} \text{ s}^{-1}$. Using k_5 as $7 \times 10^8 \text{ M}^{-1} \text{ s}^{-1}$, it was found that the simulated decay kinetics of $\text{NMP}\cdot$ are slower than the observed ones. Probably the slow rise of $\text{NMP}\cdot$ is comparable to the decay of $\text{NMP}\cdot$. The value of k_7 was varied until the simulated decays were close to the observed decays from pH 4 to 5. k_7 was then found to be $2 \times 10^8 \text{ M}^{-1} \text{ s}^{-1}$. The rates for the formation and decay of $\text{NMP}\cdot$ were then calculated. It was found that the decay rate is faster than (at pH 3) or close to (at pH around 4.5) the rate of formation of $\text{NMP}\cdot$. Hence the rise kinetics of NMPH^+ should match the rise kinetics of PYH_2^+ as observed. The rate constants obtained at 443 nm are actually k_5 at pH 3 to 4.5 (Reaction 4.5 is the rate determining step).

When the coupled differential equations involving Reactions 4.5, 4.7, 4.8, 4.9, 4.10 and 4.11 were solved by numerical integration, the concentrations of NMP^+ , NMPH^+ , PYH^+ and NMPH at various times.

were obtained. The forward rate constants for Reaction 4.10 and 4.11 were assumed to be $10^9 \text{ M}^{-1} \text{ s}^{-1}$ and the backward rate constants were then calculated from the equilibrium constants. It was found that the pseudo first order rate constants for the formation of PYH^+ match the observed rate constants (within 90 %). The concentration of NMPH at various pH's (from pH 3 to pH 7) are only about 10^{-6} of that of NMPH^+ . This then confirms our conclusion that disproportionation is not important in the present system (Section 4.6.1).

4.11 FURTHER WORK AND APPLICATIONS

4.11.1 Further Work

In the present study all rate constants were determined by optical flash photolysis. Since PYH_2^+ is a radical, its kinetics could be monitored by FPESR. Hence, this technique could be used to confirm the rate constants reported here.

PYH_2^+ can be generated by chemically reducing PYH^+ using ascorbic acid. From its first derivative ESR spectrum, it was found that there are some magnetic fields which correspond to crossover points of the NMPH^+ ESR spectrum. The kinetics of PYH_2^+ could be then monitored at these magnetic fields without the interference from NMPH^+ . k_5 and k_8 and possibly k_9 could thus be determined.

When a 10^{-4} M NMP^+ solution is used, the rise time of PYH_2^+ is about 10 μs . Without using the 100 kHz modulation it is possible to obtain response times down to 1 μs , but the signal - to - noise is poor. When not using the 100 kHz modulation the magnetic field should be set at the first derivative crossover point of the ESR signal since the response is proportional to the ESR absorption intensity.

The major problems in this method are how to improve the signal - to noise ratio and how to prevent shifting of the magnetic field since the linewidth of the ESR signal of PYH_2^+ is very narrow.

Using a UV light source and quartz optics in the optical flash photolysis experiments, it might be possible to detect the optical spectrum of X. From its decay kinetics, one should be able

to measure k_6 . The pH dependence of k_5/k_6 could then be used to confirm our proposal that this ratio decreases as pH increases (pH > 3).

4.11.2 Possible Applications

NMPH^+ is not stable under aerobic conditions. Hence, it is not a very suitable compound to use as a substrate in a photochemical system to decompose water to hydrogen and oxygen. Ishizu et al. (17) reported that NMPH^+ was strongly bound to deoxyribonucleic acid. This association stabilizes NMPH^+ against air oxidation because NMPH^+ is sterically protected from oxygen attack. Evans and Bolton (82) recently reported that there was a strong interaction between NMPH^+ and sodium dodecyl sulfate micelles, again stabilizing the molecule NMPH^+ . The binding site is in the hydrocarbon region a few angstroms below the polar head group. Thus, NMPH^+ could be stabilized by deoxyribonucleic acid or by micelles in aerobic solution.

This system could be used to couple with another reduction half cell which can sensitize the decomposition of water to hydrogen upon irradiation. The NMPH^+ thus formed during the light period could possibly regenerate the starting material of the reduction half cell electrochemically in the dark, making the reaction reversible.

4.12 SUMMARY

The photochemistry of NMP^+ in aqueous solution was investigated using a combination of electron spin resonance and optical flash photolysis techniques.

The formation of NMPH^+ was confirmed by the similarity of the optical absorption spectrum of the light induced species to that of a NMPH^+ perchlorate solution, the change in the ESR signal pattern when the solvent was changed from H_2O to D_2O , and the analysis of the ESR spectrum which indicates that there is a proton attached to the nitrogen. The formation of PYH^+ was detected by its characteristic optical absorption maxima at various pH values.

A mechanism is proposed (page 63) in terms of the formation of a solvent adduct of the unprotonated excited singlet state of NMP^+ . This intermediate donates an $\cdot\text{OH}$ radical to NMP^+ in a concerted reaction to form PYH_2^+ and $\text{NMP}\cdot$ (Reaction 4.5) which is then protonated forming NMPH^+ (Reaction 4.7) or giving back the starting material NMP^+ (Reaction 4.6). PYH_2^+ then reacts with NMP^+ giving NMPH^+ and PYH^+ (Reaction 4.8). But $\text{PYH}\cdot$, which can be generated through the ionization of PYH_2^+ (Reaction 4.10), can also react with NMP^+ giving $\text{NMP}\cdot$ and PYH^+ (Reaction 4.9). Most of the forward rate constants were determined. The disproportionation reactions (Reaction 4.11 or 4.12) were found to be rather unimportant under the experimental conditions. The rate constants for these reactions are summarized in Table 4.7.

The quantum yields of the formation of NMPH^+ were determined to be 0.29 ± 0.03 at pH 7, at 476.2 nm and 1.1 at pH 3 by an ESR

Table 4.7

Summary of the Rate Constants Obtained
in Optical Flash Photolysis Experiments

	Rate Constant ($M^{-1} s^{-1}$)
k_5	7.7×10^8
k_7	2.0×10^8
k_8	1.0×10^6
k_9	7.0×10^8

technique which does not require a prior knowledge of the absorption coefficient of the radical at the wavelength of the incident light.

Formate and acetate were found to quench the formation of PYH^+ . Probably other organic substances may also be used to facilitate the formation of NMPH^+ which in turn may possibly act as a substrate for photochemical hydrogen production.

REFERENCES

1. H. Yoshida and T. Warashina; Bull. Chem. Soc. Japan, 44, 2950, (1971)
2. J. R. Bolton; Solar Energy, (in press)
3. F. Kehrman and E. Havas; Ber., 46, 341, (1913)
4. A. Hantzsch; Ber., 46, 1925, (1913)
5. F. Kehrman and A. Danecki; Ber., 47, 279, (1914)
6. A. Hantzsch; Ber., 49, 511, (1916)
7. R. Willstätter and J. Piccard; Ber., 41, 1458, (1908)
8. A. R. Forrester, J. M. Hay and R. H. Thomson; Organic Chemistry of Stable Free Radicals, Academic Press, (1968)
9. L. Michaelis; Chem. Revs., 16, 243, (1935)
10. J. W. Newton and M. D. Kamen; Biochim. Biophys. Acta, 25, 462, (1957)
11. R. Hill and D. A. Walker; Plant Physiol., 34, 240, (1959)
12. D. M. Geller and F. Lipmann; J. Biol. Chem., 235, 2478, (1960)
13. D. M. Geller; J. Biol. Chem., 244, 971, (1969)
14. W. S. Zaugg; J. Biol. Chem., 239, 3964, (1964)
15. J. R. White and H. H. Dearman; Proc. Natl. Acad. Sci. USA, 54, 887, (1965)
16. W. S. Zaugg, L. P. Vernon and A. Tirpack; Proc. Natl. Acad. Sci. USA, 51, 232, (1964)
17. K. Ishizu, H. H. Dearman, M. T. Huang and J. R. White; Biochem., 8, 1238, (1969)

18. M. Nishikimi, N. A. Rao and K. Yagi; *Biochem. Biophys. Res. Commun.*, 46, 849, (1972)
19. J. M. McCord and I. Fridovich; *J. Biol. Chem.*, 244, 6049, (1969)
20. C. Chayet, R. H. Steele and B. S. Breckinridge; *Biochem. Biophys. Res. Commun.*, 10, 390, (1963)
21. K. Cost, J. R. Bolton and A. W. Frenkel; *Photochem. Photobiol.*, 5, 883, (1966)
22. K. Cost, J. R. Bolton and A. W. Frenkel; *Proc. Natl. Acad. Sci. USA*, 57, 868, (1967)
23. K. Cost and J. R. Bolton; *Photochem. Photobiol.*, 18, 423, (1973)
24. H. McIlwain; *J. Chem. Soc. Part 2*, 1704, (1937)
25. W. Rubaszewska and Z. R. Grabowski; *J. Chem. Soc. Perkin II*, 417, (1975)
26. J. Dobkowski and W. Rubaszewska; *Roczniki Chemii*, 50, 1435, (1976)
27. P. S. Rao and E. Hayon; *Anal. Chem.*, 48, 564, (1976)
28. D. Märzotko, R. Wachowiak and J. R. Warchol; *Acta Histochem.*, 46, 150, (1973)
29. F. Kehrman; *Ber.*, 48, 1931, (1915)
30. Y. Takagi, K. Akasaka, T. Imoto, H. Kawai and K. Ishizu; *Chem. Lett.*, 847, (1972)
31. C. Dufraissé, A. Etienne and E. Toromanoff; *Compt. Rend.*, 232, 2379 (1951) and 235, 759, (1952)
32. E. Toromanoff; *Ann. Chim. (Paris)*, 1, 115, (1956)
33. M. Kleinerman, L. Azzaraga and S. P. McGlynn in P. Kallman and M. Spruch (eds.); *Luminescence of Organic and Inorganic Materials*, New York, (1962)
34. A. Grabowski and B. Pakula; *Photochem. Photobiol.*, 9, 339, (1969)
35. Th. Förster; *Z. Elektrochem.*, 54, 42, (1950)

36. D. D. Perrin; Dissociation Constants of Organic Bases in Aqueous Solution, Butterworths, New York, (1969)
37. D. N. Bailey, D. K. Roe and D. M. Hercules; J. Chem. Soc., 90, 6291, (1969)
38. G. A. Davis, J. D. Gresser and P. A. Carapellucci; J. Am. Chem. Soc., 93, 2179, (1971)
39. S. M. Japar and E. W. Abrahamson; J. Am. Chem. Soc., 93, 4140, (1971)
40. S. Wake, H. Inour, Y. Otsuji and E. Imoto; Tetrahedron Letters, 28, 2415, (1970)
41. H. Kawata, S. Niizuma and H. Kokubun; Chem. Lett., 1369, (1976)
42. E. Friedheim and L. Michaelis; J. Biol. Chem., 91, 355, (1931)
43. W. M. Clark, B. Cohen and H. D. Gibbs; U. S. Pub. Health Repts., Suppl. No. 54, (1926)
44. M. Voriskova; Collect. Czech. Chem. Commun., 12, 607, (1947)
45. J. E. Wertz and J. R. Bolton; Electron Spin Resonance: Elementary Theory and Practical Applications, McGraw Hill, New York, (1972)
46. P. W. Atkins and M. C. R. Symons; The Structure of Inorganic Radicals, Elsevier Publishing Company, Amsterdam, (1967)
47. A. Carrington and A. D. McLachlan; Introduction to Magnetic Resonance with Applications to Chemistry and Chemical Physics, Harper and Row, (1967)
48. G. Porter in P. G. Ashmore, F. S. Dainton and T. M. Sugden (eds.); Photochemistry and Reaction Kinetics, Cambridge University Press, London, (1967)
- G. Porter and M. A. West in Weissberger and G. Hammes (eds.); Techniques of Chemistry; Volume 6, Part 2, John Wiley and Sons. Inc., (1973)
49. K. B. Eisenthal; Acc. Chem. Res., 8, 118, (1975)

50. T. J. Bennett, R. C. Smith and T. H. Wilmschurst; Chem. Commun., 307, 513, (1967)
51. J. R. Bolton and K. Cost; Photochem. Photobiol., 18, 417, (1973)
52. K. Cost and J. R. Bolton; Photochem. Photobiol., 20, 251, (1974) and 20, 263, (1974)
53. J. T. Warden, S. Mohanty and J. R. Bolton; Biochem. Biophys. Res. Commun., 59, 872, (1974)
54. J. R. Bolton and J. T. Warden in W. R. Ware (ed.); Creation and Detection of the Excited State, Volume 2, Marcel Dekker Inc., New York, (1974)
55. E. G. Janzen; Acc. Chem. Res., 4, 31, (1971)
56. E. G. Janzen and C. I. P. Liu; J. Magn. Resonance, 9, 510, (1973)
57. J. R. Bolton, R. K. Clayton and D. W. Reed; Photochem. Photobiol., 9, 209, (1969)
58. B. Segal, M. Kaplan and G. Fraenkel; J. Chem. Phys., 43, 4191, (1965)
59. J. R. Bolton, D. C. Borg and H. M. Swartz in H. M. Swartz, J. R. Bolton and D. C. Borg (eds.); Biological Applications of Electron Spin Resonance, Wiley Interscience, New York, (1972)
60. D. B. Loveland and T. N. Tozer; J. of Physics (E), 5, 535, (1972)
61. P. R. Bevington; Data Reduction and Error Analysis for the Physical Sciences, McGraw Hill, (1969)
62. J. N. Demas and G. A. Crosby; J. Phys. Chem., 75, 991, (1971)
63. C. A. Heller, R. A. Henry, B. A. McLaughlin and D. E. Bliss; J. Chem. Eng. Data, 19, 214, (1974)
64. H. McCombie and H. Archibald; J. Chem. Soc., 123, 3279, (1923)
65. T. E. King; J. Biol. Chem., 238, 4032, (1963)
66. G. Vincow in E. T. Kaiser and L. Kevin (eds.); Radical Ions, Interscience Publishers, (1968)

67. P. A. Loach and K. Walsh; *Biochem.*, 8, 1908, (1969)
68. P. A. Loach and D. L. Sekura; *Biochem.*, 7, 2642, (1968)
69. C. P. Poole, Jr.; *Electron Spin Resonance: A Comprehensive Treatise on Experimental Techniques*, Interscience Publishers, (1967)
70. A. R. McIntosh; private communication
71. J. A. Weil and J. K. Anderson; *J. Chem. Soc.*, 5567, (1965)
72. J. R. Harbour, V. Chew and J. R. Bolton; *Can. J. Chem.*, 52, 3547, (1974)
73. G. E. Adams, J. W. Boag, J. Carrant and B. D. Michael in M. Ebert, J. P. Keene, A. J. Swallow and J. H. Baxendale (eds.); *Pulse Radiolysis*, Academic Press, New York, (1965)
74. K. P. Clark and H. I. Stonehill; *J. Chem. Soc., Faraday Trans. I*, 68, 577, (1972)
75. K. P. Clark and H. I. Stonehill; *J. Chem. Soc., Faraday Trans. I*, 68, 1676, (1972)
76. C. E. Burchill, D. M. Smith and J. L. Charlton; *Can. J. Chem.*, 54, 505, (1976)
77. J. E. Charlton, R. G. Smerchanski and C. E. Burchill; *Can. J. Chem.*, 54, 512, (1976)
78. K. P. Clark and H. I. Stonehill; *J. Chem. Soc. Faraday Trans. I*, 73, 722, (1977)
79. R. H. Dekker, B. N. Shrinivasan, J. R. Huber and K. Weiss; *Photochem. Photobiol.*, 18, 457, (1973)
80. R. R. Düren, R. H. Dekker, H. C. A. van Beek and W. Berends; *Photochem. Photobiol.*, 23, 163, (1976)
81. MIMIC Source - Language Program; Computing Centre, University of Western Ontario, London, Ontario
82. C. A. Evans and J. R. Bolton; *J. Am. Chem. Soc.*, 99, 4502, (1977)

APPENDIX 1

THE COMPUTER PROGRAM FOR THE DOUBLE
INTEGRATION

```

DIMENSION Y(1024),YY(1024),HT(1024),YP(1024)
1  TYPE 2
2  FORMAT( //, 'NAME OF DATA FILE', //, ' ENTER END
   POINTS TO BE READ IN 14'//)
   ACCEPT 8, FILEN
8  FORMAT(A5)
   ACCEPT 91,N
91  FORMAT(14)
   CALL IFILE(1,FILEN)
   READ(1,5)(Y(J),J=1,N)
5  FORMAT(8F7.0)
   PRINT 56
56  FORMAT(' NUMBER OF PTS IN A GROUP IN 14'//)
   ACCEPT 88, NOG
88  FORMAT(14)
   NG=N/NOG
   J=0
   ANOG=NOG
   DO 60 I=1,NG
   SUM=0.
   DO 61 K=1,NOG
   JJ=J+K
   SUM=SUM+Y(JJ)
61  CONTINUE
   YY(I)=(SUM/ANOG)
   J=J+NOG
60  CONTINUE
   SIGMAY=0.
   DO 24 I=1,NG
   HT(I)=YY(I)-YY(I)
   SIGMAY=SIGMAY+HT(I)
24  CONTINUE

```

```

35 PRINT 35
   FORMAT(' SCAN RANGE OF SPECTRUM IN F6.0'//)
   ACCEPT 33,SCANR
33  FORMAT(F6.0)
   D=SCANR*ANOG/1024.
   ANG=NG
   BB=-2.*SIGMAY/(D*ANG*(ANG+1.))
   SAREA=0.
   DO 99 I=1,NG
   AI=I
   SAREA=(2.*ANG-3.*AI+1.)*HT(I)+SAREA
99  CONTINUE
   AREA=D*D*SAREA/3.
201 PRINT 20,FILEN,NOG,NG,AREA
20  FORMAT(' FILE NAME IS ',A5,/, ' NUMBER OF POINTS
1 IN A GROUP ',I4,/, ' TOTAL NUMBER OF GROUPS ',
2I4,/, ' AREA IS ',F10.0,//)
   SUM=0.
   SB=BB*D*D/2.
   DO 77 I=1,NG
   AI=I
   SUM=SUM+HT(I)
   YP(I)=D*SUM+SB*(AI*AI+AI)
77  CONTINUE
   CALL MAXMIN (YP,NG,YMAX,YMIN)
59  TYPE 58
58  FORMAT(' TYPE PLOT FOR A PLOT; TYPE NO'//)
   ACCEPT 8, PP
   IF (PP.EQ.'NO') GO TO 96
   IF (PP.NE.'PLOT') GO TO 59
   CALL APLOTT(YMAX,YMIN,YP,NG)
96  TYPE 14
14  FORMAT (' TYPE YES FOR ABSORPTION CURVE DATA;
1 TYPE NO'//)
   ACCEPT 8, CONP
   IF (CONP.EQ.'NO') GO TO 95
   IF (CONP.NE.'YES') GO TO 96
15  PRINT 5,(YP(J),J=1,NG)
95  PRINT 65
65  FORMAT(' TYPE NEWW FOR NEW DATA SET,
1 OTHERWISE TYPE STOP'//)
   ACCEPT 8, CONT
   IF (CONT.EQ.'NEWW') GO TO 1
   IF (CONT.NE.'STOP') GO TO 95
   STOP
   END

```

```

SUBROUTINE MAXMIN(YP,NG,YMAX,YMIN)
DIMENSION YP(1024)
YMAX=YP(1)
YMIN=YP(1)
K=1
L=1
DO 10 I=2,NG
IF(YP(I).GT.YMAX) GO TO 11
IF(YP(I).GT.YMIN) GO TO 10
YMIN=YP(I)
L=I
GO TO 10
11 YMAX=YP(I)
K=I
10 CONTINUE
AO=YP(NG)
PRINT 12, YMAX,YMIN,K,L,AO
12 FORMAT( ' MAXIMUM VALUE IS=',F10.2,/,
1' MINIMUM VALUE IS=',F10.2,/, ' ADDRESS OF MAXIMUM
2 IS=',I5,/, ' ADDRESS OF MINIMUM IS=',I5/,
3' VALUE OF LAST ADD. IS=',F5.2/)
RETURN
END

```

```

SUBROUTINE APLOTT(YMAX,YMIN,YP,NG)
DIMENSION YP(1024)
A=YMAX-YMIN
B=NG-1
9 PRINT 10
10 FORMAT(' TYPE POINT TO OBTAIN POINT PLOT, LINEE
1 TO OBTAIN LINE PLOT'//)
ACCEPT 11,COND
11 FORMAT (A5)
IF(COND.EQ.'POINT') GO TO 12
TYPE 13
13 FORMAT(/,' PLTL'//)
GO TO 15
12 TYPE 14
14 FORMAT(/,' PLTP'//)
DO 16 I=1,NG
AI=I
IHQR=(AI-1.)*9999./B
IVERT=(YP(I)-YMIN)*9999./A
TYPE 17,IHQR,IVERT
17 FORMAT(IX,I4,IX,I4)
16 CONTINUE
TYPE 18
18 FORMAT(/,' PLTT'//)
TYPE 22
22 FORMAT(' TYPE AGAIN TO PLOT THE SAME DATA'//)
ACCEPT 11,CON
IF(CON.EQ.'AGAIN') GO TO 9
RETURN
END

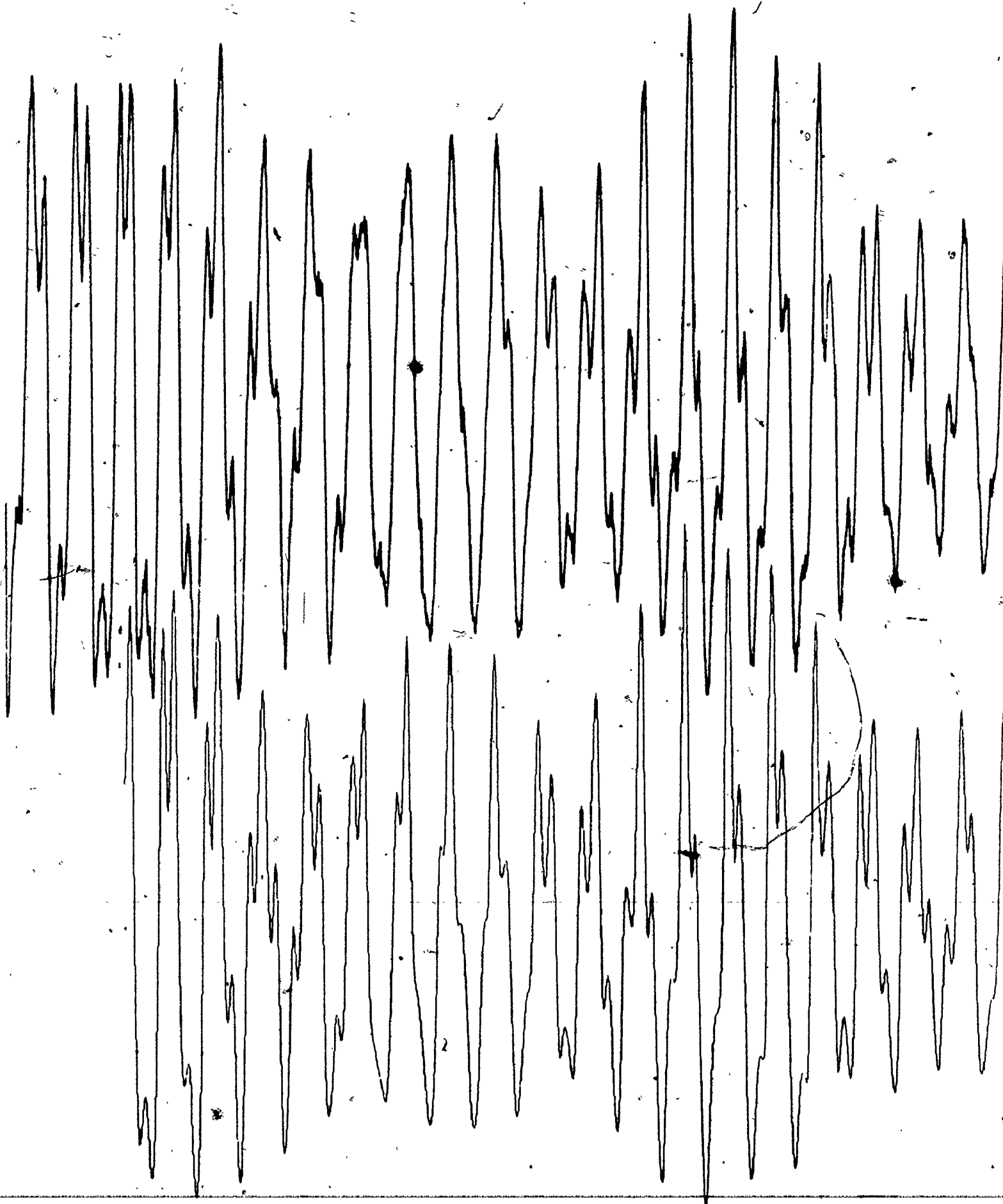
```

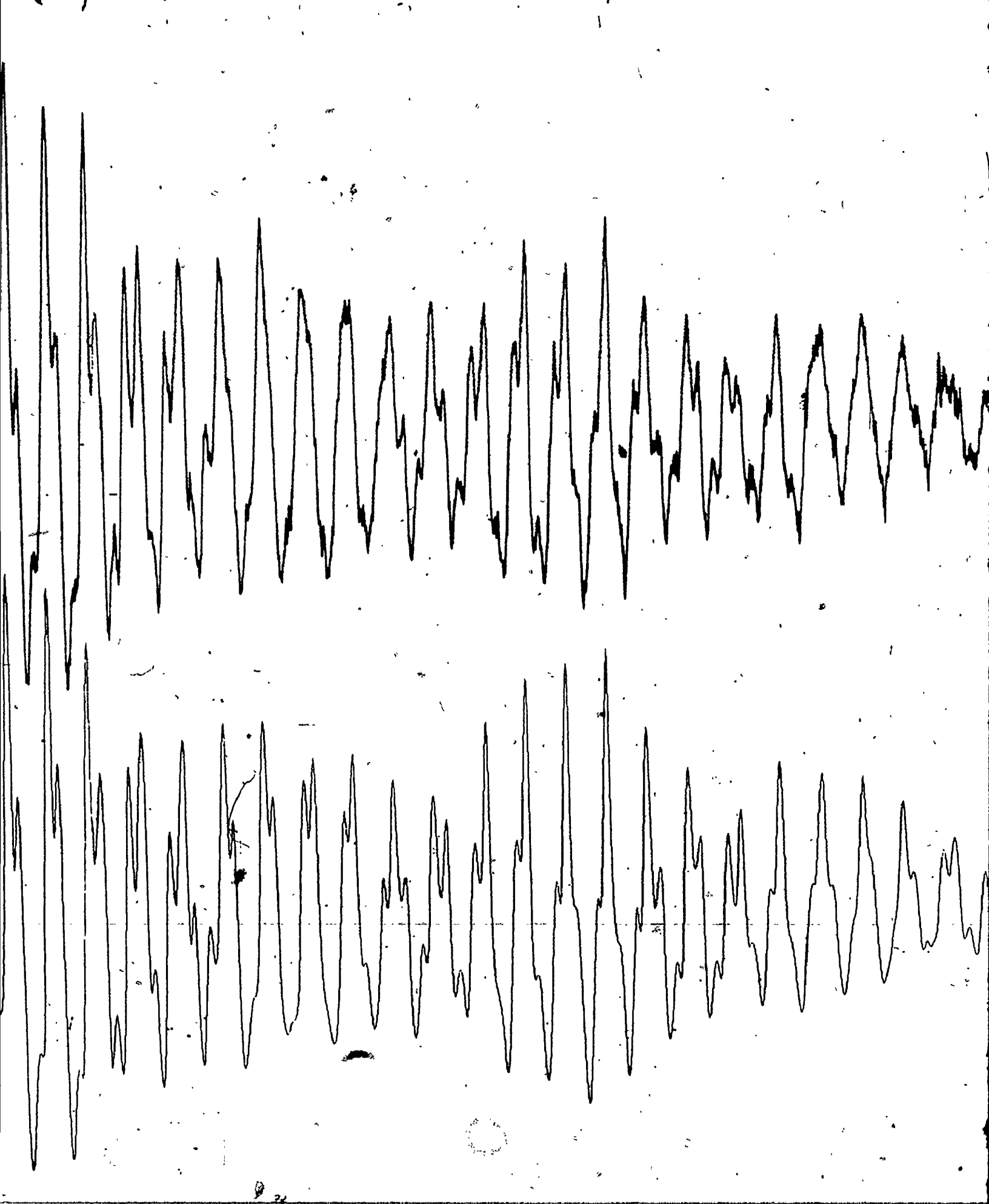
APPENDIX 2

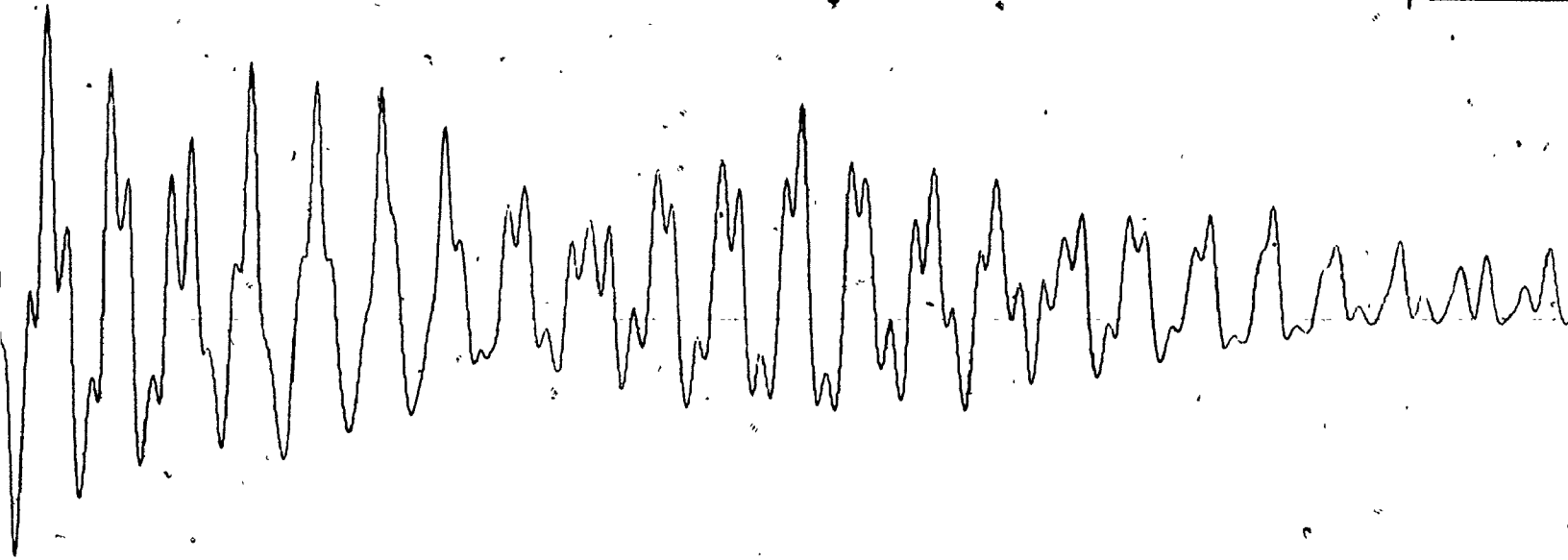
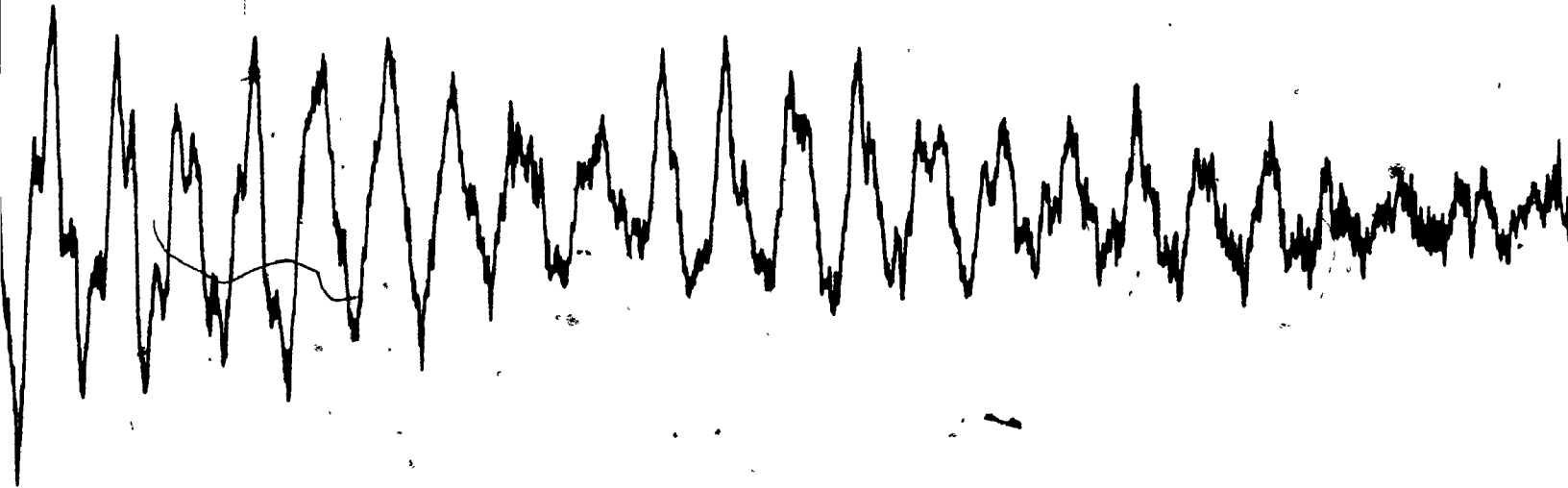
The Experimental Second Derivative of NMPH^+ ESR Spectrum (top) and the Computer Simulated Spectrum (bottom) Using the Hyperfine Splitting Constants Listed in Table 4.1.

Modulation amplitude 0.063 G, time constant 1 s, scan time 30 min./20 G, microwave power 1 mW, modulation frequencies 100 kHz and 1 kHz, linewidth used in the simulation 0.12 G.

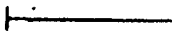
Note that the peak of the second derivative line is towards to top of the page.







2 G





2 G

